

Röntgenkristallographische Analyse zur Bestimmung von Struktur-Funktionsbeziehungen
zur toxischen Metalloendopeptidase AsaP1 sowie zur Haloalkan Dehalogenase DppA

Inauguraldissertation

zur

Erlangung des akademischen Grades
doctor rerum naturalium (Dr. rer. nat.)
an der Mathematisch-Naturwissenschaftlichen Fakultät

der

Ernst-Moritz-Arndt-Universität Greifswald

vorgelegt von
Xenia Bogdanović
geboren am 15.09.1981
in Belgrad

Greifswald im Januar 2012

Dekan: Prof. Dr. Klaus Fesser

1. Gutachter : Prof. Dr. Winfried Hinrichs

2. Gutachter: Prof. Dr. Norbert Sträter

Tag der Promotion: 14. Juni 2012

Inhaltsverzeichnis

Inhaltsverzeichnis	i
Einleitung	iii
Einleitung zur Metalloendopeptidase AsaP1	1
<i>Aeromonas salmonicida</i> subsp. <i>achromogenes</i> als Krankheitserreger.....	1
Atypische Furunkulose - Klinische Symptome, Verlauf und Virulenzfaktoren.....	2
AsaP1 – <i>Aeromonas salmonicida</i> subsp. <i>achromogenes</i> Protease 1.....	3
Aspzinkin-Proteasen	4
Propeptidstrukturen bakterieller Enzyme.....	5
Ergebnisteil zur Metalloendopeptidase AsaP1.....	9
Toxoidkonstruktion von AsaP1 und Untersuchungen zu deren Aktivität und Prozessierung.....	9
Kristallisation und röntgendiffraktometrische Untersuchungen von AsaP1 _{E294A} und AsaP1 _{E294Q}	10
Einfluss der Temperatur während des Kristallisierungsansatzes auf Präzipitatbildung und Kristallform	11
Kristallstrukturanalyse der AsaP1 Metalloendopeptidase im Komplex mit dem Propeptid.....	13
Einleitung zur Haloalkan Dehalogenase DppA	18
Halogenierte Kohlenwasserstoffe.....	18
Haloalkan Dehalogenasen, Klassifikation und Einsatzmöglichkeiten	19
Ergebnisteil zur Haloalkan Dehalogenase DppA.....	23
Kristallisation und röntgendiffraktometrische Untersuchungen zu DppA.....	23
Strukturelle Analyse der Haloalkan Dehalogenase DppA aus <i>Plesiocystis pacifica</i> SIR-I.....	23
Literatur	26
Publikationsliste.....	35

Einleitung

Proteine erfüllen in allen Organismen die unterschiedlichsten Funktionen. Es gibt Strukturproteine, katalytische Proteine, Transport- und Speicherproteine, Regulationsproteine, Proteine des Immunsystems, Signalproteine und viele mehr. Alle Proteine sind Verbindungen aus etwa 20, chemisch unterschiedlichen Aminosäuren, wobei Zusammensetzung, Länge und Sequenz von Protein zu Protein variiert. Die zahlreichen Möglichkeiten der Verknüpfung unterschiedlicher Aminosäuren wie auch die möglichen Faltungen der Polypeptidkette erlauben sehr vielfältige und hoch spezifische Funktionen von Proteinen im Metabolismus einer jeden Zelle. Ein genaues Verständnis jedes einzelnen dieser Prozesse erfordert Kenntnis über die exakte räumliche Struktur der beteiligten Proteine, möglichst im atomaren Maßstab.

Mit Hilfe der Proteinkristallographie kann die atomare Struktur von Proteinmolekülen auf molekularer Ebene aufgeklärt werden. Die Kenntnis der räumlichen Struktur eines Proteinmoleküls erlaubt die Entwicklung von Modellvorstellungen über Struktur-Funktionsbeziehungen und hat zu wesentlichen Fortschritten in vielen Bereichen der Grundlagenforschung sowie der Struktur basierten Wirkstoffentwicklung beigetragen.

Diese Arbeit beschäftigt sich zum einen mit der Röntgenstrukturaufklärung einer bakteriellen Metalloendopeptidase: AsaP1. Diese ist der hauptsächliche Virulenzfaktor von einigen atypischen *Aeromonas salmonicida* Stämmen, die als Krankheitserreger für diverse Fischarten zu massiven Verlusten in Aquakulturen führen. Die Substraterkennung und Spezifität von AsaP1 konnte anhand der Struktur geklärt werden und es wird erstmalig die Propeptidstruktur von Aspargin-Proteasen strukturell beschrieben.

Der zweite Teil der Arbeit befasst sich mit der Strukturaufklärung einer Haloalkan Dehalogenase, die biotechnologisch von Interesse ist.

Teile der Arbeit sind bereits veröffentlicht oder zur Begutachtung eingereicht (siehe Publikationsliste, Seite 35). Die Publikationen sind der Arbeit angehängt und die Ergebnisse werden nach einer Einleitung zum jeweiligen Thema kurz zusammenfassend beschrieben und diskutiert.

Einleitung zur Metalloendopeptidase AsaP1

***Aeromonas salmonicida* subsp. *achromogenes* als Krankheitserreger**

Bakterien der Gattung *Aeromonas* sind allgegenwärtige, Gram-negative, Oxidase-positive, Glukose fermentierende, fakultative Anaerobier, die autochthon in aquatischer Umgebung sind. Sie wurden sowohl in Brack-, Süß- und Salzwasser als auch in chlorierten und nicht chlorierten Wasserkreisläufen weltweit nachgewiesen, wobei die Anzahl der Bakterien in den wärmeren Monaten zunimmt¹.

Die Art *Aeromonas salmonicida* (*A. salmonicida*) wird heute in fünf Unterarten unterteilt: subsp. *salmonicida*, subsp. *masoucida*, subsp. *smithia*, subsp. *achromogenes* und subsp. *pectinolytica*^{2; 3}. Die Abgrenzung und Taxonomie ist wenig eindeutig und es existieren zunehmend mehr Unterarten, deren Zuordnung noch aussteht. Die Einteilung erfolgt vornehmlich über biochemische Charakteristika (u.a.: Pigmentbildung, Gasbildung mit Glukose als Nährstoff, Empfindlichkeit gegenüber Antibiotika). Auch die Unterteilung in typische und atypische Unterarten ist üblich, wobei alle Arten, die von *A. salmonicida* subsp. *salmonicida* abweichende Reaktionen auf spezifische Nachweisreaktionen aufweisen, als atypische bezeichnet werden⁴.

Viele Unterarten von *A. salmonicida* sind bekannte Krankheitserreger für aquatische Organismen mit breitem Wirtspektrum. Gewöhnlich werden alle Krankheitsbilder bei Knochenfischen, die durch *A. salmonicida* ausgelöst werden, als Furunkulose bezeichnet - eine septikämische Erkrankung, die zur Bildung von Geschwüren in der Haut führt und die durch unterschiedliche Infektionsverläufe gekennzeichnet ist. Häufig werden auch die inneren Organe, wie Herz und Niere, befallen. Die Krankheit verläuft oftmals tödlich, vor allem bei jungen und geschwächten Tieren.

Furunkulose ist bei der Weltorganisation für Tiergesundheit (Office Internationale des Épizooties, OIE) weder als anzeigenpflichtige noch als meldepflichtige Krankheit gelistet. Dennoch ist Furunkulose eine hoch infektiöse, bakterielle Krankheit für Salmoniden, die das Potential für eine schnelle Ausbreitung mit ernsthaften ökonomischen Folgen besitzt. Der Ausbruch der Krankheit in Aquakulturen kann zur völligen Ausmerzung der Fischbestände führen. Neben den in Zucht gehaltenen und zu den wirtschaftlich wichtigen Salmoniden⁵, Karpfen⁶, Hecht, Dorsch, Aal, Steinbutt und Heilbutt⁷ werden auch wildlebende Fischarten befallen^{5; 8; 9; 10}. Fische in Zucht werden allerdings sehr viel häufiger befallen was zu großen Problemen und Kosten führt – direkt, durch häufig vollständigen Verlust des Fischbestandes sowie indirekt, durch entstehende Kosten für Antibiotika und Impfungen^{5; 7; 8; 10; 11}. Die Krankheit führt bei wildlebenden Fischen nur selten zum Tod aufgrund der stressärmeren

Lebensbedingungen⁷. *A. salmonicida* hat kein zoonotisches Potential und stellt somit für den Menschen kein Gesundheitsrisiko dar.

Die verschiedenen *A. salmonicida* Unterarten bilden unterschiedliche extrazelluläre Produkte, die eine von der Bakterienart abhängige Zusammensetzung an Enzymen und Proteinen aufzeigen und die für den jeweiligen Verlauf der Krankheit ausschlaggebend sind. Der Krankheitsverlauf, Epizootiologie, Diagnostik sowie Resistenzen und Impfmöglichkeiten der typischen Furunkulose sind bereits umfangreich dargestellt^{5; 12}.

Findet man atypische *A. salmonicida* Unterarten als Erreger (z.B.: *A. salmonicida* subsp. *achromogenes*) spricht man von atypischer Furunkulose. Innerhalb der Unterarten *A. salmonicida* subsp. *achromogenes* wurde eine heterogene Gruppe von Bakterienstämmen gefunden, die als Erreger der atypischen Furunkulose gelten und viele verschiedene Fischarten infizieren^{1; 13; 14; 15; 16; 17; 18; 19}.

Atypische *A. salmonicida* Stämme als Auslöser für Infektionen wurden bisher von etwas mehr als 20 Fischarten in Zucht und 30 wildlebenden Fischarten - hauptsächlich in Regionen der nördlichen Hemisphäre aber auch in Australien und Chile - berichtet^{20; 21}. Diese treten neuerdings vermehrt in Aquakulturen von Kabeljau (*Gadus morhua* (L.)), Atlantischem Heilbut (*Hippoglossus hippoglossus* (L.)), geflecktem-, bzw. gestreiftem Seewolf (*Anarhichas minor* (O.) bzw. (*Anarhichas lupus* (L.)) und Steinbutt (*Scophthalmus maximus* (L.)) auf.

Darüber hinaus sind atypische *A. salmonicida* Stämme nachgewiesene Pathogene für Salmoniden und Zierfische^{22; 23}.

Atypische Furunkulose - Klinische Symptome, Verlauf und Virulenzfaktoren

Charakteristisch für Infektionen durch atypische *A. salmonicida* Stämme sind Appetitlosigkeit, ein dunkleres Erscheinungsbild des Fisches sowie eine erhöhte Mortalität. Atypische Furunkulose ist eine systemische Infektion und häufig durch eine Sepsis gekennzeichnet. Zudem werden starke Blutungen an den Flossen beobachtet und eiternde Geschwüre, die meist an den Flanken auftreten. Die Geschwüre sind im Vergleich zu Infektionen durch *A. salmonicida* subsp. *salmonicida* nicht so tiefgreifend¹³. Die Kiemen sind oft fahl mit flohstichartigen Blutungen, wohingegen in den inneren Organen und Schleimhäuten häufig großflächigere Blutungen auftreten. Eine Hyperämie der inneren Organe kann mitunter beobachtet werden. Die Krankheit kann je nach Alter und Umgebung der befallenen Fische, der unterschiedlichen Abwehrreaktionen der infizierten Fischarten sowie infizierender Bakterienstämme einen unterschiedlichen Verlauf aufzeigen.

Virulenzfaktoren, die in atypischen *A. salmonicida* Stämmen gefunden wurden sind das A-Protein (*A-layer/S-layer*), Lipopolysaccharide (LPS)²⁴, Eisen bindende Proteine in der äußeren Membran (IROMPs -iron binding outer membrane proteins)²⁵, das C1q bindende Porin²⁶, die Aspargin-Metalloendopeptidase AsaP1¹⁵, die Serinprotease AspA (auch P1 genannt) und die Cholesterol-Acyltransferase GCAT²⁷. Die zellassoziierten Virulenzfaktoren wie das A-Protein, Komponenten der Lipopolysaccharide oder die Eisen bindenden Proteine der äußeren Membran werden sowohl in typischen als auch in atypischen Stämmen von *A. salmonicida* gefunden. Die Beschaffenheit der Exotoxine der extrazellulären Produkte zeigt jedoch eine weitaus größere Varianz.

Die Glycerophospholipid:cholesterol-acyltransferase gilt als hauptsächliches letales Exotoxin bei typischen *A. salmonicida* Stämmen und zeigt eine cytotoxische Wirkung, wohingegen das hauptsächliche Toxin der Bakterienstämme, die zum Erscheinungsbild der atypischen Furunkulose führen, die Metalloendopeptidase AsaP1 ist.

AsaP1 – *Aeromonas salmonicida* subsp. *achromogenes* Protease 1

Die Protease AsaP1 wurde aus dem extrazellulären Produkt (ECP) von *Aeromonas salmonicida* subsp. *achromogenes* Stamm 265-87 isoliert und als Metalloendopeptidase identifiziert. Es konnte sowohl eine caseinolytische ($2,2 \text{ U } \mu\text{g}^{-1}$) als auch eine schwach gelantinolytische ($0,23 \text{ U } \mu\text{g}^{-1}$) Aktivität nachgewiesen werden. Die proteolytische Aktivität liegt bei $5 \text{ U } \mu\text{g}^{-1}$ ²⁸. Es handelt sich um ein-toxisches Protein, das in gereinigter Form und intraperitonealer Applikation bei Atlantischem Lachs einen LD₅₀-Wert von $0,03 \mu\text{g g}^{-1}$ Fisch aufweist; bei Mäusen ist der LD₅₀-Wert um das sechsfache höher^{28; 29}. Das ECP des Bakteriums ohne die Protease zeigt keine tödliche Wirkung^{15; 28; 29; 30; 31}. Das unbehandelte ECP ist cytotoxisch, wohingegen die isolierte Protease AsaP1 keine cytotoxischen Eigenschaften zeigt²⁸.

Das Vorhandensein von AsaP1 im ECP einiger atypischer *A. salmonicida* Stämme korreliert mit dem Auftreten der pathogenen Wirkung, der Letalität und der caseinolytischen Aktivität des ECP³⁰. Subletale Konzentrationen von AsaP1, die intramuskulär bei Atlantischem Lachs injiziert werden, rufen vergleichbare Symptome hervor wie sie bei Fischen beobachtet werden, die mit atypischer Furunkulose infiziert sind²⁸.

Eine Vielzahl von Symptomen der atypischen Furunkulose ist auf die Expression von AsaP1 zurück zu führen. Dies sind Läsionen und Geschwüre in der Haut, degenerative Veränderungen und Nekrosen in der darunter liegenden Muskulatur, blasses Kiemen und eine generelle Blutarmut der inneren

Organe³². AsaP1 ist hoch immunogen in Salmoniden und Antikörper gegen AsaP1 führen zu einer passiven Immunisierung bei Infektionen durch *A. salmonicida* subsp. *achromogenes*³¹.

AsaP1 ist ein entscheidender Virulenzfaktor von *A. salmonicida* subsp. *achromogenes*^{28; 32} und wurde bisher noch nicht im ECP typischer *A. salmonicida* Stämme nachgewiesen¹⁵.

Die Expression der Protease ist durch *Quorum-Sensing* reguliert³³.

Aspzinkin-Proteasen

Die Protease AsaP1 wird nach der MEROPS-Nomenklatur³⁴ der M35 Familie (Deuterolysin) innerhalb des Sub-Clan MA(M) im Clan MA der Metalloendopeptidasen eingeordnet. Proteasen der M35 oder Deuterolysin Familie zeigen ein konserviertes HExxH-Motiv innerhalb der Helix des aktiven Zentrums. Die beiden Histidine koordinieren das Zinkion des aktiven Zentrums und das Glutamat ist essentiell für die Katalyse. Das zweite charakteristische Merkmal ist das GTxDxxYG-Motiv in einem Loop C-terminal zur Helix des aktiven Zentrums. Dieser Loop enthält den dritten Zinkliganden - ein Aspartat. Der Sub-Clan MA(M) wird auch als Metzinkin-Proteasen (engl. *metzincins*)³⁵ bezeichnet und der Sub-Clan MA(E) als Gluzinkin-Proteasen (engl. *gluzincins*)³⁶. Keine der Proteasen, die zur M35-Familie zählen, zeigt einen konservierten '*Met-turn*', der für Familien des Sub-Clan MA(M) innerhalb des Clan MA charakteristisch ist. Die M35 Familie wurde erstmals von Fushimi *et al.*³⁷ als Aspzinkin-Proteasen (engl. *aspzincins*) definiert für Peptidasen mit einem konservierten HExxH + D Motiv. Allerdings findet man Peptidasen mit Aspartat als drittem Zinkliganden auch in den Protease-Familien M6, M7 und M64.

Bisher sind fünf Peptidasen der M35 Familie oder der Aspzinkin-Proteasen charakterisiert. Penicillolysin aus *Penicillium citrinum* (M35.001), Deuterolysin aus *Aspergillus oryzae* (M35.002) und die peptidyl-Lys Metalloendopeptidase aus *Grifola frondosa* (*GfMEP* – *Grifola frondosa* metalloendopeptidase) (M35.004) wurden bereits zusammenfassend beschrieben^{38; 39; 40}. Die fünfte Peptidase ist die AVR-Pita Peptidase aus *Magnaporthe* sp. (M35.005)⁴¹.

Für Deuterolysin und Penicillolysin konnte eine Preferenz für basische Substrate nachgewiesen werden wie zum Beispiel Histon-Proteine, Protamin und Salmin^{38; 42}. Eine basische Aminosäure wie Arginin oder Lysin ist allgemein bevorzugt in der P1' Position (Nomenklatur siehe⁴³) und ist erforderlich für die hoch spezifische *GfMEP*, die nur Xaa-Lys Peptidbindungen spaltet, wobei Xaa sogar Prolin sein kann^{44; 45}.

Die Strukturen von *GfMEP*⁴⁶ und von Deuterolysin⁴⁷ sind bereits beschrieben und weisen eine hohe Ähnlichkeit auf. Die Tertiärstruktur der Aspzinkine besteht aus zwei Domänen, die durch eine lange

Furche getrennt sind. In dieser Furche befindet sich das aktive Zentrum. Die Helix des aktiven Zentrums beinhaltet das HExxH-Motiv und ist Teil der N-terminalen Domäne. Der konservierte Loop mit dem GTxDxxYG-Motiv ist Teil der C-terminalen Domäne. Die N-terminale Domäne beinhaltet ein viersträngiges β -Faltblatt, welches durch zwei Disulfidbrücken stabilisiert wird. Die C-terminale Domäne besteht überwiegend aus α -Helices.

Die beiden Histidine, die das Zinkion komplexieren, sind genau durch eine Helixwindung voneinander getrennt. Der vierte Zinkligand ist ein Wassermolekül. Dieses Wassermolekül wird sowohl vom Zinkion als auch vom katalytischen Glutamat polarisiert und greift den Carbonyl-Kohlenstoff der zu spaltenden Peptidbindung nukleophil an. Es entsteht ein negativ geladener, tetraedrischer Übergangszustand. Die Energie des Übergangszustandes wird durch Interaktion des entstehenden Oxyanion mit dem Zinkion sowie durch Ausbildung einer Wasserstoffbrückenbindung zur phenolischen OH-Gruppe des Tyrosins des GTxDxxYG-Motivs herabgesetzt. Dieses katalytische Prinzip wird in Aspzinkinen⁴⁶, in Gluzinkinen⁴⁸, in Astacinen⁴⁹, in Serralysinen und in der Familie der Carboxypeptidase A⁵⁰ gefunden und entspricht der Oxyanionentasche von Serinproteasen⁵¹. Das Zinkion ist zu diesem Zeitpunkt durch die drei Zinkliganden, das katalytische Wassermolekül und die Carbonyl-Gruppe des Substrates pentakoordiniert.

Das Proton des katalytischen Wassermoleküls wird auf den neu entstehenden N-Terminus übertragen. Dies wird vom katalytischen Glutamat vermittelt, welches eine Salzbrücke zu der am N-Terminus auftretenden positiven Ladung ausbildet und diese stabilisiert. Sowohl die an das Zinkion gebundene Carboxylat-Gruppe des neu entstandenen C-Terminus, wie auch der an das Glutamat gebundene N-Terminus werden freigesetzt, sobald das katalytische Wassermolekül im aktiven Zentrum ersetzt wird.

Über die Protease-Einheit hinaus, besitzt AsaP1 noch eine vergleichbar große Propeptid-Domäne (ca. 170 Aminosäuren) und eine Signal-Sequenz. Das Signal-Peptid vermittelt die Translokation über die Cytoplasmamembran durch einen SEC-abhängigen, generellen Translokationsschritt. Bis auf die Peptidyl-Lys Metalloendopeptidase aus *Pleurotus ostreatus* (PoMEP) werden alle bisher bekannten Aspzinkin-Proteasen als Pro-Protein synthetisiert und weisen eine vergleichbar große Propeptid-Domäne (ca. 170 AS) auf.

Propeptidstrukturen bakterieller Enzyme

Bakterien sekretieren eine Vielzahl verschiedener Proteine ins extrazelluläre Milieu. Darunter sind Toxine und hydrolytische Enzyme wie Proteasen, Lipasen und Nukleaseen. Diese werden meist als Prä-

Pro-Proteine (oder Zymogene) synthetisiert und bestehen aus einer Signal-Sequenz ('Prä'-Part), die für die Translokation des Proteins über die Cytoplasmamembran benötigt wird, einem Propeptid und dem reifen Protein. Das Propeptid kann zwischen Signalsequenz und Enzym liegen, oder C-terminal lokalisiert sein. Die eigentliche enzymatische Funktion ist allerdings unabhängig von der Propeptid-Struktur, da es abgespalten wird und im aktiven Enzym nicht enthalten ist. Das Propeptid fungiert meist als Faltungshelfer, indem es Kontakte mit anderen Proteinen oder auch Kontakte innerhalb der Polypeptidkette verhindert, die zu Fehlfaltungen oder Proteinaggregation führen⁵². Werden Proteine ohne ihr Propeptid synthetisiert, sind sie meist nicht in der Lage in ihre native Form zu falten. Propeptide, die für die Faltung eines Proteins essentiell sind, werden als *intramolecular chaperones* (IMCs) bezeichnet. Sie sind meist kovalent verknüpft mit dem Protein, dessen Faltung sie unterstützen⁵³. Die kovalente Verknüpfung ist jedoch keine Voraussetzung für die Funktion als Faltungshelfer. Im Gegensatz zu *molecular chaperones* (MCs) besitzen IMCs ein sehr enges Substratspektrum und sind meist auf das Protein spezialisiert von dessen Polypeptid sie abgespalten werden. IMCs wirken als spezifische Katalysatoren, da sie die Aktivierungsenergie für die Faltung eines spezifischen Proteins herabsetzen⁵⁴, während MCs (z.B.: Hitzeschockproteine) bei der Renaturierung einer Vielzahl verschiedener Proteine beteiligt sind.

Erstmals wurde die IMC-Funktion des Propeptides bei Subtilisin E gezeigt. Reifes Subtilisin E ist nicht in der Lage nach Denaturierung zurück in die aktive Form zu falten. Erst durch Zugabe des Propeptids, erfolgt eine Renaturierung und Reaktivierung des Enzyms⁵⁵. Im Fall der α -lytischen Protease findet ohne Propeptid die Ausbildung von Sekundärstrukturen statt und das Protein befindet sich in einem Intermediärzustand, der dem '*molten globule*'-Zustand gleicht. Durch Zugabe des Propeptides faltet das Protein in seine endgültige, aktive, dreidimensionale Form⁵⁶.

Es gibt auch IMCs, die nicht kovalent mit ihrem Protein verknüpft sind; z.B.: einige Lipasen aus *Pseudomonas* spp. benötigen eine Lipase spezifische Foldase Lif, die als separates Polypeptid synthetisiert wird⁵⁷. Es sind viele IMCs bekannt die aktiv die Faltung eines Enzyms unterstützen, indem sie mit kinetisch blockierten Intermediaten während der Proteinfaltung interagieren.

Allerdings agieren nicht alle IMCs auf die gleiche Weise. Zum Beispiel ist das PapD Protein aus *E. coli* ein spezifisches IMC, welches in die Pili-Biogenese involviert ist. Es bindet an Pili-Untereinheiten, um eine vorzeitige Oligomerisierung der Untereinheiten im Periplasma zu verhindern⁵⁸. Ebenso verhindert das Propeptid des α -Toxins aus *Clostridium septicum* eine Aggregation durch spezifische Interaktion⁵⁹. Die Funktion der IMCs entspricht in diesen Beispielen der Funktion von MCs. Auch ist die Spezifität für nur ein Protein nicht immer gegeben, da das Propeptid der *Staphylococcus hyicus* Lipase, welches die proteolytische Degradation von Faltungsintermediaten verhindert⁶⁰, auch die

Degradation des *E. coli* OmpA-Protein abwendet, wenn dieses als Prä-Pro-OmpA in Gram-positiven Bakterien exprimiert wird⁶¹.

Neben der Rolle als Faltungshelfer konnten weitere Funktionen von bakteriellen Propeptiden beobachtet werden. So bildet zum Beispiel das Propeptid der *Neisseria gonorrhoeae* IgA Protease einen Translokationstunnel in der äußeren Membran, durch den die Protease ins extrazelluläre Milieu gelangt⁶². Einige Proteine, wie z.B.: LasA und LasD aus *Pseudomonas aeruginosa* werden als gefaltete Proteine zusammen mit dem Propeptid über die äußere Membran transportiert. Es liegt daher nahe, dass das Propeptid eine Sequenz enthält, die von dem Translokationskomplex erkannt wird.

Die Propeptid vermittelte Faltung des Proteins findet meist im Periplasma statt und resultiert in korrekt gefaltetes, aktives Enzym. Die Prozessierung zum aktiven Enzym kann sowohl intramolekular⁶³ als auch intermolekular erfolgen^{63; 64; 65} und geht nicht immer direkt mit einer Aktivierung einher. Das abgetrennte Propeptid bleibt häufig an das Enzym gebunden und wirkt als spezifischer, kompetitiver Inhibitor im Periplasma⁶⁶, um eine vorzeitige Aktivierung proteolytischer Enzyme zu verhindern und um sicher zu stellen, dass das Enzym erst an seinem Bestimmungsort, dem extrazellulären Milieu, die vollständige Aktivität erreicht. Die Dissoziation des Propeptides vom Enzym ist Voraussetzung für die Enzymaktivität und muss daher streng reguliert werden. So dissoziert das Propeptid der α-lytischen Protease aus *Clostridium septicum* nicht unmittelbar nach der proteolytischen Spaltung von der Protease, sondern erst wenn das pro-Toxin an seinen Rezeptor in der Membran gebunden ist, wo es zu einer multimeren Pore assembliert. Die Bildung des Oligomers ist wahrscheinlich der Auslöser der Dissoziation⁵⁹. Die Dissoziation könnte auch durch Interaktionen mit dem Translokationskomplex in der äußeren Membran begünstigt werden⁶⁷.

Für eine Vielzahl von Enzymen konnte gezeigt werden, dass N-terminale Propeptide sowohl als Faltungshelfer fungieren als auch eine inhibitorische Funktion ausüben^{68; 69; 70; 71; 72; 73}. Dabei ist wahrscheinlich die strukturelle Information des Propeptides von Bedeutung, da Chimären aus Propeptid und Enzym verschiedener Organismen auf die gleiche Weise funktionieren wie die nativen Enzyme, obwohl nur eine sehr geringe Sequenzidentität innerhalb der Propeptid-Domäne vorliegt^{74; 75}. Häufig korreliert auch die inhibitorische Funktion des Propeptides mit der Fähigkeit als IMC zu funktionieren⁷⁶.

Strukturell sind bereits mehrere bakterielle Propeptid-Domänen aus verschiedenen Protease-Familien beschrieben und auch einige Aktivierungsmechanismen sind bekannt^{77; 78; 79; 80; 81; 82; 83; 84; 85; 86}.

Die jeweiligen Mechanismen der IMCs, der Inhibition und der Aktivierung verschiedener Protease-Familien unterscheiden sich deutlich auf molekularer Ebene und sie sind meist sehr spezifisch für das jeweilige Enzym. Häufig wirkt das Propeptid als Faltungshelfer bis die Struktur des aktiven Zentrums

voll ausgebildet ist und strukturell dem der aktiven, reifen Protease entspricht. Es folgt typischerweise eine limitierte Proteolyse der Polypeptidkette des Zymogens, die zu einer Konformationsänderung des Enzyms führt. Das Propeptid übernimmt dann die Funktion eines Inhibitors indem es das aktive Zentrum des Enzyms blockiert. Durch Dissoziation des Propeptids vom Enzym wird dieses schließlich aktiviert⁸⁷.

Proteolytische Enzyme sind neben ihrer Funktion als bakterielle Toxine auch bei einer Vielzahl anderer Krankheitsbilder beteiligt, übernehmen aber auch für den Organismus essentielle Aufgaben. Das Verständnis der propeptidvermittelten Aktivierung eines bestimmten Enzyms bietet eine vielversprechende Möglichkeit zur Entwicklung von hoch spezifischen Protease-Inhibitoren in der pharmazeutischen Industrie^{88; 89}.

Ergebnisteil zur Metalloendopeptidase AsaP1

Toxoidkonstruktion von AsaP1 und Untersuchungen zu deren Aktivität und Prozessierung

Von Johanna Schwenteit vom Institut für Experimentelle Pathologie der Universität Reykjavík wurden vier Toxide von AsaP1 hergestellt⁹⁰. Diese unterscheiden sich von der aktiven Protease durch jeweils eine Punktmutation, wobei für die katalytische Aktivität essentielle Aminosäuren ausgetauscht wurden. Das katalytisch essentielle Glutamat (Glu²⁹⁴) des HExxH-Motivs wurde durch ein Alanin (AsaP1_{E294A}) und ein Glutamin (AsaP1_{E294Q}) ersetzt. Das Tyrosin (Tyr³⁰⁹) aus dem GTxDxxYG-Motiv wurde durch Alanin (AsaP1_{Y309A}) und Phenylalanin (AsaP1_{Y309F}) ausgetauscht.

Alle vier Mutanten von AsaP1 sowie die Wildtyp-Protease (AsaP1_{rek}) wurden von Johanna Schwenteit in pJOE3075 kloniert und in *E. coli* Pri3715 exprimiert. Es wurden signifikante Unterschiede im Wachstum der *E. coli* Zellen festgestellt (siehe Manuskript 1, Abbildung 1) (Johanna Schwenteit), die auf die Expression der jeweiligen AsaP1 Variante zurückzuführen sind⁹⁰. Auch die caseinolytische Aktivität (Johanna Schwenteit) variiert bei den verschiedenen AsaP1 Varianten. Die des rekombinant exprimierten Wildtyp-Enzyms (AsaP1_{rek}) ist geringer, als die des Enzyms aus *Aromonas salmonicida* subsp. *achromogenes* (AsaP1_{WT}). Von den vier Mutanten zeigt lediglich AsaP1_{Y309F} eine caseinolytische Aktivität, die jedoch zum rekombinant exprimierten AsaP1_{rek} vermindert ist. Die Mutanten AsaP1_{E294Q}, AsaP1_{E294A} sowie AsaP1_{Y309A} zeigen keine caseinolytische Aktivität⁹⁰. Das unterschiedliche Wachstum der verschiedenen *E. coli* Stämme korreliert mit der caseinolytischen Aktivität der exprimierten AsaP1-Varianten, wobei die *E. coli* Stämme, die Varianten mit der höchsten caseinolytischen Aktivität exprimieren, die geringste Wachstumsrate aufzeigen.

Das Protein in reiner Form wurde von Johanna Schwenteit für die Analyse der Letalität und Pathogenität verwendet. Alle Fische, denen natives AsaP1_{WT} oder rekombinantes AsaP1_{rek} injiziert wurde, starben innerhalb von 12 Stunden, wohingegen keine der vier AsaP1 Mutanten eine letale Wirkung zeigte, ungeachtet der hohen Dosis, die injiziert wurde. Die pathologischen Befunde zeigen vergleichbare Ergebnisse bei AsaP1_{WT} und AsaP1_{rek}. Die Veränderungen sind abhängig von der Konzentration an eingesetztem Protein und sind mit den bereits beschriebenen Anzeichen atypischer Furunkulose vergleichbar³².

Keine der heterolog exprimierten AsaP1-Varianten (AsaP1_{rek} und die vier Mutanten) wird ins extrazelluläre Milieu sekretiert (siehe Manuskript 1, Abbildung 3). Alle Proteine wurden im Cytoplasma oder im Periplasma der *E. coli* Zellen nachgewiesen. Dies könnte durch unterschiedliche Sekretionswege

in *E. coli* im Vergleich zu *A. salmonicida* erklärt werden; insbesondere der Translokationsschritt über die äußere Membran könnte in den Organismen unterschiedlich realisiert werden. Weiterhin konnte ein Größenunterschied zwischen der aktiven Protease AsaP1_{WT} (19 kDa) exprimiert in *Aeromonas salmonicida* subsp. *achromogenes* und AsaP1_{rek} (22 kDa) festgestellt werden, das in *E. coli* exprimiert wurde.

AsaP1_{E294A} und AsaP1_{E294Q} zeigen eine Größe von 37 kDa; dies entspricht dem unprozessierten Enzym, das neben der Protease noch die Propeptid-Domäne enthält. Die Prozessierung zum nativen Enzym findet nur bei caseinolytisch aktiven AsaP1-Varianten statt. Die inaktive Mutanten AsaP1_{E294A} und AsaP1_{E294Q} werden durch Zugabe von AsaP1_{rek} prozessiert (siehe Manuskript 1, Abbildung 4). Dies deutet auf eine autoproteolytische Prozessierung der Protease AsaP1. Ebenso wird ersichtlich, dass die Protease sich aufgrund der hohen Aktivität autoproteolytisch zersetzt.

Rekombinant erzeugtes AsaP1_{rek} ist ohne Aktivierungsmechanismus aktiv, im Gegensatz zu Pro-Deuterolysin, welches durch Zugabe von ZnCl₂ oder Trypsin aktiviert werden muss^{37; 91}. Darüber hinaus ist nur wenig bekannt über den Aktivierungsschritt von Aspzinkin-Proteasen, wohingegen die Aktivierungsmechanismen für Gluzinkins (Proteasen der Thermolysin-Familie) und für Metzinkins (Proteasen der Astacin-Familie) bereits aufgeklärt werden konnten^{78; 92}.

Alle vier Mutanten sowie AsaP1_{rek} rufen eine Immunantwort in Arktischem Saibling (*Salvelinus alpinus*) hervor und Antikörper gegen das extrazelluläre Produkt von *A. salmonicida* subsp. *achromogenes* konnten nachgewiesen werden (siehe Manuskript 1, Abbildung 2, 5, 6). Der Einsatz von Toxoid-Impfstoffen ist für Tetanus und Diphtherie bereits realisiert^{93; 94}. Es konnte gezeigt werden, dass bei Cholera genetisch erzeugte Toxoid-Impfstoffe effizienter sind als inaktivierte Toxine^{95; 96}. Die durch Mutagenese erzeugten Toxoide von AsaP1 bilden somit geeignete Ausgangsmoleküle für eine Impfstoffentwicklung und ein interessantes Target für eine strukturelle Untersuchung.

Kristallisation und röntgendiffraktometrische Untersuchungen von AsaP1_{E294A} und AsaP1_{E294Q}

Zur strukturellen Charakterisierung der Toxoide AsaP1_{E294A} und AsaP1_{E294Q} wurden diese in *E. coli* Pri3705 exprimiert und anschließend über Nickel-Affinitätschromatographie und Größenausschlusschromatographie gereinigt.

Sowohl AsaP1_{E294A} als auch AsaP1_{E294Q} kristallisierte in der monoklinen Raumgruppe C2 mit ähnlichen Gitterkonstanten (siehe Manuskript 2, Tabelle 1 und Abbildung 1). Kristalle von AsaP1_{E294A} und AsaP1_{E294Q} wurden unter Cryo-Bedingungen vermessen und beugen Röntgenstrahlen bis zu einer Auflösung von

2,0 Å an einem Drehanoden-Röntgengenerator. Auch durch Messen mit intensiverer Strahlung am Synchrotron konnte die Auflösung der Kristalle nicht verbessert werden⁹⁷.

Die Struktur konnte durch Molekularen Ersatz (*molecular replacement*) gelöst werden. Als Suchmodell diente GfMEP (PDB Eintrag 1g12). Das Polypeptid des Suchmodells beinhaltet allerdings nur die aktive Protease (Aminosäuren 182-348) ohne Propeptid. Die GfMEP Protease weist eine Sequenzidentität von 43% zur Protease-Einheit von AsaP1 (Aminosäuren 172-343) auf. Mit den anfänglichen Phasen lässt sich eine Elektronendichte für die Protease berechnen, die eindeutig den Verlauf des Polypeptides erkenn lässt. Elektronendichte für das Propeptid ist deutlich schwächer, aber interpretierbar.

In der endgültigen Elektronendichtheckarte fehlt die Verbindung von Propeptid zur Protease sowohl bei AsaP1_{E294A} als auch bei AsaP1_{E294Q}. Daraufhin wurde versucht Proteinkristalle höherer Streukraft zu erzeugen. Ebenso wurde versucht das Protein in einem anderen Kristallsystem zu kristallisieren, welches vermutlich eine andere Interaktion der Proteinmoleküle aufzeigt und somit eventuell die Verknüpfung erkennen lässt.

Für AsaP1_{E294A} konnte eine weitere Kristallisationsbedingung gefunden werden. Ist die Proteinkonzentration im Bereich von 10-12 mg ml⁻¹ bildet sich ein orthorhombisches Gittersystem (*P*2₁2₁2), wohingegen ein monoclines Gitter (*C*2) ausgebildet wird bei höherer Proteinkonzentration (16-25 mg ml⁻¹). Die Gitter zeigen unterschiedliche Zellkonstanten und unterscheiden sich beide von den oben genannten⁹⁸.

Die Kristalle bei höherer Proteinkonzentration zeigen deutliche Risse und Spalten und es ist zudem vermehrte Präzipitatbildung im Kristallisationsansatz zu erkennen. Die Methode, die zur Optimierung dieser Kristalle geführt hat, ist nachfolgend beschrieben.

Einfluss der Temperatur während des Kristallisationsansatzes auf Präzipitatbildung und Kristallform

Die Proteinkristallisation wird von vielen unterschiedlichen Faktoren beeinflusst. Hier wird der Einfluss der Temperatur während des Kristallisationsansatzes beschrieben, der bei der Kristallisation von AsaP1_{E294A} zu beobachten war.

Die oben genannten monoclinen Kristalle von AsaP1_{E294A} weisen große Risse und Wachstumsfehler auf. Zudem ist deutliche Präzipitatbildung zu erkennen.

Das Präzipitat bildet sich bereits beim Vermischen von Protein- und Reservoirlösung während des Kristallisationsansatzes. Durch Kühlen der Reservoirlösung (4 °C) konnte die Präzipitatbildung vermindert werden und die Kristalle zeigten definierte Kanten und Flächen sowie weniger Risse. Wurde der gesamte

Kristallisationsansatz auf Eis durchgeführt (Kristallisationsplatte auf Eis, gekühlte Reservoirlösungen (4 °C) und gekühlte Pipettenspitzen (-20 °C)) konnte der gewünschte Effekt noch verstärkt werden (siehe Manuskript 3, Abbildung 1).

Zudem konnte auch eine etwas erhöhte Auflösung für Kristalle gemessen werden, die unter gekühlten Bedingungen kristallisiert wurden. Alle Kristallisationsplatten wurden bei 20 °C inkubiert. Es wurde lediglich beim Ansetzen der Kristallisationsplatten gekühlt⁹⁸.

Eine Reduktion der Protein- oder der Präzipitant-Konzentration zeigte einen leichten Rückgang der Präzipitatbildung, hatte allerdings keinen Einfluss auf die Form der Kristalle. Es waren lediglich weniger Kristalle pro Tropfen zu beobachten.

Wurde das Experiment mit gekühlten Reservoirlösungen, gekühlten Spitzen und der Kristallisationsplatte auf Eis durchgeführt, die Kristallisationsplatte allerdings bei 4 °C statt bei 20 °C inkubiert, konnte keine Kristallisation beobachtet werden, sondern nur Phasenseparation. Es ist nicht klar, ob sich bei niedrigen Temperaturen keine Kristallisationskeime ausbilden oder ob das Kristallwachstum nicht stattfindet. Wahrscheinlich bilden sich Kristallisationskeime während die Proteinlösung langsam von 4 °C auf 20 °C erwärmt wird.

Die Wahrscheinlichkeit, dass sich ein Kristallisationskeim ausbildet und somit ein Kristall wachsen kann ist höher, umso weiter das Kristallisationssystem in den Übersättigungsbereich gebracht wird. Allerdings steigt damit ebenso die Wahrscheinlichkeit einer übermäßigen Keimbildung und Präzipitatbildung⁹⁹. Zudem ist im Übersättigungsbereich die Geschwindigkeit, mit der die Kristalle wachsen, erhöht und es kommt zu Defekten und Gitterstörungen. Die Temperatur kann ein Parameter sein, der das Kristallisationssystem in den Bereich der Übersättigung bringt. Die fehlerhaften Kristalle und die ungeordnete Aggregation der Proteinmoleküle (Präzipitat) sind ein Zeichen für das Erreichen der übersättigten Phase, das neben der hohen Proteinkonzentration und der Zusammensetzung des Präzipitanten möglicherweise auch auf die Temperatur zurückzuführen ist.

Es könnte sein, dass das Protein bei niedrigeren Temperaturen eine höhere Löslichkeit aufweist und der hier beschriebene Effekt darauf zurückzuführen ist, dass eine geringere Übersättigung bei niedrigerer Temperatur eintritt. Die Abhängigkeit der Proteinlöslichkeit von der Temperatur ist eine spezifische Eigenschaft jedes Proteins und der entsprechenden Pufferbedingung; sie wurde für AsaP1 nicht quantitativ ermittelt.

Blow *et al.*¹⁰⁰ zeigten, dass durch eine Änderung der Temperatur von 10 °C auf 20 °C eine Trennung von Keimbildung und Kristallwachstum bei Lysozym erzeugt werden konnte und dass mit längerer Inkubationszeit bei 10 °C mehr stabile Kristallisationskeime entstehen. In den hier beschriebenen Experimenten blieb die Anzahl der gebildeten Kristalle (entspricht stabiler Kristallisationskeime)

konstant, aber die Kristallqualität verbesserte sich. In *seeding*-Experimenten konnte gezeigt werden¹⁰¹, dass die Kristallqualität mit der Qualität der eingesetzten Kristallisationskeime korreliert. Vielleicht bilden sich auch in den hier beschriebenen Experimenten besser geordnete Kristallisationskeime.

Kristallstrukturanalyse der AsaP1 Metalloendopeptidase im Komplex mit dem Propeptid

Die Röntgenkristallstrukturen von AsaP1_{E294A} und AsaP1_{E294Q} konnten mit einer Auflösung von 2.0 Å bestimmt werden (siehe Manuskript 4, Tabelle 1). Neben der Elektronendichte für die Protease ist auch Elektronendichte für das Propeptid deutlich zu erkennen. Es ist somit gelungen, erstmalig die Propeptid-Struktur von Aspzinkin-Proteasen zu zeigen. Bisher ist für Aspzinkine oder M35-Proteasen lediglich die aktive Protease strukturell beschrieben.

Mit Ausnahme der Protease PoMEP, werden alle bisher bekannten Aspzinkine als Zymogene exprimiert, und zur Aktivierung der Protease ist die Abspaltung des Propeptids nötig. Der aktive Teil der Protease weist eine hohe Sequenzidentität auf innerhalb der M35 Proteasen, wohingegen keine signifikante Homologie innerhalb der Propeptid-Sequenz erkennbar ist (siehe Manuskript 1, Abbildung 6).

Die Strukturlösung von AsaP1_{E294A} und AsaP1_{E294Q} zeigt ein Molekül in der asymmetrischen Einheit in den monoclinalen Kristallsystemen. Im orthorhombischen Kristallsystem von AsaP1_{E294A} sind zwei Monomere in der asymmetrischen Einheit (siehe Manuskript 1, Abbildung 7). Bereiche mit fehlender oder nur schwacher Elektronendichte wurden nicht in das Strukturmodell aufgenommen, was zu Lücken im Polypeptid führt. Schwache Elektronendichte am N-Terminus und in einigen Loop- bzw. Turn-Strukturen deutet auf flexible Bereiche des Proteins hin. Tatsächlich zeigt der Bereich von Asp210-Gly214, der neben GfMEP und Deuterolysin nur in der orthorhombischen Struktur von AsaP1_{E294A} zu erkennen ist, die höchste r.m.s.d. zwischen den drei unterschiedlichen Strukturen. Es zeigt sich hier, dass durch ein anderes Kristallsystem Bereiche strukturiert werden, die vorher flexibel waren.

Die ersten 22 Aminosäuren sind Teil einer Signal-Sequenz, die mit großer Wahrscheinlichkeit entfernt wird, sobald das Protein über die Cytoplasmamembran ins Periplasma transloziert wird. Der N-Terminus ist höchstwahrscheinlich nicht mehr im Molekül enthalten, da die AsaP1-Mutanten im Periplasma der *E. coli* Zelle nachgewiesen werden konnten⁹⁰.

Das Fehlen der Elektronendichte für die Aminosäurereste 160 - 171 in allen drei Strukturen verhindert die klare Zuordnung von Protease und Propeptid. Auch ist eine eindeutige Zuordnung der biologischen Funktionseinheit aufgrund von Abstandskriterien innerhalb der verschiedenen Kristallgitter nicht möglich. Die verschiedenen Kristallsysteme werden von einem Homodimer gebildet, welches im monoclinalen Kristallsystem durch kristallographische Symmetrie erzeugt wird, wohingegen im

orthorhombischen Gittersystem das Dimer die asymmetrische Einheit bildet. Es gibt zwei Möglichkeiten, die Zuordnung der Protease zum Propeptid vorzunehmen und demnach zwei mögliche Kontaktflächen – eine intra- und eine intermolekulare Wechselwirkung. Beide Interaktionsflächen wurden einer PISA-Analyse¹⁰² unterzogen und wurden für stabil in Lösung befunden (siehe Manuskript 1, Tabelle 3). Einer wurde die Möglichkeit zur Komplexbildung zugeordnet, wohingegen die andere lediglich als Ergebnis des Kristallisationseffekts zu deuten wäre. Dies stimmt mit Ergebnissen der Größenausschlusschromatographie überein, die eindeutig ein Monomer in Lösung zeigt. Demnach erfolgt die Zuordnung des Propeptides so, dass es im aktiven Zentrum der Protease-Einheit des gleichen Polypeptids bindet. Das Homodimer bildet sich lediglich im Kristall oder bei unphysiologisch hohen Proteinkonzentrationen.

Ob die Lücken im Polypeptid im Bereich 132 - 141 und 160 - 171, die die Verknüpfung von Protease und Propeptid bilden, als flexible Strukturen tatsächlich im Molekül enthalten sind oder ob diese durch einen eventuellen Prozessierungsschritt entfernt wurden, konnte bisher nicht geklärt werden.

Die beiden AsaP1-Mutanten sind strukturell identisch mit r.m.s.d.-Werten von 0,4 Å für die Protease-Untereinheit und 0,9 Å für das Propeptid. Das Propeptid besteht aus den Aminosäuren Gly23 - Gln160 und bildet eine separate Domäne; N-terminal zur Protease. Es besteht aus β-Faltblättern und verschiedenen Loop-Strukturen. Ein einzelner β-Strang (β6) bindet an das aktive Zentrum der Protease. Zwei β-Faltblätter bilden eine Art Sandwich-Struktur, wobei die Faltblätter so gegeneinander verschoben sind, dass die Aminosäureseitenketten kaum miteinander interagieren können. Das zweisträngige Faltblatt liegt senkrecht am Ende der 'Sandwich'-Struktur.

Die Protease zeigt die typische Faltung der M35 Protease-Familie oder Aspzinkine, die aus zwei Domänen besteht^{46; 47} (siehe Manuskript 1, Abbildung 1). Das Faltblatt der N-terminalen Protease-Domäne wird durch β6 des Propeptides verlängert.

In allen drei Strukturen wird das Zinkion des aktiven Zentrums über die Imidazolringe von His293 und His297 des HExxH-Motivs sowie über die Carboxylatfunktion des Asp306 des GTxDxxYG-Motivs koordiniert (siehe Manuskript 1, Abbildung 2 und Abbildung 3). Aufgrund der Bindungsabstände des Asp306 wird eine einzähnige Koordination angenommen¹⁰³ (siehe Manuskript 1, Tabelle 2). Der Wasserligand am Zinkion, der die vierte Koordinationsstelle besetzt und als Nukleophil die zu spaltende Peptidbindung angreift, ist in den beiden Monomeren der orthorhombischen Struktur vorhanden (AsaP1_{E294A}). Dies entspricht der typischen Koordination von Aspzinkin-Metalloendopeptidasen. In der monoclinalen Struktur von AsaP1_{E294A} ist an der Stelle des Wasserliganden ein Chlorid koordiniert, wie bereits beschrieben¹⁰⁴. In der Struktur von AsaP1_{E294Q} ist die Position des Zinkions zu 40% besetzt. Dies korreliert mit den zwei alternativen Konformationen, die für Asp306 gefunden wurden. Die Asp306

Konformation mit 40%iger Besetzung zeigt zum Zinkion, während die Konformation mit 60%iger Besetzung in die entgegengesetzte Richtung zeigt und über eine Wasserstoffbrücke zum Tyr309 stabilisiert wird. Elektronendichte für einen vierten Zink-Liganden ist nicht zu erkennen. Der Abstand des Carbonylsauerstoffs von Ile84 zum Zinkion beträgt 2,93 Å.

Das aktive Zentrum liegt in einer Furche, die sich zwischen der N- und C-terminalen Protease-Domäne befindet, und wird von einem Helix-Loop-Helix-Motiv gebildet. Die erste Helix beinhaltet das konservierte HExxH-Motiv und die Loop-Struktur das GTxDxxYG-Motiv. Oberhalb der Helix des aktiven Zentrums liegt β-Strang 13, der mit β6 des Propeptides interagiert. Das aktive Zentrum ist somit durch das Propeptid blockiert (siehe Manuskript 1, Abbildung 4).

Die Interaktion der Protease mit dem Propeptid erlaubt Rückschlüsse auf die Substratbindung und die Protease-Spezifität. Die Substraterkennung beruht zum einen auf einer Sekundärstrukturerkennung von β6 mit β13, wobei die Möglichkeit besteht, dass sich die Sekundärstruktur des β6 erst durch die Interaktion mit β13 ausbildet. Zum anderen ist die Substrat-Erkennung durch die Beschaffenheit der Substratbindungstaschen gegeben (siehe Manuskript 1, Abbildung 5). In P1' Position befindet sich Lys85 in P2 Position Leu83, beide Aminosäuren sind Teil des β6. Das Ile84 in P1 Position zeigt aufgrund der β-Strang-Struktur in die entgegengesetzte Richtung. Für Lys85 ist eine spezifische Interaktion zu erkennen mit Phe259, Asp285, Asp330 und Glu333. Das Phe259 interagiert mit den hydrophoben Methylengruppen des Lys85 während die negativ geladenen Carboxylatgruppen von Asp285, Asp330, Glu333 sich am Boden der S1' Bindetasche befinden und mit der positiv geladenen Aminogruppe des Lys85 interagieren. Die Bindungsabstände entsprechen gut definierten Wasserstoffbrückenbindungen und die Bindungswinkel und Interaktionspartner bestätigen eine positiv geladene Ammoniumgruppe der Lysinseitenkette. Das Asp330 ist in allen Aspzinkinen konserviert, wohingegen Asp285 und Glu333 nur in lysinspezifischen Aspzinkinen auftreten. In nicht lysinspezifischen Aspzinkin-Proteasen sind diese Aminosäuren durch ein Alanin und ein Glutamin ersetzt. Das Phe259 ist nicht konserviert und wird auch in lysinspezifischen Aspzinkinen häufig durch Tyrosin ersetzt. In anderen Aspzinkinen findet man an dieser Position häufig hydrophobe Aminosäuren wie Leucin oder Prolin. Die S1' Bindungstasche bei lysinspezifischen M35 Proteasen zeigt eine vorwiegend hydrophobe Umgebung mit drei negativ geladenen Aminosäureresten am Boden der Bindungstasche.

Die S2 Bindungstasche zeigt die Aminosäuren His297, Pro264, Pro66 und Val262 im Radius von 4 Å um Leu83, die eine hydrophobe Umgebung bilden. Ein Teil der S2-Bindungstasche wird vom Proteinrückgrat der Aminosäuren des GTxDxxYG-Motivs gebildet. Im Gegensatz zur S1'-Bindetasche ist die S2-Bindetasche eher unspezifisch für hydrophobe Aminosäuren ausgelegt. Allerdings wäre es auch denkbar,

dass eine kleinere hydrophobe Aminosäure, wie Alanin, in der S1'-Bindetasche bindet. Weder Lys85 noch Ile83 sind bei Aspzinkin-Proteasen konserviert.

Eine DALI-Analyse fand zwei Proteasen, die das gleiche Faltungsmotiv wie AsaP1_{E294A/Q} aufweisen und auch zur Familie der Aspzinkin-Proteasen gehören (siehe Manuskript 1, Tabelle 4). Das Protein mit dem höchsten Z-Score (28.10) ist GfMEP und das zweite ist Deuterolysin aus *Aspergillus oryzae* (Z-score 21.0). Beide Enzyme sind strukturell sehr ähnlich, was durch die r.m.s.d. der Ca-Atome verdeutlicht wird. Diese beträgt 2.0 Å für monoclines AsaP1_{E294A} zu Deuterolysin und 1.0 Å zu GfMEP. Darüber hinaus wird das Aspzinkin-Faltungsmotiv der Protease auch in anderen Proteinen gefunden, allerdings mit einem Z-score von 6,1 und weniger; hier bildet es nur einen Teil innerhalb eines größeren Proteins.

Für die Propeptid-Domäne wurden sieben Proteine mit einem ähnlichen Faltungsmotiv gefunden. Von den Proteinen, die nur aus der gesuchten Domäne bestehen, zeigt der intrazelluläre Protease-Inhibitor aus *Bacillus subtilis* den höchsten Z-score (9.3). Ein Z-score von sieben und weniger wurde für das FIXG-Related Protein aus *Vibrio parahaemolyticus* rimd 221063, das vermutliche ApaA Protein aus *Bordetella pertussis*, das ApaG Protein aus *Xanthomonas axonopodis* pv. *citri*, das ApaG Protein aus *Vibrio cholerae* und das ApaG Protein aus *Shewanella oneidensis* mr-1 ermittelt. Mit einem Z-score von 7,3 und weniger wurde die gesuchte Domäne auch als Teil von größeren Proteinen gefunden.

Die Struktur der ApaG Proteine zeigt eine Fibronectin-3-Faltung (Fn3), jedoch keine signifikante Sequenzidentität mit bisherigen Fn3-Domänen. Die Funktion der ApaG Proteine ist noch nicht geklärt, es wird allerdings vermutet, dass diese Protein-Protein Interaktionen vermitteln¹⁰⁵. Für den intrazellulären Protease-Inhibitor gibt es einen Datenbank-Eintrag, allerdings zurzeit keine Literatur. Auch hier ist die Funktion nicht eindeutig bestätigt.

Die Struktur des AsaP1 Propeptides ähnelt der des Protease-Inhibitors und der ApaG Proteine (siehe Manuskript 1, Abbildung 8). Die beiden β-Faltblätter des β-Sandwichs im AsaP1-Propeptid sind gegeneinander verschoben, so dass die Aminosäureseitenketten nur geringfügig miteinander interagieren können. Somit bildet sich keine wirkliche Sandwich Struktur aus. Innerhalb des viersträngigen β-Faltblattes ist β5 im AsaP1-Propeptid deutlich verkürzt mit nur 2 Aminosäuren. Der entsprechende β-Strang enthält vier Aminosäuren im Protease-Inhibitor und ist damit ebenfalls deutlich kürzer als in den ApaG-Proteinen. Eine weitere Gemeinsamkeit des AsaP1-Propeptides und des Protease-Inhibitors ist ein langer Loop, der sich von der Kern-Domäne entfernt. Dieser Loop beinhaltet im AsaP1-Propeptid β-Strang 6, der mit dem aktiven Zentrum der Protease interagiert. Im Protease-Inhibitor ist keine β-Strang Struktur zu erkennen. Diese Loop-Struktur ist in den ApaG Proteinen nicht vorhanden.

Es ist denkbar, dass das Propeptid von AsaP1 die gleiche Struktur aufzeigt wie der Protease-Inhibitor, wenn es alleine in Lösung vorliegt und β6 erst durch die Interaktion mit der Protease die entsprechende

Konformation annimmt (*induced fit*). Der Protease-Inhibitor wurde in *B. subtilis* entdeckt, einem Gram-positiven Bakterium, und als intrazelluläres Protein angegeben. AsaP1 aus *A. salmonicida* subsp. *achromogenes* (Gram-negativ) ist eine giftige, extrazelluläre Protease. Die Genome von *B. subtilis*, *V. parahaemolyticus*, *B. pertussis*, *V. cholerae* und *S. oneidensis* sind vollständig sequenziert, allerdings konnte keine zu AsaP1 homologe Protease gefunden werden. Nur in *X. axonopodis* konnte eine homologe M35 Protease gefunden werden. Inwiefern die Ähnlichkeiten in der Struktur auf eine gemeinsame Funktion deuten, kann zurzeit nicht beantwortet werden.

Mittels ortsgerichteter Mutagenese von AsaP1_{E294Q}, AsaP1_{E294A} und AsaP1_{rek} wurde Lys85, welches in der S1'-Bindungstasche bindet, zu Alanin mutiert. Sowohl die inaktiven Mutanten AsaP1_{E294Q/K85A} und AsaP1_{E294A/K85A} als auch die aktive Protease AsaP1_{rek/K85A} wurden von *E. coli* in Einschlusskörpern (*inclusion bodies*) exprimiert. Dies könnte darauf hin deuten, dass Lys85 eine Rolle bei der Faltung des Enzyms übernimmt, bevor dieses autoproteolytisch prozessiert wird. Es konnte gezeigt werden, dass die Interaktion des Lys85 mit dem aktiven Zentrum der inaktiven Mutanten AsaP1_{E294Q} und AsaP1_{E294A} hoch spezifisch ist und entsprechende Aminosäuren bei Lys-spezifischen Aspzinkinen konserviert sind⁴⁴. Demnach kann man davon ausgehen, dass die Peptidbindung zwischen Lys85 und Ile84 in der aktiven AsaP1 Protease gespalten würde. Die aktive Protease beginnt allerdings bei Aminosäure 172 (AsaP1) und in der Polypeptidsequenz ist in diesem Bereich kein Lysin enthalten – auch nicht bei den lysinspezifischen Proteasen GfMEP und PoMEP. Über den Prozessierungs-Mechanismus von Aspzinkin-Proteasen ist bisher nichts Genaues bekannt. Der hier gezeigte Komplex der AsaP1-Mutanten AsaP1_{E294A} und AsaP1_{E294Q} mit ihrem Propeptid ist wahrscheinlich ein Zwischenzustand des autoproteolytisch Prozessierungs-Mechanismus der Protease, der aufgrund der Inaktivität der Mutanten erfasst werden konnte. Ob es sich hierbei um einen Inhibitionskomplex handelt ist noch unklar.

Einleitung zur Haloalkan Dehalogenase DppA

Halogenierte Kohlenwasserstoffe

Halogenierte Kohlenwasserstoffe sind - wie reine Kohlenwasserstoffe - lipophile Substanzen, deren Reaktivität mit zunehmendem Halogenierungsgrad abnimmt. Die Einsatzmöglichkeiten halogenierter Kohlenwasserstoffe sind außerordentlich vielfältig und reichen beispielsweise von der Verwendung als Herbizide, Fungizide oder Insektizide in der Landwirtschaft über Kühl- und Flammenschutzmittel, Weichmacher und Treibmittel hin zum Einsatz in der chemischen Reinigung und Entfettung von technischen Anlagen. Außerdem spielen sie eine wichtige Rolle in der chemischen Industrie als Lösungsmittel sowie als Zwischen- und Ausgangsprodukte verschiedenster Synthesen.

Viele halogenierte Kohlenwasserstoffe sind giftig, nachweislich krebserregend oder stehen im Verdacht krebserregend zu sein¹⁰⁶. Zudem konnten teratogene Eigenschaften nachgewiesen werden wie auch die Wirkung selbst geringer Mengen als Xenohormone - vor allem als Xenoöstrogene. Manche Substanzen sind für Zellen an sich nicht giftig, können aber bei Entgiftungsreaktionen in der Leber zu hochgiftigen Stoffen umgebaut werden, die Leber¹⁰⁷ sowie Niere zerstören¹⁰⁶.

Eine weit größere Anzahl dieser Substanzen wurde noch nicht auf schädliche Auswirkungen und Langzeitfolgen getestet. Derweil ist der Einsatz in den Industrienationen häufig verboten oder stark eingeschränkt.

Der verbreitete Einsatz anthropogener, halogenierter Kohlenwasserstoffe macht diese vielfältige Substanzklasse heutzutage zu einer der größten Gruppe von Umweltschadstoffen. Seit 1940 werden enorme Mengen produziert und aufgrund ihrer Stabilität und Persistenz sind viele der heute verbotenen Substanzen noch weltweit präsent und akkumulieren in Wasser, Boden, Luft sowie in Gebäuden, Möbeln, Kleidungsstücken und Organismen. Über die Nahrungskette reichern sich halogenierte Kohlenwasserstoffe im Fettgewebe an¹⁰⁸.

Abfälle mit hohem Gehalt an halogenierten Kohlenwasserstoffen, insbesondere mehrfach chlorierte Substanzen, stellen in der Bundesrepublik Deutschland ein vorrangiges Entsorgungsproblem dar, seit im Frühjahr 1991 die thermische Behandlung von Abfällen auf hoher See ohne spezielle Rauchgasreinigungsverfahren verboten wurde, die insbesondere zur Entsorgung von Rückständen halogenierter Kohlenwasserstoffe üblich war¹⁰⁹. Die Entsorgung solcher Abfälle ist derzeit sehr aufwendig und kostspielig.

Der biologische Abbau von halogenierten Kohlenwasserstoffen erfolgt meist mikrobiell. Weiterhin wird auch auf einige Pilze und Pflanzen¹¹⁰ hingewiesen, die es vermögen halogenierte Substanzen umzusetzen und damit unschädlich zu machen. Eine große Anzahl verschiedener Mikroorganismen ist bekannt, die signifikant zum biologischen Abbau von halogenierten Kohlenwasserstoffen beitragen und die in der Literatur bereits umfassend beschrieben sind^{111; 112; 113; 114; 115; 116; 117; 118}. Weit verbreitet ist die Fähigkeit mono-substituierte Substanzen umzusetzen wie z.B. Chlorbenzol, Methylchlorid, Methylenchlorid oder Vinylchlorid. Schwieriger wird es Organismen zu finden, die in der Lage sind Dichlorethen, Dibromethan oder Hexachlorocyclohexan umzusetzen. *Sphingobium japonicum* (früher *Sphingomonas paucimobilis*) UT26 ist beispielsweise eines der wenigen Mikroorganismen, das in der Lage ist γ -Hexachlorocyclohexan zu metabolisieren; benötigt hierfür allerdings auch acht verschiedene Enzyme, unter denen sich drei verschiedene Dehalogenasen (LinA, LinB, LinD) befinden¹¹⁶. Bisher noch nicht bekannt und nahezu unmöglich scheint der mikrobielle Abbau von Chloroform, 1,1,1-Trichlorethan, 1,2,3-Trichlorpropan oder Trichlorethylen.

Die Fähigkeit halogenierte Kohlenwasserstoffe abzubauen ist häufig Plasmid vermittelt^{119; 120; 121} und katabole Gene für Xenobiotika sind oft auf Transposon- und Insertions-Elementen zu finden^{118; 122; 123; 124; 125}.

Die Dehalogenierungsreaktion in Mikroben wird häufig von einem spezifischem Enzym katalysiert, der Dehalogenase, oder durch spontane Dehalogenierung instabiler Intermediate realisiert¹¹⁴. Zudem gibt es Enzyme, die neben ihrem herkömmlichen Substrat auch halogenierte Substratanaloga oder chemisch verwandte Substrate umsetzen, was zu einer zufälligen Dehalogenierung führen kann.

Haloalkan Dehalogenasen, Klassifikation und Einsatzmöglichkeiten

Haloalkan Dehalogenasen (E.C. 3.8.1.5.) sind weit verbreitet in Mikroorganismen und spalten die Kohlenstoff-Halogen-Bindung halogenierter aliphatischer Kohlenwasserstoffe. Als einziges Co-Substrat wird Wasser benötigt. Es gibt keine Anzeichen für die Beteiligung von Co-Faktoren¹²⁶. Alle bisher charakterisierten Haloalkan Dehalogenasen (HDs) gehören strukturell zur Familie der α/β -Hydrolasen.

Diese große Protein-Familie wurde erstmals 1992 von Ollis *et al.*^{127; 128; 129} beschrieben. Dazu zählen Enzyme, die verschiedene Reaktionen katalysieren, eine geringe Sequenzidentität zeigen, sehr unterschiedliche Substrate umsetzen und unterschiedliche physikalische Eigenschaften aufweisen. Gemeinsam haben diese Enzyme das α/β -Hydrolase-Faltungsmotiv.

Die Hauptdomäne besteht aus einem zentralen, acht strängigen β -Faltblatt, das bis auf einen Strang ($\beta2$) parallel ausgerichtet ist und auf beiden Seiten von α -Helices umsäumt wird. Am C-terminalen Ende der

β -Strände befindet sich die sogenannte Cap-Struktur, die meist aus α -Helices gebildet wird. Die Haupt-Domäne ist bei allen α/β -Hydrolasen streng konserviert, während die Cap-Struktur hinsichtlich der Anzahl und Anordnung von Sekundärstrukturelementen stark variiert.

Das aktive Zentrum dieser Enzymfamilie wird von einer katalytischen Triade gebildet, die aus einem Nukleophil (Ser, Asp oder Cys), einem Histidin mit basischen Eigenschaften und einer katalytischen Säure (Asp oder Glu) besteht. Die Aminosäuren des aktiven Zentrums befinden sich in Loop-Strukturen, die durch das starre Gerüst, gebildet aus β -Faltblatt und umliegenden α -Helices, in die richtige Position gebracht werden. Es gibt zwei mögliche Anordnungen für die katalytische Triade. Beide Anordnungen findet man auch in der eher kleinen Gruppe der HDs.

Sehr häufig findet man Insertionen am C-terminalen Ende von β 6, β 7 und β 8. Diese Insertionen bilden die Cap-Struktur oberhalb des aktiven Zentrums, die dieses vom Solvent abschirmt und für die Substratbindung verantwortlich ist^{127; 128; 129}.

Die α/β -Hydrolase-Faltung bildet ein einfaches und effektives Gerüst, um verschiedene katalytische Triaden für verschiedene enzymatische Reaktionen und die Umsetzung diverser Substrate durch nur geringe Änderungen zu realisieren. Auch in der Natur findet man, ausgehend von einem gemeinsamen enzymatischem Vorfahren, innerhalb der α/β -Hydrolase-Familie eine weit größere Anzahl an verschiedenen katalysierten Reaktionen als in jeder anderen Hydrolase-Familie, die durch divergente Evolution entstanden ist.

Auch gibt es viele erfolgreiche Ansätze in denen Enzyme der α/β -Hydrolase-Familie durch Protein-Engineering neue Eigenschaften realisieren¹³⁰.

Der Reaktionsmechanismus von HDs setzt sich aus zwei Teilschritten zusammen. Im ersten Reaktionsschritt wird ein kovalentes Alkyl-Enzym-Intermediat durch Angriff des Nukleophils der katalytischen Triade an das Substrat gebildet. Hierdurch wird das Halogenatom als Halogenid abgespalten. Im zweiten Schritt wird das Produkt, mittels nukleophiler Substitution durch ein Hydroxydion gebildet und der entsprechende Alkohol wird freigesetzt. Das Hydroxyd wird aus einem Wassermolekül mit Hilfe des Base/Säure-Paares der katalytischen Triade gebildet.

Der erste Übergangszustand ist sehr wahrscheinlich ein penta-koordiniertes Kohlenstoffatom des Substrates, wie es in S_N2 -Reaktionen an sp^3 hybridisierten Kohlenstoffatomen auftritt, wo die negative Ladung am Halogensubstituent entsteht und von den Halogenid-stabilisierenden Aminosäuren stabilisiert wird. Dieser Reaktionsschritt ist typisch für Dehalogenasen. Die Halogenid-stabilisierenden Aminosäuren sind beispielsweise zwei Tryptophane und das entstehende Halogenid liegt zwischen den aromatischen Indolringen und wird durch die partiell positiven Wasserstoffatome der Imino-Stickstoffe stabilisiert. Der zweite Übergangszustand entspricht einem negativ geladenen, tetraedrischen

Intermediate und ist typisch für alle α/β -Hydrolasen. Auch hier wird ein kovalent gebundenes Substrat-Enzym-Intermediate hydrolysiert, wie zum Beispiel bei den Acetylcholinesterasen¹³¹ oder den Serincarboxypeptidasen¹³². Bei HDs wird jedoch zuerst das halogensubstituierte Kohlenstoffatom des Substrates angegriffen und in einem zweiten Schritt das $\text{C}\gamma$ -Atom des nukleophilen Aspartats. Der Übergangszustand der zweiten Reaktion wird vom *Oxy-Anion-Hole* stabilisiert, einem charakteristischen Merkmal aller α/β -Hydrolasen¹²⁹.

Innerhalb der HDs gibt es drei Klassen: HD-I, HD-II und HD-III¹³³. Die Einteilung erfolgt nach der Position und Identität funktionell wichtiger Aminosäurereste. Enzyme mit Asp–His–Asp (katalytische Triade) und Trp–Trp (Halogenid-stabilisierende Aminosäuren) zählen zu HDs-I, mit Asp–His–Glu und Asn–Trp werden in HDs-II und mit Asp–His–Asp und Asn–Trp in HDs-III eingeteilt.

Eine weitere Einteilung erfolgt aufgrund des Substratspektrums und der Sequenzhomologien. Hierbei werden Enzyme, die spezifisch kurzkettige, halogenierte Alkane (C2-C4) umsetzen von jenen unterschieden, die einfach-, doppelt- und mehrfach halogenierte C2-C9 Verbindungen spalten¹³⁴.

Es gibt verschiedene, miteinander verwandte HDs, die jeweils ein breites Spektrum an unterschiedlichen chlorierten, bromierten und teilweise auch jodierten Substraten umsetzen, mit einer Präferenz für primäre Kohlenstoff-Halogenbindungen. Neben Alkanen und Alkenen werden auch Cyclohexane, Haloalkohole und Halosäuren umgesetzt. Bisher ist nur ein Enzym bekannt, das in der Lage ist Fluoracetat umzusetzen; welches allerdings nicht zu HDs gezählt wird¹³⁵.

Die Substratspezifität von HDs ist im Allgemeinen eher breit und zu der eher geringen Selektivität kommen eine niedrige Umsatzrate und eine niedrige Spezifität. Krooshof *et al.* konnten zeigen, dass der geschwindigkeitsbestimmende Schritt die Freisetzung des Halogenids ist. Eine langsame konformative Umlagerung ist nötig, damit das Halogenid das Enzym verlassen kann¹³⁶.

Durch Protein-Engineering (z.B. site-directed mutagenesis, directed evolution, rational design) konnte eine Verbesserung der spezifischen Aktivität, der Enantioselektivität, der Langzeitstabilität und eine Verminderung der Produktinhibierung erzielt werden¹³⁷.

Eine der ersten Haloalkan Dehalogenasen (DhIA) wurde aus dem Mikroorganismus *Xanthobacter autotrophicus* isoliert¹³⁸ und in den 90er Jahren in der Grundwasseraufarbeitung zum Abbau von 1,2-Dichlorethan eingesetzt¹³⁹. Neben dem biologischen Abbau von Umweltschadstoffen und der Sanierung kontaminierten Boden (*bioremediation*)¹¹¹ finden HDs derzeit Anwendung als Biosensoren für toxische Chemikalien¹⁴⁰, bei der Dekontamination von Kampfstoffen¹⁴¹, im Cell Imaging und in der Proteinanalyse¹⁴² sowie als industrielle Biokatalysatoren unter anderem für die Produktion chiraler Synthesebausteine¹⁴³.

Zurzeit gibt es 14 verschiedene HDs mit nachgewiesener Dehalogenierungsaktivität von denen fünf bereits strukturell beschrieben sind: DhIA aus *X. autotrophicus* GJ10¹⁴⁴, DhaA aus *Rhodococcus* sp. TDTM0003¹⁴⁵, LinB aus *Sphingobium japonicum* (*Sphingomonas paucimobilis*) UT26¹⁴⁶), DmbA aus *Mycobacterium tuberculosis* H37Rv¹⁴⁷ und DbjA aus *Bradyrhizobium japonicum* USDA110¹⁴⁸.

Mit zunehmender Information der Struktur-Funktionsbeziehungen steigt auch die Vielfalt praktischer Einsatzmöglichkeiten von HDs.

Ergebnisteil zur Haloalkan Dehalogenase DppA

Kristallisation und röntgendiffraktometrische Untersuchungen zu DppA

Mit einer Konsensus-Sequenz von 19 verschiedenen HDs wurde in der NCBI-Datenbank eine Haloalkan Dehalogenase in *Plesiocystis pacifica* SIR-1 identifiziert (DppA). *Plesiocystis pacifica* SIR-1 ist ein Gram-negatives, marines Myxobakterium und wurde an der japanischen Küste im subtropischen Pazifik isoliert und erstmals von Izuka *et al.* beschrieben¹⁴⁹. Die Identifikation, Klonierung, Expression und Reinigung von DppA wurde von Dr. Martin Hesseler aus der Arbeitsgruppe Biotechnologie und Enzymkatalyse der Universität Greifswald vorgenommen.

Optimierte Kristalle der Haloalkan Dehalogenase DppA wurden unter Cryo-Bedingungen vermessen und beugen Röntgenstrahlen bis zu einer Auflösung von 1,95 Å an einem Drehanoden-Röntgengenerator¹⁵⁰. Die Datenprozessierung zeigt, dass DppA in der orthorhombischen Raumgruppe *P2₁2₁2* mit einem Molekül in der asymmetrischen Einheit kristallisiert (siehe Manuskript 5, Abbildung 1 und Tabelle 1).

Die Struktur konnte nach der Methode des Molekularen Ersatzes (*Molecular Replacement*) gelöst werden. Als Suchmodell diente die Haloalkan Dehalogenase DhaA von *Xanthobacter autotrophicus* GJ10 (PDB 1edb¹⁵¹) mit einer Sequenzidentität von 50%.

Das endgültige Strukturmodell von DppA, bei einer Auflösung von 2,0 Å und einem *R*-Faktor von 21,93 % beinhaltet 2311 Proteinatome (ohne Wasserstoff), die den Aminosäuren 1-297 des DppA Moleküls entsprechen, 260 Wassermoleküle und 4 Sulfatmoleküle.

Strukturelle Analyse der Haloalkan Dehalogenase DppA aus *Plesiocysti pacifica* SIR-1

Anhand des Strukturmodells lässt sich die Haloalkan Dehalogenase DppA zur α/β-Hydrolase Superfamilie zuordnen. Das Protein zeigt eine globuläre Struktur und ist in zwei Domänen geteilt (siehe Manuskript 6, Abbildung 3 und Tabelle 3). Die Hauptdomäne besteht aus einem zentralen β-Faltblatt, das aus acht β-Strängen gebildet wird. Das β-Faltblatt bildet den Kern des Proteins und ist fast vollständig aus parallelen β-Strängen aufgebaut. Die einzige Ausnahme bildet β2, der antiparallel ausgerichtet ist. Das zentrale β-Faltblatt ist von sechs α-Helices umgeben und bildet das Proteingerüst. Vier der α-Helices sind auf der einen Seite des Faltblattes platziert und zwei auf der gegenüberliegenden Seite. Die Faltung von DppA entspricht der Faltung anderer bereits bekannter Haloalkan Dehalogenasen, wobei die

Sekundärstrukturelemente der Kerndomäne sehr gut konserviert sind, die der Cap-Struktur jedoch größere Unterschiede aufzeigen.

Die zweite Domäne ist die sogenannte Cap-Struktur. Diese ist am C-terminalen Ende des β -Faltblattes lokalisiert und besteht hauptsächlich aus α -Helices. Die Cap-Struktur wird an zwei Stellen in die Grundstruktur des α/β -Hydrolase-Faltungsmotiv eingefügt. Die erste Insertion erfolgt nach $\beta 6$ und die zweite nach $\beta 7$. Die Cap-Struktur schirmt das aktive Zentrum vom umgebenden Solvent ab.

Die katalytisch wichtigen Aminosäureseitenketten von DppA sind in einer katalytischen Triade angeordnet, bestehend aus Asp123, dem Nukleophil, His278 als katalytische Base und Asp249 als katalytische Säure (siehe Manuskript 6, Abbildung 1).

Das Nukleophil Asp123 befindet sich in der Loop-Struktur zwischen $\beta 5$ und $\alpha 3$, dem sogenannten nukleophilen Ellenbogen (*nucleophilic elbow*). Der Loop wurde als γ -artig beschrieben und weist eine extrem enge Windung auf, die in einer ungünstigen Anordnung der Diederwinkel (ϕ und ψ) des Peptidrückgrats resultiert. Um sterische Hinderungen zu vermeiden besitzen die Aminosäuren in direkter Nachbarschaft zum Nukleophil (-3 - +3) kleine Aminosäureseitenketten. Das Nukleophil befindet sich genau am N-Terminus der α -Helix und somit kann deren Dipolmoment sowohl den tetraedrischen Übergangszustand als auch die negative Ladung des Nukleophils stabilisieren. Die katalytische Base ist hinter $\beta 8$ lokalisiert und die katalytische Säure befindet sich in der Loop-Struktur nach $\beta 7$. Die Position des Nukleophils und der Base ist streng konserviert und identisch für alle α/β -Hydrolasen, wohingegen die katalytische Säure entweder in der Loop-Struktur nach $\beta 6$ oder nach $\beta 7$ positioniert ist. Die Position der katalytischen Säure nach $\beta 6$ wird typischerweise in humanen Pankreaslipasen gefunden¹⁵² wohingegen die Position nach $\beta 7$ typisch für alle anderen α/β -Hydrolasen¹²⁷ ist. Innerhalb der eher kleinen Gruppe der HDs werden beide Anordnungen gefunden (siehe Manuskript 1, Abbildung 4).

Die Halogenid-stabilisierenden Aminosäuren sind Trp124 und Trp163 in DppA. Mit dieser Anordnung der Aminosäuren des aktiven Zentrums gehört DppA zur HDL-I Familie, genau wie Dhla¹³³.

Die Stabilisierung des zweiten Übergangszustandes wird, ähnlich dem *Oxy-Anion-Hole* der Serinproteasen¹⁵³, auch in allen anderen α/β -Hydrolasen, durch die Amidstickstoffatome von Glu55 und Trp124 gewährleistet. Dabei ist die Position dieser Aminosäuren hoch konserviert. Das Glu55 ist nach $\beta 3$ lokalisiert und die zweite Aminosäure (Trp125) folgt immer direkt auf das Nukleophil. Beide Aminosäuren bilden Wasserstoffbrückenbindungen zum nukleophilen Asp124 und erhöhen einerseits dessen Nukleophilie und stabilisieren andererseits den negativ geladenen Übergangszustand während der Hydrolyse.

Die Abhängigkeit der Enzymaktivität von Temperatur und pH sowie die Substratspezifität wurden von Dr. Martin Hesseler bestimmt (siehe Manuskript 6, Tabelle 1 und 2). Es konnte gezeigt werden, dass DppA

ein breites Temperatur-Optimum von 30 – 37 °C besitzt und in alkalischen Lösungen (pH 8-9) die höchste Aktivität aufzeigt. Die Substratspezifität wurde mit verschiedensten Substanzen getestet; die höchste Aktivität besitzt DppA gegenüber 1-Brombutan. Zudem werden Bromokane von kurzer bis mittlerer Kettenlänge umgesetzt. Neben 1-Brombutan werden auch 2-Brombutan sowie verzweigte Substrate umgesetzt (1,2-Dibrombutan und 1,2-Dibrompropan). Chlorierte Substrate, Halosäuren, Haloalkohole sowie das halogenierte Epoxid Epibromhydrin werden nicht umgesetzt. Mit diesem Substratspektrum bildet DppA eine neue Substrat-Spezifitäts-Klasse.

Im Gegensatz zum nächsten bisher charakterisierten Verwandten DhaA zeigt DppA keinerlei Aktivität gegenüber chlorierten Substraten. Die Substratspezifität von HDs wird hauptsächlich durch die Cap-Struktur gegeben¹⁵⁴, die die Beschaffenheit des Ein- und Ausgangstunnels und die des aktiven Zentrums bestimmt (siehe Manuskript 1, Abbildung 6 und 7). Es ist möglich, dass HDs unterschiedliche Substrat-Spezifitäten erworben haben, da die Cap-Strukturen von unterschiedlicher Herkunft sind¹²⁶. Es konnte gezeigt werden, dass die Präferenz für größere Substrate mit der Größe und Form des Eingangstunnels korreliert^{126; 146}.

In DhaA findet man *direct repeats* auf DNA-Ebene, die in DppA nicht existieren. Dies führt zur Insertion von einigen Aminosäuren nach Position 150 in DhaA und somit zu einer geringfügigen Verschiebung der Halogenid-stabilisierenden Aminosäure im Vergleich zu DppA (siehe Manuskript 6, Abbildung 5). Janssen *et al.*¹¹² konnten zeigen, dass das Auftreten dieser repetitiven Elemente mit der Fähigkeit von DhaA in Verbindung steht, neben bromierten Substraten auch chlorierte Substanzen umzusetzen. Die Tatsache, dass DppA keine Insertionen aufweist und keine chlorierten Substrate umsetzt, stimmt mit diesen Ergebnissen überein.

Durch Veränderungen innerhalb der Cap-Struktur konnte neben dem Substratspektrum auch die Enantioselektivität von HDs verbessert werden¹⁵⁵. Demnach ist die Cap-Struktur ein geeigneter Angriffspunkt zur Mutagenese für gerichtetes Proteindesign¹⁵⁶.

Literatur

1. Austin, B., Austin, D. A., Dalsgaard, I., Gudmundsdottir, B. K., Hoie, S., Thornton, J. M., Larsen, J. L., O'Hici, B. & Powell, R. (1998). Characterization of atypical *Aeromonas salmonicida* by different methods. *Syst Appl Microbiol* **21**, 50-64.
2. Holt, J. G., Krieg, N. R., Sneath, P. H. A., Staley, J. T. & Williams, S. T. (1994). *Bergey's Manual of Determinative Bacteriology*. 9 edit, Williams and Wilkins, Baltimore.
3. Pavan, M. E., Abbott, S. L., Zorzopoulos, J. & Janda, J. M. (2000). *Aeromonas salmonicida* subsp. *peptinolytica* subsp. nov., a new pectinase-positive subspecies isolated from a heavily polluted river. *Int J Syst Evol Microbiol* **50 Pt 3**, 1119-24.
4. Wiklund, T., Dalsgaard, I., Eerola, E. & Olivier, G. (1994). Characteristics of 'atypical', cytochrome oxidase-negative *Aeromonas salmonicida* isolated from ulcerated flounders (*Platichthys flesus* (L.)). *J Appl Bacteriol* **76**, 511-20.
5. Bernoth, E. M., Ellis, A. E., Midtlyng, P. J., Smith, P. . (1997). *Furunculosis: Multidisciplinary Fish Disease Research*, Academic Press, United Kingdom.
6. Mackie, T. J. & Finkelstein, M. H. (1930). Complement-fixation by the Interaction of Normal Serum and Bacterial Suspensions-a Contribution to the Study of Natural Immunity Phenomena. *J Hyg (Lond)* **30**, 1-24.
7. Toranzo, A. E., Magariños, B. & Romalde, J. L. (2005). A review of the main bacterial fish diseases in mariculture systems. *Aquaculture* **246**, 37-61.
8. Toranzo, A. E., Barreiro, S., Casal, J. F., Figueras, A., Magariños, B. & Barja, J. L. (1991). Pasteurellosis in cultured gilthead seabream (*Sparus aurata*): first report in Spain. *Aquaculture* **99**, 1-15.
9. Ellis, A. E. (1997). Immunization with bacterial antigens: furunculosis. *Dev Biol Stand* **90**, 107-16.
10. Bricknell, I. R., Bowden, T. J., Bruno, D. W., MacLachlan, P., Johnstone, R. & Ellis, A. E. (1999). Susceptibility of Atlantic halibut, *Hippoglossus hippoglossus* (L.) to infection with typical and atypical *Aeromonas salmonicida*. *Aquaculture* **175**, 1-13.
11. Ellis, A. E., do Vale, A., Bowden, T. J., Thompson, K. & Hastings, T. S. (1997). In vivo production of A-protein, lipopolysaccharide, iron-regulated outer membrane proteins and 70-kDa serine protease by *Aeromonas salmonicida* subsp. *salmonicida*. *FEMS Microbiol Lett* **149**, 157-63.
12. Austin, B. & Austin, D. A. (2007). *Bacterial fish pathogens : diseases of farmed and wild fish*, Springer ; Published in association with Praxis Pub., Dordrecht; Chichester.
13. Gudmundsdottir, B. K. & Bjornsdottir, B. (2007). Vaccination against atypical furunculosis and winter ulcer disease of fish. *Vaccine* **25**, 5512-23.
14. Bjornsdottir, B., Gudmundsdottir, S., Bambir, S. H. & Gudmundsdottir, B. K. (2005). Experimental infection of turbot, *Scophthalmus maximus* (L.), by *Aeromonas salmonicida* subsp. *achromogenes* and evaluation of cross protection induced by a furunculosis vaccine. *J Fish Dis* **28**, 181-8.
15. Gudmundsdottir, B. K., Hvanndal, I., Bjornsdottir, B. & Wagner, U. (2003). Analysis of exotoxins produced by atypical isolates of *Aeromonas salmonicida*, by enzymatic and serological methods. *J Fish Dis* **26**, 15-29.
16. Gudmundsdottir, S., Lange, S., Magnadottir, B. & Gudmundsdottir, B. K. (2003). Protection against atypical furunculosis in Atlantic halibut, *Hippoglossus hippoglossus* (L.); comparison of a commercial furunculosis vaccine and an autogenous vaccine. *J Fish Dis* **26**, 331-8.
17. Lund, V. & Mikkelsen, H. (2004). Genetic diversity among A-proteins of atypical strains of *Aeromonas salmonicida*. *Diseases of Aquatic Organisms* **61**, 257-262.

18. Magnadóttir, B., Bambir, S. H., Gudmundsdóttir, B. K., Pilström, L. & Helgason, S. (2002). Atypical *Aeromonas salmonicida* infection in naturally and experimentally infected cod, *Gadus morhua* L. *Journal of Fish Diseases* **25**, 583-597.
19. Lund, V., Jenssen, L. M. & Wesmajervi, M. S. (2002). Assessment of genetic variability and relatedness among atypical *Aeromonas salmonicida* from marine fishes, using AFLP-fingerprinting. *Diseases of Aquatic Organisms* **50**, 119-126.
20. Wiklund, T. & Dalsgaard, I. (1998). Occurrence and significance of atypical *Aeromonas salmonicida* in non-salmonid and salmonid fish species: a review. *Diseases of Aquatic Organisms* **32**, 49-69.
21. Bravo, S. (2000). Occurrence of atypical furunculosis in Chile. *Bull Eur Ass Fish Pathol* **20**, 209.
22. Hiney M, O. G. (1999). Furunculosis (*Aeromonas salmonicida*). In *Fish Diseases and Disorders* (Woo PTK, B. D., ed.), pp. 341-425. CABI Publishing, New York.
23. Johansen, L. H., Jensen, I., Mikkelsen, H., Bjørn, P. A., Jansen, P. A. & Bergh, Ø. (2011). Disease interaction and pathogens exchange between wild and farmed fish populations with special reference to Norway. *Aquaculture* **315**, 167-186.
24. Pyle, W., S., Cipriano & C., R. (1986). *Specificity of lipopolysaccharide antigens of Aeromonas salmonicida*, 31, Faculty Press, London, ROYAUME-UNI.
25. Hirst, I. D. & Ellis, A. E. (1994). Iron-regulated outer membrane proteins of *Aeromonas salmonicida* are important protective antigens in Atlantic salmon against furunculosis. *Fish & Shellfish Immunology* **4**, 29-45.
26. Merino, S., Rubires, X., Aguilar, A., Albertí, S., Hernandez-Allés, S., Benedí, V. J. & Tomas, J. M. (1996). Mesophilic *Aeromonas* sp. serogroup O:11 resistance to complement-mediated killing. *Infection and Immunity* **64**, 5302-9.
27. Lund, V., Espelid, S. & Mikkelsen, H. (2003). Vaccine efficacy in spotted wolffish *Anarhichas minor*: relationship to molecular variation in A-layer protein of atypical *Aeromonas salmonicida*. *Diseases of Aquatic Organisms* **56**, 31-42.
28. Gudmundsdottir, B. K., Hastingst, S. & Ellis, E. A. (1990). Isolation of a new toxic protease from a strain of *Aeromonas salmonicida* subspecies *achromogenes*. *Diseases of Aquatic Organisms* **9**, 199-208.
29. Gudmundsdottir, S. & Gudmundsdottir, B. (2001). Induction of inflammatory cytokines by extracellular products and LPS of the fish pathogen *Aeromonas salmonicida* ssp. *achromogenes* in mice and mouse cell cultures. *Vet Immunol Immunopathol* **81**, 71-83.
30. Gunnlaugsdottir, B. & Gudmundsdottir, B. K. (1997). Pathogenicity of atypical *Aeromonas salmonicida* in Atlantic salmon compared with protease production. *J Appl Microbiol* **83**, 542-51.
31. Magnadottir, B., Gudmundsdottir, S. & Gudmundsdottir, B. K. (1995). Study of the humoral response of Atlantic salmon (*Salmo salar* L.), naturally infected with *Aeromonas salmonicida* ssp. *achromogenes*. *Vet Immunol Immunopathol* **49**, 127-42.
32. Arnadottir, H., Hvanndal, I., Andresdottir, V., Burr, S. E., Frey, J. & Gudmundsdottir, B. K. (2009). The AsaP1 peptidase of *Aeromonas salmonicida* subsp. *achromogenes* is a highly conserved deuterolysin metalloprotease (family M35) and a major virulence factor. *J Bacteriol* **191**, 403-10.
33. Schwenteit, J., Gram, L., Nielsen, K. F., Fridjonsson, O. H., Bornscheuer, U. T., Givskov, M. & Gudmundsdottir, B. K. (2011). Quorum sensing in *Aeromonas salmonicida* subsp. *achromogenes* and the effect of the autoinducer synthase Asal on bacterial virulence. *Vet Microbiol* **147**, 389-97.
34. Rawlings, N. D., Barrett, A. J. & Bateman, A. (2010). MEROPS: the peptidase database. *Nucleic Acids Research* **38**, D227-D233.
35. Stöcker, W. & Bode, W. (1995). Structural features of a superfamily of zinc-endopeptidases: the metzincins. *Current Opinion in Structural Biology* **5**, 383-390.

36. Adekoya, O. A. & Sylte, I. (2009). The Thermolysin Family (M4) of Enzymes: Therapeutic and Biotechnological Potential. *Chemical Biology & Drug Design* **73**, 7-16.
37. Fushimi, N., Ee, C. E., Nakajima, T. & Ichishima, E. (1999). Aspzincin, a family of metalloendopeptidases with a new zinc-binding motif. Identification of new zinc-binding sites (His(128), His(132), and Asp(164)) and three catalytically crucial residues (Glu(129), Asp(143), and Tyr(106)) of deuterolysin from *Aspergillus oryzae* by site-directed mutagenesis. *J Biol Chem* **274**, 24195-201.
38. Ichishima, E. (2004). Penicillolysin. In *Handbook of Proteolytic Enzymes* (Barrett, A. J., Rawlings,N.D. & Woessner,J.F., ed.), Vol. 2 edn (eds), pp. 784-786. Elsevier, London
39. Tatsumi, H. (2004). Deuterolysin. In *In Handbook of Proteolytic Enzymes* (Barrett, A. J., Rawlings, N.D. & Woessner,J.F., ed.), Vol. 2 end, pp. 786-788. Elsevier, London.
40. Takio, K. (2004). Peptidyl-Lys metalloendopeptidase. In *In Handbook of Proteolytic Enzymes* (Barrett, A. J., Rawlings,N.D. & Woessner,J.F. eds, ed.), Vol. 2 edn, pp. 788-792. 788-792 vols. Elsevier, London.
41. Zhou, E., Jia, Y., Singh, P., Correll, J. C. & Lee, F. N. (2007). Instability of the Magnaporthe oryzae avirulence gene AVR-Pita alters virulence. *Fungal Genet Biol* **44**, 1024-34.
42. Doi, Y., Lee, B. R., Ikeguchi, M., Ohoba, Y., Ikoma, T., Tero-Kubota, S., Yamauchi, S., Takahashi, K. & Ichishima, E. (2003). Substrate Specificities of Deuterolysin from *Aspergillus oryzae* and Electron Paramagnetic Resonance Measurement of Cobalt-substituted Deuterolysin. *Bioscience, Biotechnology, and Biochemistry* **67**, 264-270.
43. Schechter, I. & Berger, A. (1967). On the size of the active site in proteases. I. Papain. *Biochemical and Biophysical Research Communications* **27**, 157-162.
44. Nonaka, T., Hashimoto, Y. & Takio, K. (1998). Kinetic Characterization of Lysine-Specific Metalloendopeptidases from *Grifola frondosa* and *Pleurotus ostreatus* Fruiting Bodies. *Journal of Biochemistry* **124**, 157-162.
45. Raijmakers, R., Neerincx, P., Mohammed, S. & Heck, A. J. R. (2010). Cleavage specificities of the brother and sister proteases Lys-C and Lys-N. *Chemical Communications* **46**, 8827-8829.
46. Hori, T., Kumazaka, T., Yamamoto, M., Nonaka, N., Tanaka, N., Hashimoto, Y., Ueki, U. & Takio, K. (2001). Structure of a new 'aspzincin' metalloendopeptidase from *Grifola frondosa*: implications for the catalytic mechanism and substrate specificity based on several different crystal forms. *Acta Crystallogr D Biol Crystallogr* **57**, 361-8.
47. McAuley, K. E., Jia-Xing, Y., Dodson, E. J., Lehmbeck, J., Østergaard, P. R. & Wilson, K. S. (2001). A quick solution: ab initio structure determination of a 19 kDa metalloproteinase using ACORN. *Acta Crystallogr D Biol Crystallogr* **57**, 1571-1578.
48. Holden, H. M., Tronrud, D. E., Monzingo, A. F., Weaver, L. H. & Matthews, B. W. (1987). Slow-and fast-binding inhibitors of thermolysin display different modes of binding: crystallographic analysis of extended phosphonamide transition-state analogues. *Biochemistry* **26**, 8542-53.
49. Grams, F., Dive, V., Yiotakis, A., Yiallouros, I., Vassiliou, S., Zwilling, R., Bode, W. & Stocker, W. (1996). Structure of astacin with a transition-state analogue inhibitor. *Nat Struct Biol* **3**, 671-5.
50. Kim, H. & Lipscomb, W. N. (1991). Comparison of the structures of three carboxypeptidase A-phosphonate complexes determined by x-ray crystallography. *Biochemistry* **30**, 8171-8180.
51. Bode, W., Meyer, E. & Powers, J. C. (1989). Human leukocyte and porcine pancreatic elastase: x-ray crystal structures, mechanism, substrate specificity, and mechanism-based inhibitors. *Biochemistry* **28**, 1951-1963.
52. Hendrick, J. P. & Hartl, F. (1993). Molecular Chaperone Functions of Heat-Shock Proteins. *Annual Review of Biochemistry* **62**, 349-384.
53. Inouye, M. (1991). Intramolecular chaperone: the role of the pro-peptide in protein folding. *Enzyme* **45**, 314-21.

54. Eder, J., Rheinheimer, M. & Fersht, A. R. (1993). Folding of subtilisin BPN': characterization of a folding intermediate. *Biochemistry* **32**, 18-26.
55. Ikemura, H. & Inouye, M. (1988). In vitro processing of pro-subtilisin produced in Escherichia coli. *Journal of Biological Chemistry* **263**, 12959-12963.
56. Silen, J. L. & Agard, D. A. (1989). The [alpha]lytic protease pro-region does not require a physical linkage to activate the protease domain in vivo. *Nature* **341**, 462-464.
57. Rosenau, F., Tommassen, J. & Jaeger, K.-E. (2004). Lipase-Specific Foldases. *ChemBioChem* **5**, 152-161.
58. Striker, R., Jacob-Dubuisson, F., Freiden, C. & Hultgren, S. J. (1994). Stable fiber-forming and nonfiber-forming chaperone-subunit complexes in pilus biogenesis. *Journal of Biological Chemistry* **269**, 12233-12239.
59. Sellman, B. R. & Tweten, R. K. (1997). The propeptide of Clostridium septicum alpha toxin functions as an intramolecular chaperone and is a potent inhibitor of alpha toxin-dependent cytotoxicity. *Molecular Microbiology* **25**, 429-440.
60. Demleitner, G. & Götz, F. (1994). Evidence for importance of the Staphylococcus hyicus lipase pro-peptide in lipase secretion, stability and activity. *FEMS Microbiol Lett* **121**, 189-197.
61. Meens, J., Herbort, M., Klein, M. & Freudl, R. (1997). Use of the pre-pro part of Staphylococcus hyicus lipase as a carrier for secretion of Escherichia coli outer membrane protein A (OmpA) prevents proteolytic degradation of OmpA by cell-associated protease(s) in two different gram-positive bacteria. *Applied and Environmental Microbiology* **63**, 2814-20.
62. Klauser, T., Krämer, J., Otelberger, K., Pohlner, J. & Meyer, T. F. (1993). Characterization of the Neisseria Igα-core: The Essential Unit for Outer Membrane Targeting and Extracellular Protein Secretion. *J Mol Biol* **234**, 579-593.
63. Li, Y. & Inouye, M. (1996). The Mechanism of Autoprocessing of the Propeptide of Prosubtilisin E: Intramolecular or Intermolecular Event? *J Mol Biol* **262**, 591-594.
64. McIver, K., Kessler, E. & Ohman, D. E. (1991). Substitution of active-site His-223 in Pseudomonas aeruginosa elastase and expression of the mutated lasB alleles in Escherichia coli show evidence for autoproteolytic processing of proelastase. *Journal of Bacteriology* **173**, 7781-7789.
65. Gustin, J. K., Kessler, E. & Ohman, D. E. (1996). A substitution at His-120 in the LasA protease of Pseudomonas aeruginosa blocks enzymatic activity without affecting propeptide processing or extracellular secretion. *Journal of Bacteriology* **178**, 6608-17.
66. Kessler, E. & Safrin, M. (1994). The propeptide of Pseudomonas aeruginosa elastase acts as an elastase inhibitor. *Journal of Biological Chemistry* **269**, 22726-22731.
67. Braun, P. & Tommassen, J. (1998). Function of bacterial propeptides. *Trends in Microbiology* **6**, 6-8.
68. Fu, X., Inouye, M. & Shinde, U. (2000). Folding Pathway Mediated by an Intramolecular Chaperone. *Journal of Biological Chemistry* **275**, 16871-16878.
69. Baker, D., Sohl, J. L. & Agard, D. A. (1992). A protein-folding reaction under kinetic control. *Nature* **356**, 263-265.
70. Ramos, C., Winther, J. R. & Kielland-Brandt, M. C. (1994). Requirement of the propeptide for in vivo formation of active yeast carboxypeptidase Y. *Journal of Biological Chemistry* **269**, 7006-7012.
71. Lee, Y.-C., Ohta, T. & Matsuzawa, H. (1992). A non-covalent NH₂-terminal pro-region aids the production of active aqualysin I (a thermophilic protease) without the COOH-terminal pro-sequence in Escherichia coli. *FEMS Microbiol Lett* **92**, 73-77.
72. Carmona, E., Dufour, É., Plouffe, C., Takebe, S., Mason, P., Mort, J. S. & Ménard, R. (1996). Potency and Selectivity of the Cathepsin L Propeptide as an Inhibitor of Cysteine Proteases†. *Biochemistry* **35**, 8149-8157.

73. van den Hazel, H. B., Kielland-Brandt, M. C. & Winther, J. R. (1993). The propeptide is required for in vivo formation of stable active yeast proteinase A and can function even when not covalently linked to the mature region. *Journal of Biological Chemistry* **268**, 18002-18007.
74. Tang, B., Nirasawa, S., Kitaoka, M., Marie-Claire, C. & Hayashi, K. (2003). General function of N-terminal propeptide on assisting protein folding and inhibiting catalytic activity based on observations with a chimeric thermolysin-like protease. *Biochemical and Biophysical Research Communications* **301**, 1093-1098.
75. Marie-Claire, C., Yabuta, Y., Suefuji, K., Matsuzawa, H. & Shinde, U. (2001). Folding pathway mediated by an intramolecular chaperone: the structural and functional characterization of the aqualysin I propeptide. *J Mol Biol* **305**, 151-165.
76. Li, Y., Hu, Z., Jordan, F. & Inouye, M. (1995). Functional Analysis of the Propeptide of Subtilisin E as an Intramolecular Chaperone for Protein Folding. *Journal of Biological Chemistry* **270**, 25127-25132.
77. Gamble, M., Künze, G., Dodson, E. J., Wilson, K. S. & Jones, D. D. (2011). Regulation of an intracellular subtilisin protease activity by a short propeptide sequence through an original combined dual mechanism. *Proceedings of the National Academy of Sciences* **108**, 3536-3541.
78. Gao, X., Wang, J., Yu, D.-Q., Bian, F., Xie, B.-B., Chen, X.-L., Zhou, B.-C., Lai, L.-H., Wang, Z.-X., Wu, J.-W. & Zhang, Y.-Z. (2010). Structural basis for the autoprocessing of zinc metalloproteases in the thermolysin family. *Proceedings of the National Academy of Sciences* **107**, 17569-17574.
79. Li, D., Li, H., Wang, T., Pan, H., Lin, G. & Li, H. (2010). Structural basis for the assembly and gate closure mechanisms of the Mycobacterium tuberculosis 20S proteasome. *EMBO J* **29**, 2037-2047.
80. Iacovache, I., Degiacomi, M. T., Pernot, L., Ho, S., Schiltz, M., Dal Peraro, M. & van der Goot, F. G. (2011). Dual Chaperone Role of the C-Terminal Propeptide in Folding and Oligomerization of the Pore-Forming Toxin Aerolysin. *PLoS Pathog* **7**, e1002135.
81. Olsen, J. G., Dagil, R., Niclasen, L. M., Sørensen, O. E. & Kragelund, B. B. (2009). Structure of the Mature Streptococcal Cysteine Protease Exotoxin mSpeB in Its Active Dimeric Form. *J Mol Biol* **393**, 693-703.
82. Demidyuk, I. V., Gromova, T. Y., Polyakov, K. M., Melik-Adamyan, W. R., Kuranova, I. P. & Kostrov, S. V. (2010). Crystal Structure of the Protealysin Precursor. *Journal of Biological Chemistry* **285**, 2003-2013.
83. Kim, J.-S., Kluskens, L. D., de Vos, W. M., Huber, R. & van der Oost, J. (2004). Crystal Structure of Fervidolysin from Fervidobacterium pennivorans, a Keratinolytic Enzyme Related to Subtilisin. *J Mol Biol* **335**, 787-797.
84. Jain, S. C., Shinde, U., Li, Y., Inouye, M. & Berman, H. M. (1998). The crystal structure of an autoprocessed Ser221Cys-subtilisin E-propeptide complex at 2.0 Å resolution. *J Mol Biol* **284**, 137-144.
85. Roy, R. S., Kim, S., Baleja, J. D. & Walsh, C. T. (1998). Role of the microcin B17 propeptide in substrate recognition: solution structure and mutational analysis of McbA1 26. *Chemistry & biology* **5**, 217-228.
86. Smith, J., Zaluzec, E., Wery, J., Niu, L., Switzer, R., Zalkin, H. & Satow, Y. (1994). Structure of the allosteric regulatory enzyme of purine biosynthesis. *Science* **264**, 1427-1433.
87. Khan, A. R. & James, M. N. G. (1998). Molecular mechanisms for the conversion of zymogens to active proteolytic enzymes. *Protein Science* **7**, 815-836.
88. Scott, C. J. & Taggart, C. C. (2010). Biologic protease inhibitors as novel therapeutic agents. *Biochimie* **92**, 1681-1688.
89. Steele, D. L., El-Kabbani, O., Dunten, P., Windsor, L. J., Kammlott, R. U., Crowther, R. L., Michoud, C., Engler, J. A. & Birktoft, J. J. (2000). Expression, characterization and structure determination of an active site mutant (Glu202-Gln) of mini-stromelysin-1. *Protein Engineering* **13**, 397-405.

90. Schwenteit, J., Bogdanović, X., Fridjonsson, O. H., Bornscheuer, U. T., Hinrichs, W. & Gudmundsdottir, B. K. Construction of four toxoids of AsaP1, a lethal toxic aspzincin metalloendopeptidase of *Aeromonas salmonicida* subsp. *achromogenes*, and studies of its activity and processing. *submitted*.
91. Tatsumi, H., Murakami, S., Tsuji, R. F., Ishida, Y., Murakami, K., Masaki, A., Kawabe, H., Arimura, H., Nakano, E. & Motai, H. (1991). Cloning and expression in yeast of a cDNA clone encoding *Aspergillus oryzae* neutral protease II, a unique metalloprotease. *Mol Gen Genet* **228**, 97-103.
92. Guevara, T., Yiallouros, I., Kappelhoff, R., Bissdorf, S., Stöcker, W. & Gomis-Rüth, F. X. (2010). Proenzyme Structure and Activation of Astacin Metallopeptidase. *Journal of Biological Chemistry* **285**, 13958-13965.
93. Scheifele, D. W. & Ochnio, J. (2002). Hepatitis A vaccine: Is it being used to best advantage? *Canadian Medical Association Journal* **167**, 44-45.
94. Kim, K.-H., Kim, Y.-K., Kim, N. H., Chang, S. H., Lee, J., Park, E.-A., Park, S. E., Eun, B. W., Lee, H. & Lee, H. J. Immunogenicity and safety of LBVH0101, a new *Haemophilus influenzae* type b tetanus toxoid conjugate vaccine, compared with Hiberix™ in Korean infants and children: A randomized trial. *Vaccine*.
95. Giannini, G., Rappuoli, R. & Ratti, G. (1984). The amino-acid sequence of two non-toxic mutants of diphtheria toxin: CRM45 and CRM197. *Nucleic Acids Research* **12**, 4063-4069.
96. Robbins, J. B., Schneerson, R., Trollfors, B., Sato, H., Sato, Y., Rappuoli, R. & Keith, J. M. (2005). The Diphtheria and Pertussis Components of Diphtheria-Tetanus Toxoids-Pertussis Vaccine Should Be Genetically Inactivated Mutant Toxins. *Journal of Infectious Diseases* **191**, 81-88.
97. Bogdanovic, X., Singh, R. K., Hentschke, J., Gudmundsdottir, B. K. & Hinrichs, W. (2009). Crystallization and preliminary X-ray diffraction studies of AsaP1_E294A and AsaP1_E294Q, two inactive mutants of the toxic zinc metallopeptidase AsaP1 from *Aeromonas salmonicida* subsp. *achromogenes*. *Acta Crystallogr Sect F Struct Biol Cryst Commun* **65**, 695-7.
98. Bogdanovic, X. & Hinrichs, W. (2011). Influence of temperature during crystallization setup on precipitate formation and crystal shape of a metalloendopeptidase. *Acta Crystallographica Section F* **67**, 421-423.
99. McPherson, A. (1990). Current approaches to macromolecular crystallization. *European Journal of Biochemistry* **189**, 1-23.
100. Blow, D. M., Chayen, N. E., Lloyd, L. F. & Saridakis, E. (1994). Control of nucleation of protein crystals. *Protein Science* **3**, 1638-1643.
101. Terese, B. (2003). Seeds to crystals. *Journal of Structural Biology* **142**, 66-76.
102. Krissinel, E. & Henrick, K. (2007). Inference of Macromolecular Assemblies from Crystalline State. *J Mol Biol* **372**, 774-797.
103. Harding, M. M. (2006). Small revisions to predicted distances around metal sites in proteins. *Acta Crystallogr D Biol Crystallogr* **62**, 678-82.
104. Yen, N., Bogdanović, X., Palm, G., Kühl, O. & Hinrichs, W. (2010). Structure of the Ni(II) complex of *Escherichia coli* peptide deformylase and suggestions on deformylase activities depending on different metal(II) centres. *Journal of Biological Inorganic Chemistry* **15**, 195-201.
105. Cicero, D. O., Contessa, G. M., Pertinhez, T. A., Gallo, M., Katsuyama, A. M., Paci, M., Farah, C. S. & Spisni, A. (2007). Solution structure of ApaG from *Xanthomonas axonopodis* pv. *citri* reveals a fibronectin-3 fold. *Proteins* **67**, 490-500.
106. Bull, R. J., Reckhow, D. A., Li, X., Humpage, A. R., Joll, C. & Hrudey, S. E. (2011). Potential carcinogenic hazards of non-regulated disinfection by-products: haloquinones, halo-cyclopentene and cyclohexene derivatives, N-halamines, halonitriles, and heterocyclic amines. *Toxicology* **286**, 1-19.
107. Kimbrough, R. D. (1979). The Carcinogenic and other Chronic Effects of Persistent Halogenated Organic Compounds. *Annals of the New York Academy of Sciences* **320**, 415-418.

108. Shinsuke, T. (1988). PCB problems in the future: Foresight from current knowledge. *Environmental Pollution* **50**, 5-28.
109. Hubert Schneemann, G. W. (1995). *Hagers Handbuch der pharmazeutischen Praxis*. Waren und Dienste, Folgebd. 1, Springer
110. Gribble, G. W. (2003). The diversity of naturally produced organohalogens. *Chemosphere* **52**, 289-97.
111. Bosma, T., Damborsky, J., Stucki, G. & Janssen, D. B. (2002). Biodegradation of 1,2,3-trichloropropane through directed evolution and heterologous expression of a haloalkane dehalogenase gene. *Appl Environ Microbiol* **68**, 3582-7.
112. Janssen, D. B., Dinkla, I. J. T., Poelarends, G. J. & Terpstra, P. (2005). Bacterial degradation of xenobiotic compounds: evolution and distribution of novel enzyme activities. *Environmental Microbiology* **7**, 1868-1882.
113. Fetzner, S. (1998). Bacterial dehalogenation. *Applied Microbiology and Biotechnology* **50**, 633-657.
114. Fetzner, S. & Lingens, F. (1994). Bacterial dehalogenases: biochemistry, genetics, and biotechnological applications. *Microbiol Rev* **58**, 641-85.
115. Megharaj, M., Ramakrishnan, B., Venkateswarlu, K., Sethunathan, N. & Naidu, R. (2011). Bioremediation approaches for organic pollutants: a critical perspective. *Environ Int* **37**, 1362-75.
116. Nagata, Y., Endo, R., Ito, M., Ohtsubo, Y. & Tsuda, M. (2007). Aerobic degradation of lindane (γ -hexachlorocyclohexane) in bacteria and its biochemical and molecular basis. *Applied Microbiology and Biotechnology* **76**, 741-752.
117. Segev, O., Meusel, W., Friedenberger, M., Brenner, A. & Kushmaro, A. (2009). Aerobic biodegradation of the brominated flame retardants, dibromoneopentyl glycol and tribromoneopentyl alcohol. *Biodegradation* **20**, 621-7.
118. Wackett, L. P. (2004). Evolution of Enzymes for the Metabolism of New Chemical Inputs into the Environment. *Journal of Biological Chemistry* **279**, 41259-41262.
119. Chatterjee, D. K. & Chakrabarty, A. M. (1982). Genetic rearrangements in plasmids specifying total degradation of chlorinated benzoic acids. *Molecular and General Genetics MGG* **188**, 279-285.
120. Chaudhry, G. R. & Huang, G. H. (1988). Isolation and characterization of a new plasmid from a Flavobacterium sp. which carries the genes for degradation of 2,4-dichlorophenoxyacetate. *Journal of Bacteriology* **170**, 3897-3902.
121. Don, R. H. & Pemberton, J. M. (1981). Properties of six pesticide degradation plasmids isolated from Alcaligenes paradoxus and Alcaligenes eutrophus. *Journal of Bacteriology* **145**, 681-686.
122. Kawasaki, H., Tsuda, K., Matsushita, I. & Tonomura, K. (1992). Lack of homology between two haloacetate dehalogenase genes encoded on a plasmid from Moraxella sp. strain B. *Journal of General Microbiology* **138**, 1317-1323.
123. Poelarends, G. J., Kulakov, L. A., Larkin, M. J., van Hyckama Vlieg, J. E. T. & Janssen, D. B. (2000). Roles of Horizontal Gene Transfer and Gene Integration in Evolution of 1,3-Dichloropropene- and 1,2-Dibromoethane-Degradative Pathways. *Journal of Bacteriology* **182**, 2191-2199.
124. Fukumori, F. & Saint, C. P. (1997). Nucleotide sequences and regulational analysis of genes involved in conversion of aniline to catechol in *Pseudomonas putida* UCC22(pTDN1). *Journal of Bacteriology* **179**, 399-408.
125. Dogra, C., Raina, V., Pal, R., Suar, M., Lal, S., Gartemann, K.-H., Holliger, C., van der Meer, J. R. & Lal, R. (2004). Organization of lin Genes and IS6100 among Different Strains of Hexachlorocyclohexane-Degrading *Sphingomonas paucimobilis*: Evidence for Horizontal Gene Transfer. *Journal of Bacteriology* **186**, 2225-2235.

126. Damborský, J. & Koča, J. (1999). Analysis of the reaction mechanism and substrate specificity of haloalkane dehalogenases by sequential and structural comparisons. *Protein Engineering* **12**, 989-998.
127. Ollis, D. L., Cheah, E., Cygler, M., Dijkstra, B., Frolov, F., Franken, S. M., Harel, M., Remington, S. J., Silman, I., Schrag, J. & et al. (1992). The alpha/beta hydrolase fold. *Protein Eng* **5**, 197-211.
128. Holmquist, M. (2000). Alpha/Beta-hydrolase fold enzymes: structures, functions and mechanisms. *Curr Protein Pept Sci* **1**, 209-35.
129. Carr, P. D. & Ollis, D. L. (2009). Alpha/beta hydrolase fold: an update. *Protein Pept Lett* **16**, 1137-48.
130. Jochens, H., Hesseler, M., Stiba, K., Padhi, S. K., Kazlauskas, R. J. & Bornscheuer, U. T. (2011). Protein Engineering of α/β -Hydrolase Fold Enzymes. *ChemBioChem* **12**, 1508-1517.
131. Froede, H. C. & Wilson, I. B. (1984). Direct determination of acetyl-enzyme intermediate in the acetylcholinesterase-catalyzed hydrolysis of acetylcholine and acetylthiocholine. *Journal of Biological Chemistry* **259**, 11010-11013.
132. Douglas, K. T., Nakagawa, Y. & Kaiser, E. T. (1976). Mechanistic studies of carboxypeptidase Y. Kinetic detection of an acyl-enzyme intermediate in trimethylacetate esterase action. *Journal of the American Chemical Society* **98**, 8231-8236.
133. Chovancová, E., Kosinski, J., Bujnicki, J. M. & Damborský, J. (2007). Phylogenetic analysis of haloalkane dehalogenases. *Proteins: Structure, Function, and Bioinformatics* **67**, 305-316.
134. Nagata, Y., Miyauchi, K., Damborsky, J., Manova, K., Ansorgova, A. & Takagi, M. (1997). Purification and characterization of a haloalkane dehalogenase of a new substrate class from a gamma-hexachlorocyclohexane-degrading bacterium, *Sphingomonas paucimobilis* UT26. *Appl Environ Microbiol* **63**, 3707-10.
135. Chan, P. W. Y., Yakunin, A. F., Edwards, E. A. & Pai, E. F. (2011). Mapping the Reaction Coordinates of Enzymatic Defluorination. *Journal of the American Chemical Society* **133**, 7461-7468.
136. Krooshof, G. H., Floris, R., Tepper, A. W. J. W. & Janssen, D. B. (1999). Thermodynamic analysis of halide binding to haloalkane dehalogenase suggests the occurrence of large conformational changes. *Protein Science* **8**, 355-360.
137. Janssen, D. B. (2004). Evolving haloalkane dehalogenases. *Curr Opin Chem Biol* **8**, 150-9.
138. Keuning, S., Janssen, D. B. & Witholt, B. (1985). Purification and characterization of hydrolytic haloalkane dehalogenase from *Xanthobacter autotrophicus* GJ10. *Journal of Bacteriology* **163**, 635-639.
139. Stucki, G. & Thüer, M. (1994). Increased removal capacity for 1,2-dichloroethane by biological modification of the granular activated carbon process. *Applied Microbiology and Biotechnology* **42**, 167-172.
140. Bidanova, S., Chaloupkova, R., Damborský, J. & Prokop, Z. (2010). Development of an enzymatic fiber-optic biosensor for detection of halogenated hydrocarbons. *Analytical and Bioanalytical Chemistry* **398**, 1891-1898.
141. Prokop, Z., Opluštil, F., DeFrank, J. & Damborský, J. (2006). Enzymes fight chemical weapons. *Biotechnology Journal* **1**, 1370-1380.
142. Los, G. V., Encell, L. P., McDougall, M. G., Hartzell, D. D., Karassina, N., Zimprich, C., Wood, M. G., Learish, R., Ohana, R. F., Urh, M., Simpson, D., Mendez, J., Zimmerman, K., Otto, P., Vidugiris, G., Zhu, J., Darzins, A., Klaubert, D. H., Bulleit, R. F. & Wood, K. V. (2008). HaloTag: A Novel Protein Labeling Technology for Cell Imaging and Protein Analysis. *ACS Chemical Biology* **3**, 373-382.
143. Paul E, S. (1999). Dehalogenases applied to industrial-scale biocatalysis. *Current Opinion in Biotechnology* **10**, 365-369.
144. Franken, S. M., Rozeboom, H. J., Kalk, K. H. & Dijkstra, B. W. (1991). Crystal structure of haloalkane dehalogenase: an enzyme to detoxify halogenated alkanes. *Embo J* **10**, 1297-302.

145. Newman, J., Peat, T. S., Richard, R., Kan, L., Swanson, P. E., Affholter, J. A., Holmes, I. H., Schindler, J. F., Unkefer, C. J. & Terwilliger, T. C. (1999). Haloalkane dehalogenases: structure of a Rhodococcus enzyme. *Biochemistry* **38**, 16105-16114.
146. Marek, J., Vevodova, J., Smatanova, I. K., Nagata, Y., Svensson, L. A., Newman, J., Takagi, M. & Damborsky, J. (2000). Crystal structure of the haloalkane dehalogenase from *Sphingomonas paucimobilis* UT26. *Biochemistry* **39**, 14082-6.
147. Mazumdar, P. A., Hulecki, J. C., Cherney, M. M., Garen, C. R. & James, M. N. G. (2008). X-ray crystal structure of *Mycobacterium tuberculosis* haloalkane dehalogenase Rv2579. *Biochim Biophys Acta* **1784**, 351-362.
148. Prokop, Z., Sato, Y., Brezovsky, J., Mozga, T., Chaloupkova, R., Koudelakova, T., Jerabek, P., Stepankova, V., Natsume, R., van Leeuwen, J. G. E., Janssen, D. B., Florian, J., Nagata, Y., Senda, T. & Damborsky, J. (2010). Enantioselectivity of Haloalkane Dehalogenases and its Modulation by Surface Loop Engineering. *Angewandte Chemie International Edition* **49**, 6111-6115.
149. Iizuka, T., Jojima, Y., Fudou, R., Hiraishi, A., Ahn, J.-W. & Yamanaka, S. (2003). *Plesiocystis pacifica* gen. nov., sp. nov., a marine myxobacterium that contains dihydrogenated menaquinone, isolated from the Pacific coasts of Japan. *Int J Syst Evol Microbiol* **53**, 189-195.
150. Bogdanovic, X., Hesseler, M., Palm, G. J., Bornscheuer, U. T. & Hinrichs, W. (2010). Crystallization and preliminary X-ray diffraction studies of the putative haloalkane dehalogenase DppA from *Plesiocystis pacifica* SIR-I. *Acta Crystallogr Sect F Struct Biol Cryst Commun* **66**, 828-30.
151. Verschueren, K. H. G., Franken, S. M., Rozeboom, H. J., Kalk, K. H. & Dijkstra, B. W. (1993). Refined X-ray Structures of Haloalkane Dehalogenase at pH 6·2 and pH 8·2 and Implications for the Reaction Mechanism. *J Mol Biol* **232**, 856-872.
152. Schrag, J. D., Winkler, F. K. & Cygler, M. (1992). Pancreatic lipases: evolutionary intermediates in a positional change of catalytic carboxylates? *Journal of Biological Chemistry* **267**, 4300-3.
153. Blow, D. (1990). More of the catalytic triad. *Nature* **343**, 694-695.
154. Pries, F., van den Wijngaard, A. J., Bos, R., Pentenga, M. & Janssen, D. B. (1994). The role of spontaneous cap domain mutations in haloalkane dehalogenase specificity and evolution. *J Biol Chem* **269**, 17490-4.
155. Damborsky, J., Chaloupkova, R., Pavlova, M., Chovancova, E. & Brezovsky, J. (2010). Structure-Function Relationships and Engineering of Haloalkane Dehalogenases. In *Handbook of Hydrocarbon and Lipid Microbiology* (Timmis, K. N., ed.), pp. 1081-1098. Springer Berlin Heidelberg.
156. Chaloupkova, R., Sykorova, J., Prokop, Z., Jesenska, A., Monincova, M., Pavlova, M., Tsuda, M., Nagata, Y. & Damborsky, J. (2003). Modification of activity and specificity of haloalkane dehalogenase from *Sphingomonas paucimobilis* UT26 by engineering of its entrance tunnel. *J Biol Chem* **278**, 52622-8.

Publikationsliste

Im Rahmen dieser Arbeit diskutierte Publikationen und Anteile der jeweiligen Autoren:

Veröffentlichung I: Xenia Bogdanović, Rajesh K. Singh, Johanna Hentschke, Bjarnheiður K. Guðmundsdóttir and Winfried Hinrichs. *Crystallization and preliminary X-ray diffraction studies of AsaP1_{E294A} and AsaP1_{E294Q}, two inactive mutants of the toxic zinc metallopeptidase AsaP1 from Aeromonas salmonicida subsp. *achromogenes* AsaP1.* *Acta Cryst.* (2009). F65, 695–697

X. Bogdanović: Proteinexpression, -Reinigung und -Kristallisation, Aufnahme der Datensätze und Auswertung, Verfassen des Manuskripts; R. K. Singh: Unterstützung bei der Datensammlung; J. Hentschke: Konstruktion der Expressionsstämme; B. K. Guðmundsdóttir: Bereitstellung der Expressionsstämme im Rahmen der Kooperation, Diskussion des Manuskripts; W. Hinrichs: Diskussion des Manuskripts

Veröffentlichung II: Xenia Bogdanović and Winfried Hinrichs. *Influence of temperature during crystallization setup on precipitate formation and crystal shape of a metalloendopeptidase.* *Acta Cryst* (2011). F67, 421-423

X. Bogdanović: Alle experimentellen Arbeiten, Verfassen und Diskussion des Manuskriptes; W. Hinrichs: Diskussion des Manuskripts

Veröffentlichung III: Johanna Schwenteit*, Xenia Bogdanović*, Olafur H. Friðjónsson, Arnthor Aevarsson, Uwe T. Bornscheuer, Winfried Hinrichs and Bjarnheiður K. Guðmundsdóttir. *Construction of four toxoids of AsaP1, a lethal toxic aspzincin metalloendopeptidase of Aeromonas salmonicida subsp. *achromogenes*, and studies of its activity and processing.* Submitted.

J. Schwenteit: Toxoid-Konstruktion, Herstellung der Expressionsstämme, Wachstumskurve und caseinolytische Aktivität, Analyse der Pathogenität und Letalität der Toxoide, Verfassen und Diskussion des Manuskripts; X. Bogdanović: Proteinreinigung, Nachweis der autoproteolytischen Prozessierung, Überprüfung des Expressionslevels sowie der Lokalisation der Toxoide, Verfassen und Diskussion des Manuskripts; O. H. Friðjónsson: Betreuung der Toxoid-Konstruktion und molekularbiologischer Arbeiten; A. Aevarsson: Unterstützung bei der Planung der Toxoide; U. T. Bornscheuer: Korrektur und Betreuung der experimentellen Arbeiten von Johanna Schwenteit, Beitrag zur Diskussion; W. Hinrichs: Korrektur und Betreuung der experimentellen Arbeiten von Xenia Bogdanović, Beitrag zur Diskussion ; B. K. Guðmundsdóttir: Unterstützung und Aufsicht der Tierversuche, Korrektur und Diskussion des Manuskript

Veröffentlichung IV: Xenia Bogdanović, Johanna Schwenteit, Rajesh K. Singh, Bjarnheiður K. Guðmundsdóttir and Winfried Hinrichs. *Structure of two different inactive mutants of AsaP1 an aspzincin metalloendopeptidase in complex with its propeptide.* Manuscript in Vorbereitung.

X. Bogdanović: Protein-Expression, -Reinigung und -Kristallisation, Datensammlung und Prozessierung, Strukturlösung, Refinement und Analyse der Struktur, Verfassen und Diskussion des Manuskripts; J. Schwenteit: Konstruktion der Expressionsstämme und Diskussion des Manuskriptes; R. K. Singh: Unterstützung bei der Datensammlung; B. K. Guðmundsdóttir und W. Hinrichs: Korrektur und Diskussion des Manuskripts

Veröffentlichung V: **Xenia Bogdanović**, Martin Hesseler, Gottfried J. Palm, Uwe T. Bornscheuer and Winfried Hinrichs. *Crystallization and preliminary X-ray diffraction studies of the putative haloalkane dehalogenase DppA from Plesiocystis pacifica SIR-I*. **Acta Cryst (2010) F66**, 828–830

X. Bogdanović: Proteinkristallisation, Datensammlung und Auswertung, Verfassen und Diskussion des Manuskriptes; M. Hesseler: Konstruktion des Expressionsstammes, Proteinreinigung, Verfassen des Manuskriptes; G. J. Palm: Unterstützung beim Indizieren des Datensatzes; U. T. Bornscheuer: Betreuung der experimentellen Arbeiten von Martin Hesseler, Diskussion des Manuskriptes; W. Hinrichs: Betreuung der experimentellen Arbeiten von Xenia Bogdanovic, Diskussion des Manuskriptes.

Veröffentlichung VIII: Martin Hesseler*, **Xenia Bogdanović***, Aurelio Hidalgo, Jose Berenguer, Gottfried J. Palm, Winfried Hinrichs and Uwe T. Bornscheuer. *Cloning, functional expression, biochemical characterization, and structural analysis of a haloalkane dehalogenase from Plesiocystis pacifica SIR-1*. **Appl Microbiol Biotechnol (2011)** 91:1049–1060

M. Hesseler, A. Hidalgo, J. Berenguer: Konstruktion des Expressionsstammes, Proteinreinigung, Untersuchungen zur Substratspezifität, Bestimmung von Temperatur- und pH-Optima für enzymatische Aktivität, Analyse der Struktur, Docking-Experimente, Verfassen und Diskussion des Manuskriptes; X. Bogdanović: Kristallisation, Datensammlung und -Prozessierung, Strukturlösung, Refinement und Analyse der Struktur, Verfassen und Diskussion des Manuskriptes; G. J. Palm: Unterstützung beim Indizieren des Datensatzes; W. Hinrichs und U. T. Bornscheuer: Diskussion und Korrektur des Manuskriptes.

* Gleichberechtigte Erstautoren

Journal name: VETERINARY MICROBIOLOGY

Title:

Toxoid construction of AsaP1, a lethal toxic aspzinin metalloendopeptidase of *Aeromonas salmonicida* subsp. *achromogenes*, and studies of its activity and processing

A running head title:

AsaP1: activity, processing and immunogenicity of the aspzincin metalloendopeptidase

Authors: Johanna Schwenteit^{1, 2‡}, Xenia Bogdanović^{3‡}, Olafur H. Fridjonsson⁴, Arnthor

Aevarsson⁴, Uwe T. Bornscheuer², Winfried Hinrichs³ and Bjarnheidur K. Gudmundsdottir^{1*}

¹ Institute for Experimental Pathology, University of Iceland, Keldur v/Vesturlandsveg, IS-112 Reykjavík, Iceland.

² Institute of Biochemistry, Dept. of Biotechnology and Enzyme Catalysis and ³ Dept. of Structural Biology, Greifswald University, Felix Hausdorff-Str. 4, 17487 Greifswald, Germany.

⁴ Matís ohf, Vínlandsleið 12, 113 Reykjavík, Iceland

E-mails in the same order

johanna.schwenteit@gmx.de

xenia.bogdanovic@uni-greifswald.de

olafur.h.fridjonsson@matis.is

arnthor.aevarsson@matis.is

uwe.bornscheuer@uni-greifswald.de

winfried.hinrichs@uni-greifswald.de

27 bjarngud@hi.is

28

29 [‡] authors with equal contribution

30 *Corresponding author: Mailing address: Institute for Experimental Pathology, University of
31 Iceland, Keldur v/Vesturlandsveg, IS-112 Reykjavík. Phone: +354 5674700 Fax: +354
32 5673979. E-mail: bjarngud@hi.is

33

34 ABSTRACT

35 AsaP1 is a toxic aspzincin metalloendopeptidase secreted by the fish pathogen *Aeromonas*
36 *salmonicida* subsp. *achromogenes*. The protease is highly immunogenic and antibodies
37 against AsaP1 provide passive protection against infection with *A. salmonicida* subsp.
38 *achromogenes*. The protease is expressed as 37 kDa pre-pro-protein and processed to an
39 active enzyme of 19 kDa in *A. salmonicida* subsp. *achromogenes*.

40 Recombinant expression of AsaP1_{rec} in *E. coli* resulted in a protease of 22 kDa that is not
41 secreted. AsaP1_{rec} induces pathological changes in Atlantic salmon comparable to those
42 induced by native AsaP1_{wt}.

43 Toxoids were realized by single exchange of an amino acid residue in the active site region
44 of the protease. Four different AsaP1 mutants (AsaP1_{E294A}, AsaP1_{E294Q}, AsaP1_{Y309A} and
45 AsaP1_{Y309F}) were successfully constructed by one step site directed mutagenesis, expressed in
46 *E. coli* BL21 C43 as pre-pro-protein and purified by His-tag affinity chromatography and gel
47 filtration.

48 Three of the resulting mutants (AsaP1_{E294A}, AsaP1_{E294Q} and AsaP1_{Y309A}) were not
49 caseinolytic active and are detected as unprocessed pre-pro-proteins of 37 kDa. Caseinolytic
50 active AsaP1_{rec} and a mutant with reduced activity, AsaP1_{Y309F}, were processed to a size of
51 22 kDa. Furthermore AsaP1_{rec} is able to process the inactive mutants to the mature size of
52 22 kDa, allowing the conclusion that AsaP1 is autocatalytically processed.

53 All four mutants AsaP1_{E294A}, AsaP1_{E294Q}, AsaP1_{Y309A} and AsaP1_{Y309F} are non-toxic in fish
54 but induce a specific anti-AsaP1 antibody response in Arctic charr and are therefore true
55 toxoids.

56

57 KEYWORDS

58 *Aeromonas salmonicida* subsp. *achromogenes*; AsaP1; Aspzincin metalloendopeptidase;

59 Toxoid; Autoprocessing

60

61 1. Introduction

62 *Aeromonas salmonicida* subsp. *achromogenes* is the causative agent of atypical furunculosis
63 in many fish species, including Atlantic salmon (*Salmon salar*, L.), Arctic charr (*Salvelinus*
64 *alpinus*, L.), rainbow trout (*Oncorhynchus mykiss*, Walbaum), Atlantic cod (*Gadus morhua*,
65 L.), and Atlantic halibut (*Hippoglossus hippoglossus*, L.) (Gudmundsdottir and Bjornsdottir,
66 2007).

67 It has been shown that detoxified, concentrated extracellular products (ECP) of
68 *Aeromonas salmonicida* subsp. *achromogenes* induces a better immune protection against
69 atypical furunculosis in Atlantic salmon than killed bacterial cells. The protection correlated
70 with an increased antibody response against the extracellular protease AsaP1
71 (Gudmundsdottir and Magnadottir, 1997). AsaP1 is a major extracellular virulence factor of
72 *A. salmonicida* subsp. *achromogenes*, with a LD₅₀ of 30 ng/g fish (Arnadottir et al., 2009;
73 Gudmundsdottir et al., 1990). Expression of the protease is quorum sensing regulated
74 (Schwenteit et al., 2011).

75 AsaP1 is a M35 aspzincin metalloendopeptidase, expressed as a precursor with
76 propeptide and signal sequence (37 kDa) and is processed to the 19 kDa mature enzyme in
77 *A. salmonicida* subsp. *achromogenes*. AsaP1 was successfully cloned in *Escherichia coli*
78 resulting in recombinant AsaP1_{rec} for construction of an AsaP1 deficient strain of *A.*
79 *salmonicida* subsp. *achromogenes* (Arnadottir et al., 2009). Extracellular proteases of Gram-
80 negative bacteria are usually expressed as pre-pro-peptides comprising a signal sequence, a
81 propeptide and the protease domain. The signal sequence promotes translocation across the
82 cytoplasmic membrane by a sec-dependent, general secretory pathway, whereas several
83 different functions have been assigned to the propeptide. Activation of bacterial
84 metallopeptidases by intramolecular autocatalysis is well known (Gao et al., 2010).
85 Propeptide functions have been associated with inhibition of protease activity within the
86 bacterial cell and chaperone activity (Häse and Finkelstein, 1993). For many proteases,

87 including AsaP1, the exact function of the propeptide is still unknown as well as the precise
88 mechanism of maturation.

89 Peptidases in family M35 contain two zinc binding histidines and a catalytic glutamate
90 in a HExxH motif. The side chain of Glu supports the nucleophilic attack of a water molecule
91 on the scissile peptide bond (Fushimi et al., 1999). A third ligand is an Asp located in the
92 highly conserved aspzincin motif GTxDxxYG; it also contains a Tyr that stabilizes the
93 tetrahedral intermediate of the catalyzed reaction, comparable to the oxyanion hole of serine
94 proteases (Bryan et al., 1986; Kraut, 1977). Furthermore, it may provide a hydrophobic
95 environment in the substrate binding site supporting the substrate specificity of the enzyme
96 (Hori et al., 2001).

97 There are several studies demonstrating the efficacy of toxoid enriched vaccines in
98 evoking protective immunity in fish (Collado et al., 2000; Magariños et al., 1994; Santos et
99 al., 1991). The aims of this study were to construct AsaP1 toxoids by exchanging catalytically
100 important amino acids.

101 2. Material and Methods

102 2.1 *Bacterial strains, plasmids and culture conditions*

103 *E. coli* BL21 C43 [OverExpress C43 (DE3): F⁻OmpT, hsdSB (rB⁻, mB⁻), gal, dcm (DE3)]
104 (Dumon-Seignovert et al., 2004) was used as expression strain, whereas *E. coli* TOP10
105 [F⁻mcrA, Δ(mrr-sdRMS-mcrBC), Φ80lacZΔM15, ΔlacX74, recA1araD139, Δ(ara-leu)7697,
106 galU, galK, rpsL, (StrR) endA1, nupGcells] (InvitrogenTM) was used for cloning. *E. coli*
107 strains were routinely grown in LB-media (Bertani, 1951) containing 100 µg/ml ampicillin at
108 37°C with 200 rpm agitation. If necessary, 1.5% agar was added to the media. Bacterial
109 growth was monitored by OD measurement at 600 nm.

110 The plasmid pTriplEx_*asaP1* previously constructed (Arnadottir et al., 2009) was used
111 for isolation of the *asaP1* gene (GenBank: AF550405.3) and pJOE3075 (Wegerer et al., 2008)
112 was used for over-expression of AsaP1 and its mutants. *A. salmonicida* subsp. *achromogenes*,
113 strain Keldur265-87, was used for isolation of native AsaP1 (Gudmundsdottir et al., 1990).

114

115 2.2 *Construction of AsaP1 mutants*

116 To clone the *asaP1* gene two primers (Table 1; *asaP1*-nde-f and *asaP1*-bgl-h-r) were used to
117 amplify a 1032 bp gene fragment in the plasmid pTriplEx_*asaP1*. The primers included
118 restriction sites for cloning into pJOE3075 by double digest and ligation.

119 The resulting plasmid pJOE_*asaP1* was used as a template for further mutant construction.

120 Based on comparison to other metalloproteases, two amino acid residues were assumed to
121 play an important role either in substrate binding or catalytic mechanism: Glu294 and Tyr309.

122 One-step site-directed mutagenesis (5 µl 10 x HF-buffer; 200 ng template; 1 µl f-primer [100
123 pmol]; 1 µl r-primer [100 pmol]; 200 µM dNTP's; 2U Pfx (Invitrogen) ad 50 µl) (94°C 3';
124 (94°C 1'; 52°C 1'; 68°C 10') x 15; 68°C 1 h), adapted from a previously described method
125 (Zheng et al., 2004), was used to exchange the two amino acid residues, E294 and Y309, by
126 single point mutations (*asaP1*_{E294A}, *asaP1*_{E294Q} and *asaP1*_{Y309F}) and two point mutations

127 (*asaP1_{Y309A}*) using primers listed in Table 1. Mutants were screened by digestion of an
128 additional *Kpn*I restriction site introduced in one of the corresponding primers by a silent
129 point mutation. The successful construction of all four mutants, AsaP1_{E294Q}, AsaP1_{E294A},
130 AsaP1_{Y309F} and AsaP1_{Y309A} was confirmed by sequencing.

131

132

133 *2.3 Protein expression and purification*

134 Expression of recombinant *asaP1* and its mutant genes (*asaP1_{E294}*, *asaP1_{E294Q}*, *asaP1_{Y309A}*
135 and *asaP1_{Y309F}*) in pJOE E3075 in *E. coli* BL21 C43 was induced by 1 mM L-rhamnose (final
136 concentration) at a bacterial OD_{600 nm} of 0.5 at 37°C, subsequently the temperature was
137 reduced to 22°C. To monitor bacterial growth, an empty *E. coli* BL21 strain served as control.
138 Cells were incubated overnight, harvested by centrifugation 15 min at 1800 x g, resuspended
139 in 20 mM Tris–HCl pH 7.6 containing 300 mM NaCl and lysed by sonication (1min, 50%).
140 The crude extract was applied to a Ni²⁺- immobilized metal affinity (PorosMC)
141 chromatography column with 20 mM Tris–HCl pH 7.6, 300 mM NaCl, 50 mM imidazole.
142 The protein was eluted with 20 mM Tris–HCl pH 7.6, 300 mM NaCl, 200 mM imidazole
143 using a linear gradient from 0% to 100% elution buffer. Fractions containing recombinant
144 AsaP1 (AsaP1_{rec}), AsaP1_{E204A}, AsaP1_{E294Q}, AsaP1_{Y309A} or AsaP1_{Y309F} mutants were pooled
145 and concentrated by ultrafiltration before applying on a size exclusion chromatography
146 column (Superdex200). The buffer for gel filtration comprised 20 mM Tris–HCl pH 7.6 and
147 300 mM NaCl. The protein concentration was determined by UV absorption
148 ($\epsilon_{280\text{ nm}} = 31\ 400\ \text{M}^{-1}\ \text{cm}^{-1}$).

149

150

151 *2.4 Screening for expression level, protein localization and protein size*

152 Recombinant proteins were expressed for 3 h at 22 °C following induction, and then cells
153 were isolated by centrifugation as previously described in section 2.4. The pellets were
154 resuspended in spheroblast buffer (100 mM Tris-HCl ph 8.5, 0.5 mM EDTA, 500 mM
155 Saccharose) at 4°C and incubated on ice for 10 min before centrifugation for 20 min at
156 6000 × g. Supernatants were removed and the pellets incubated for 5 min at 37°C.
157 Afterwards, cells were resuspended in 50 ml cold water, incubated on ice for 10 min and
158 centrifuged for 30 min at 10000 × g. The pellets were resuspended in 2 ml of 20 mM Tris–
159 HCl pH 7.6, 300 mM NaCl and cells were lysed by sonication and centrifuged for 30 min at
160 13000 × g. Samples (20µl) were taken from the supernatants of each step and the final pellet.
161 The samples were mixed with sample buffer, heated 10 min at 96°C and applied on a 12%
162 SDS-PAGE (Laemmli, 1970). The gels were either stained with Coomassie Brilliant Blue
163 R250 or applied to Western blotting using polyclonal mouse α -AsaP1 antibody for protein
164 detection (Gudmundsdottir et al., 2003).

165

166

167 *2.5 Stability of AsaP1_{rec} and its mutants*

168 Protein samples used (1 mg/ml) were AsaP1_{E294Q}, AsaP1_{E294A} and AsaP1_{rec} purified by
169 affinity chromatography, but without size exclusion chromatography. Stability of the proteins
170 was analysed at 4°C and 20°C, respectively. Furthermore, mixtures of recombinant AsaP1_{rec}
171 either with AsaP1_{E294Q} or AsaP1_{E294A} were analysed with and without 50 mM EDTA.
172 Samples were fractionated to 10 µl each and incubated separately for 1, 3, 5, 7, 9, 12, 14, 17,
173 and 18 d before adding sample buffer and heating for 10 min at 95°C. Samples were analysed
174 by 12% SDS-PAGE and stained by Coomassie Brilliant Blue R250.

175

176

177 *2.6 Experimental fish*

178 Atlantic salmon (*Salmo salar*, L.) fingerlings, mean weight 30.0 g, from Stofnfiskur, Iceland
179 were used for estimation of the pathogenic and lethal effect of proteins and juvenile Arctic
180 charr (*Salvelinus alpinus*, L.), mean weight 34.1 g, from Íslandsbleikja, Iceland were used for
181 immunizations. The fish were kept in 170 l (salmon) and 400 l (charr) tanks with continuously
182 running fresh water at $10 \pm 2^{\circ}\text{C}$ and were acclimatized for one week prior to treatment. Prior
183 to intra peritoneal (i.p.) injection, all fish were anaesthetised with MS222 (Pharmaq, Vistor
184 hf.) and marked with Alcian blue dye (salmon) or Visible Implant Fluorescent Elastomer dye
185 (Northwest Marine Technology, Salisbury, U.K) (charr). The density of fish in the tanks was
186 3 kg/tank or less. Oxygen concentration, temperature, and mortality were monitored daily
187 during the experiments. The fish were free of infections, according to standard routine
188 diagnostics performed at the Icelandic Fish-Disease Reference Laboratory, The experiments
189 were approved and performed according to the Icelandic Animal Research Authority
190 (approval no. YDL03080041/023BE).

191
192
193 *2.7 Analysis of lethality and pathogenicity of recombinant proteins*
194 Two salmon fingerlings were in each experimental group. Estimation of lethality was
195 performed by intraperitoneal (i.p.) injection of His-tag purified AsaP1_{rec} and the respective
196 AsaP1 mutants (0.18 µg/ g fish). Mortality was monitored daily for 7 days. Pathogenicity of
197 native (AsaP1_{wt}) and recombinant (AsaP1_{rec}) AsaP1 was compared by i.p. injection with 1 ng/
198 g fish or 5 ng/ g fish protein dissolved in 100 µl of phosphate buffered saline (PBS). Control
199 fish received 100 µl PBS. Gross pathological changes were described 48 h post injection and
200 samples taken from liver, kidney, spleen, and heart for histological examination. The samples
201 were fixed in 10% buffered formalin, embedded in paraffin wax, sectioned and stained with
202 Giemsa before microscopic examination.

203

204 2.8 Analysis of proteolytic activity of AsaP1 mutants

205 Proteolytic activity was analysed by radial diffusion method and substrate SDS-PAGE as
206 previously described (Gudmundsdóttir, 1996). Casein-agarose plates with 4 mm wells were
207 used for radial diffusion analysis and 12% SDS gels containing 0.1% casein and stained with
208 Coomassie Brilliant Blue R250 were used for substrate SDS-PAGE.

209

210

211 2.9 Analysis of immunogenicity of AsaP1 mutants in Arctic charr

212 Arctic charr were immunized i.p. (100 µl) with the four AsaP1 mutants (AsaP1_{E294A},
213 AsaP1_{E294Q}, AsaP1_{Y309A} and AsaP1_{Y309F}) (100 µg/ fish) emulsified with Freund's incomplete
214 adjuvant (FIA). The mutants AsaP1_{E294A} and AsaP1_{Y309F} were also injected without FIA.

215 Fish were cultivated for 12 weeks after immunization, before caudal blood was sampled. Sera
216 were isolated from each sample as previously described (Gudmundsdottir and Magnadottir,
217 1997) and kept at -20°C until used.

218 Specific antibody activity against AsaP1 was analysed by a double sandwich ELISA,
219 modified of a previously described method (Magnadottir and Gudmundsdottir, 1992), and
220 confirmed by Western blot. All samples were analysed in duplicates at 1:50 dilution. The
221 antigen used was ECP of *A. salmonicida* subsp. *achromogenes*, strain Keldur265-87, freshly
222 prepared by cellophane overlay method (Gudmundsdottir et al., 2003), in coating buffer
223 (Sigma) (20 µg protein/ ml). Bound serum antibodies were detected by polyclonal mouse α-
224 salmon IgM antibodies 1:1000 (Magnadottir and Gudmundsdottir, 1992), followed by
225 conjugated goat α-mouse antibody (Sigma) labeled with alkaline phosphatase 1:1000. Color
226 was developed with *p*-nitophenyl phosphate (Sigma) and reaction stopped using 3 M NaOH.
227 OD was read at 405 nm. Antibody endpoint titre was determined with the same ELISA assay
228 for five fish per group giving high OD readings. Sera were analysed in dilution series from
229 1:50 up to 1:12400. Twice the average value of OD readings at 405 nm of the PBS injected

230 control group was considered to be the cut-off value in antibody titre calculation ($OD_{405nm} =$
231 0.16). Immunogenicity of AsaP1_{rec} and the four AsaP1 mutants was analysed in Western blots
232 immunostained with sera from immunized charr, using immunostaining with polyclonal
233 murine α -AsaP1 antibodies as a positive control and sera from PBS-injected fish as a negative
234 control. ECP of strain Keldur265-87 was used as an antigen for native AsaP1.

235

236 *2.10 Statistical analysis*

237 Growth rates of *E. coli* expressing AsaP1_{rec} and its four mutants were diagrammed and
238 statistical differences analysed by GraphPad Prism5. Student's t-test with Welsh correction
239 was used to estimate statistical differences of ELISA readings compared to the PBS injected
240 control group.

241 3. Results

242 *3.1 AsaP1 mutant construction and expression*

243 Two amino acid residues, Glu294 and Tyr309, of AsaP1, were successfully replaced by
244 glutamine and alanine in case of Glu294 and phenylalanine and alanine in case of Tyr309, by
245 site-directed mutagenesis.

246 All four AsaP1 mutants as well as the wild type protease were recombinantly
247 expressed in *E. coli* BL21 C43. Significant differences were detected in growth of the *E. coli*
248 strains expressing the different proteins (Figure 1). *E. coli* expressing AsaP1_{rec} was impaired
249 in growth with a 27-fold lower OD (0.23) than *E. coli* expressing the inactive mutant
250 AsaP1_{E294A} (OD = 6.3). *E. coli* expressing AsaP1_{Y309F} was growing to a higher OD than *E.*
251 *coli* expressing AsaP1_{rec}, but the growth was significantly lower than growth of *E. coli* cells
252 expressing the other three mutants. Furthermore, AsaP1_{rec} was processed in *E. coli* to the
253 mature size of 22 kDa, whereas it is processed to 19 kDa in *A. salmonicida* subsp.
254 *achromogenes* (data not shown). AsaP1_{E294A}, AsaP1_{E294Q} and AsaP1_{Y309A} were detected at 37
255 kDa, the size of the polypeptide with propeptide and protease domain. Only the mutant
256 AsaP1_{Y309F}, showing a reduced caseinolytic activity, was detected at 22 kDa (Figure 2),
257 corresponding to the size of AsaP1_{rec} expressed in *E. coli*. None of the five recombinant
258 proteins (AsaP1_{rec} and four AsaP1 mutants) expressed by *E. coli* were secreted, but found
259 within the expressing bacterial cell (Figure 3).

260

261 *3.2 Activity of the four AsaP1 mutants recombinant expressed in E. coli BL21 C43*

262 Three of four constructed AsaP1 mutants did not have detectable caseinolytic activity
263 (AsaP1_{E294A}, AsaP1_{E294Q} and AsaP1_{Y309A}). AsaP1_{Y309F} was still caseinolytic active, as
264 indicated by a 4 mm clearing zone in the radial diffusion assay and a clearing zone in the
265 substrate SDS-PAGE at 22 kDa (data not shown); though its activity was reduced compared

266 to the recombinant AsaP1_{rec} (7 mm) and the ECP of *A. salmonicida* subsp. *achromogenes*
267 Keldur265-87 (30 mm).

268 All fish injected with 180 ng/g fish of native or recombinant AsaP1_{rec} died within 12 h,
269 but none of the four AsaP1 mutants was lethal to salmon in this concentration. Fish injected
270 with PBS was not affected. Gross and microscopic changes obtained in fish injected with
271 sublethal doses of native (AsaP1_{wt}) or recombinant peptidase (AsaP1_{rec}) 48h post treatment
272 were comparable in all four fish. Gross pathological changes obtained were pale gills and
273 anemic viscera in the body cavity. Descriptions of histopathological changes are shown in
274 Table 2. The changes obtained are dose dependent and comparable to those described in
275 infected fish (Arnadottir et al., 2009).

276

277 *3.3 Stability of recombinant AsaP1 and its four mutants*

278 Protein samples of AsaP1_{E294A}, AsaP1_{E294Q} and AsaP1_{rec} were analysed by SDS-PAGE after
279 incubation at 4°C and 20°C for 10 and 18 days, respectively. The two inactive mutants
280 AsaP1_{E294A} and AsaP1_{E294Q} show equal stability, which is demonstrated in Figure 4 for
281 AsaP1_{E294A}. At 4°C, a strong band at 37 kDa was visible up to 18 days, indicating the
282 presence of the unprocessed enzyme, which is stable owing to inactivity of the mutant. In
283 principle, AsaP1_{E294A} at 20°C shows the same degradation pattern as at 4°C. However, the
284 protein is less stable, because the protein bands at a lower molecular weight are stronger and
285 the band at 37 kDa decreases faster. For AsaP1_{rec} only one faint band is visible at 22 kDa,
286 indicating the mature form of the protease, which is stable at 4°C up to 18 days, but at 20 °C
287 this band disappears at day 12. The protease is highly active and self-degradation is
288 presumably the reason for decreasing intensity.

289 A mixture of recombinant, still active AsaP1_{rec} with inactive AsaP1_{E294A} at 4°C shows
290 another degradation pattern than inactive AsaP1_{E294A}. The precursor at 37 kDa disappears and
291 there is one prominent band around 19 kDa at day 18. Recombinant AsaP1 mixed with

292 AsaP1_{E294A} at 20°C shows the same degradation pattern, in principle, but less degradation
293 products. A band at the size of the mature recombinant protease (22 kDa) appears at day 10.
294 At day 18 the prominent band has a size around 19 kDa, corresponding probably to a
295 denaturation product of the matured protease domain of the inactive mutant.

296 The mixture of recombinant AsaP1_{rec} and AsaP1_{E294A} with 500 mM EDTA at 4°C
297 shows the pre-pro-peptide at 37 kDa up to day 18 and only weak bands with faster mobility
298 on the gel, but no prominent band at 22 kDa or 19 kDa, respectively. At 20°C the band at
299 37 kDa is also stable and protein bands with faster mobility show the degradation pattern of
300 the inactive mutant AsaP1_{E294A}.

301

302 *3.4 AsaP1 mutants induce a specific antibody response in Arctic charr*

303 All four AsaP1 mutants induced an antibody response in Arctic charr, which was detected 12
304 weeks after immunization (Figure 5). All AsaP1 mutants were emulsified with Freund's
305 incomplete adjuvant (FIA) before immunization. Additionally the mutants AsaP1_{E294A} and
306 AsaP1_{Y309F} were also injected without adjuvant. Immunization with PBS emulsified in FIA
307 served as negative control.

308 Antibody activity of the different groups against the ECP of *A. salmonicida* subsp.
309 *achromogenes* (anti-AsaP1 antibody response) is shown in Figure 5A. Fish in the PBS-FIA
310 control group did not have a positive anti-AsaP1 antibody response.

311 Antibody response of fish injected with AsaP1_{E294A}-FIA, AsaP1_{Y309A}-FIA,
312 AsaP1_{Y309F}-FIA and AsaP1_{Y309F} differed significantly from the PBS-FIA group, but antibody
313 responses to AsaP1_{E294Q}-FIA and AsaP1_{E294A} were not significant ($p > 0.08$). A significant
314 difference ($p = 0.002$) was between the groups injected with AsaP1_{E294A}-FIA and AsaP1_{E294A}
315 without the adjuvant, indicating the importance of the adjuvant in enhancing the immune
316 response.

317 Anti-ECP endpoint titres of selected sera from 5 fish in each group are shown in
318 Figure 5 B. Fish in all groups had significant anti-AsaP1 titres ($p < 0.01$). The group
319 immunized with AsaP1_{E294A}-FIA had significantly higher titres than fish in the other groups
320 ($p < 0.05$), but difference between the other groups was not statistically significant ($p > 0.07$).

321 Specific antibody activity against AsaP1_{wt} was analysed by Western blot (Figure 6).
322 The results reveal that sera from all four groups of fish vaccinated by AsaP1 mutants
323 immunostained a dominant band with the size of AsaP1_{wt} (19 kDa) in the ECP.

324 The results from ELISA and Western blot analysis indicate that all four mutants
325 induced specific anti-AsaP1 immunity, but also that AsaP1_{E294A} has the highest antigenicity.

326

327

328 4. Discussion

329 In this study, toxoids of the extracellular protease AsaP1 of *A. salmonicida* subsp.
330 *achromogenes* were successfully constructed, recombinantly expressed and functionally
331 characterized. Toxoid construction was realized by point mutations in the *asaP1* gene
332 replacing single amino acid residues, which are assumed to be mandatory for the catalytic
333 mechanism. Furthermore, the AsaP1_{rec} protein was recombinantly expressed and isolated and
334 its activity including pathogenicity was compared to that of the native AsaP1_{wt} peptidase.

335 Glu294 within the conserved HExxH motif, which is crucial for catalysis in other zinc
336 peptidases (Hooper, 1994), was replaced by alanine and glutamine, resulting in the
337 caseinolytic inactive mutants AsaP1_{E294A} and AsaP1_{E294Q}, confirming the catalytic role of
338 Glu294. Within the central GTxDxxYG motif of aspzincin metalloproteases, Tyr309 has been
339 supposed to support substrate recognition and to stabilize the tetrahedral intermediate of the
340 catalyzed reaction (Hori et al., 2001), comparable to the oxyanion hole in serine proteases
341 (Bryan et al., 1986; Kraut, 1977). This amino acid residue was replaced by alanine and
342 phenylalanine in AsaP1_{Y309A} and AsaP1_{Y309F}, respectively.

343 Besides, the recombinant AsaP1_{rec} only AsaP1_{Y309F} shows caseinolytic activity
344 detected in a zymogram at 22 kDa, the size of the mature enzyme expressed in *E. coli*.
345 AsaP1_{Y309A} has no remaining caseinolytic activity, indicating the importance of Tyr309 in the
346 catalytic mechanism. Recombinant AsaP1_{rec} is caseinolytic active without any activation
347 procedure, in contrast to prodeuterolysin, that has to be activated by ZnCl₂ or incubation with
348 trypsin (Fushimi et al., 1999).

349 The other constructed mutants, AsaP1_{E294A}, AsaP1_{E294Q} and AsaP1_{Y309A} were
350 caseinolytic inactive, but all four mutants, including AsaP1_{Y309F} were found to be non-lethal
351 to Atlantic salmon despite a high injection dose. His-tag purified proteins were i.p. injected in
352 6 fold higher concentrations than the LD₅₀ of native AsaP1 purified from the ECP of *A.*
353 *salmonicida* subsp. *achromogenes*. The recombinant AsaP1 protease was highly aggressive

354 against the expressing *E. coli* strain, as indicated by decreasing optical density of *E. coli*
355 culture 7 hours after induction of AsaP1_{rec} expression. However caseinolytic activity was
356 reduced compared to native AsaP1. Pathogenicity of AsaP1_{rec} was comparable to that of
357 AsaP1_{wt}, in the injection doses studied.

358 *A. salmonicida* subsp. *achromogenes* secrets AsaP1_{wt} as 19 kDa mature enzyme
359 (Arnadottir et al., 2009; Gudmundsdottir et al., 1990), but AsaP1_{rec} is processed to a 22 kDa
360 mature enzyme in *E. coli* (Hvanndal, 2003). The present study shows that AsaP1_{rec} is, as
361 expected, not secreted, but found in the periplasma and cytoplasma, respectively. Loss in
362 activity of AsaP1_{rec} compared to AsaP1_{wt} is presumably caused by the different processing
363 status. It remains to be elucidated, whether AsaP1_{wt} is further processed by translocation over
364 the outer membrane, presumably leading to the 3 kDa size difference, or if there is another
365 reason.

366 The processing to the mature enzyme is strongly dependent on protease activity, as
367 inactive mutants of AsaP1 remained at the status of the unprocessed precursor, which is
368 indicated by the size of 37 kDa. AsaP1_{rec} was able to process inactive mutants in absence of
369 protease inhibitors. However, if EDTA was added, the inactive mutants, as well as AsaP1_{rec},
370 remained unprocessed. These results indicate an autocatalytic processing step, as suggested
371 for deuterolysin by Fushimi et al. (1999). Maturation processes of thermolysin like proteases
372 representing gluzincins and of astacin as an example for metzincins have been described in
373 literature (Gao et al., 2010; Guevara et al., 2010). The maturation mechanism of aspzincins is
374 only poorly described so far (Fushimi et al., 1999).

375 All four mutants are detectable by polyclonal, murine α -AsaP1 antibodies, showing that the
376 epitopes recognized by the antibodies are not lost by exchange of amino acids. Furthermore,
377 all four AsaP1 mutants are non-toxic, and immunogenic in Arctic charr. Antibodies in the sera
378 of Arctic charr, immunized with the different AsaP1 mutants, were specific against AsaP1_{wt}.

379 protease secreted by *A. salmonicida* subsp. *achromogenes*. These results show that four
380 toxoids were genetically established: AsaP1_{E294A}, AsaP1_{E294Q}, AsaP1_{Y309A} and AsaP1_{Y309F}.
381 The AsaP1_{E294A} mutant was the most potent immunogen of the four mutants and its
382 antigenicity was significantly better than that of AsaP1_{E294Q}. The difference is most likely due
383 to variations in the side chains of Ala and Glu, but more studies are required to describe its
384 nature. Antigenicity of AsaP1_{Y309A} and AsaP1_{Y309F} was comparable. It is noteworthy, that
385 AsaP1_{E294A} emulsified with adjuvant raised a significantly improved antibody response, in
386 contrast to its injection without adjuvant, demonstrating the importance of adjuvants for
387 vaccine development.

388 The toxoids of AsaP1 are interesting targets for vaccine development. AsaP1 is highly
389 immunogenic and passive immunization with anti-AsaP1 antibodies gives a protection against
390 *A. salmonicida* subsp. *achromogenes* infection in Atlantic salmon (*Salmo salar*, L.)
391 (Gudmundsdottir and Magnadottir, 1997). It has been reported that infection with an *asaP1*
392 deletion strain leads to an impaired virulence and weakened defence mechanisms in fish
393 (Arnadottir et al., 2009). It is possible to inactivate AsaP1 by formalin and heat treatment,
394 which may affect other important bacterial antigens. Studies on the diphtheria vaccine have
395 shown that the genetically inactivated toxin is much more efficient as vaccine compared to the
396 chemically inactivated toxin (Giannini et al., 1984; Robbins et al., 2005). The development of
397 the enzymatically inactive but highly immunogenic AsaP1_{E294A} toxoid is therefore considered
398 to be an improvement to the chemically inactivated toxin, considering the use of AsaP1 as a
399 vaccine component.

400 The human pathogens *Aeromonas hydrophila* and *Aeromonas caviae*, belonging to the
401 same genus as *A. salmonicida*, produce AsaP1-like proteases (Beatson et al., 2011; Seshadri et
402 al., 2006). This and the importance of the extracellular protease, AsaP1, in virulence of *A.*

403 *salmonicida* subsp. *achromogenes* makes it an interesting target for further studies on its
404 processing and the role of its pre-pro-peptide.

405 Further studies of the potency of the toxoids, especially the AsaP1_{E294A} toxoid, in
406 inducing protection against atypical furunculosis caused by *A. salmonicida* subsp.
407 *achromogenes* are also highly significant.

408

409 6. Acknowledgements

410 This project was funded by the Icelandic Centre for Research (RANNIS; R-090015/5384) and
411 the University of Iceland Research Found. We thank Britta Girbärdt and Leona Berndt for
412 their skilful technical assistance. Thanks are also due to the staff of Sandgerði for taking care
413 of the fish during challenge and immunization experiments.

414

- 415 7. References
- 416 Arnadottir, H., Hvanndal, I., Andresdottir, V., Burr, S.E., Frey, J., Gudmundsdottir, B.K.,
- 417 2009. The AsaP1 peptidase of *Aeromonas salmonicida* subsp. *achromogenes* is a
- 418 highly conserved deuterolysin metalloprotease (family M35) and a major virulence
- 419 factor. *J. Bacteriol.* 191, 403-410.
- 420 Beatson, S.A., das Gracas de Luna, M., Bachmann, N.L., Alikhan, N.F., Hanks, K.R.,
- 421 Sullivan, M.J., Wee, B.A., Freitas-Almeida, A.C., Dos Santos, P.A., de Melo, J.T.,
- 422 Squire, D.J., Cunningham, A.F., Fitzgerald, J.R., Henderson, I.R., 2011. Genome
- 423 sequence of the emerging pathogen *Aeromonas caviae*. *J. Bacteriol.* 193, 1286-1287.
- 424 Bertani, G., 1951. Studies on lysogenesis. I. The mode of phage liberation by lysogenic
- 425 *Escherichia coli*. *J. Bacteriol.* 62, 293-300.
- 426 Bryan, P., Pantoliano, M.W., Quill, S.G., Hsiao, H.Y., Poulos, T., 1986. Site-directed
- 427 mutagenesis and the role of the oxyanion hole in subtilisin. *Proc. Natl. Acad. Sci. USA*
- 428 83, 3743-3745.
- 429 Collado, R., Fouz, B., Sanjuan, E., Amaro, C., 2000. Effectiveness of different vaccine
- 430 formulations against vibriosis caused by *Vibrio vulnificus* serovar E (biotype 2) in
- 431 European eels *Anguilla anguilla*. *Dis. Aquat. Organ.* 43, 91-101.
- 432 Dumon-Seignovert, L., Cariot, G., Vuillard, L., 2004. The toxicity of recombinant proteins in
- 433 *Escherichia coli*: a comparison of overexpression in BL21(DE3), C41(DE3), and
- 434 C43(DE3). *Protein Expr. Purif.* 37, 203-206.
- 435 Fushimi, N., Ee, C.E., Nakajima, T., Ichishima, E., 1999. Aspzincin, a family of
- 436 metalloendopeptidases with a new zinc-binding motif. *J. Biol. Chem.* 274, 24195-
- 437 24201.
- 438 Gao, X., Wang, J., Yu, D.Q., Bian, F., Xie, B.B., Chen, X.L., Zhou, B.C., Lai, L.H., Wang,
- 439 Z.X., Wu, J.W., Zhang, Y.Z., 2010. Structural basis for the autoprocessing of zinc

- 440 metalloproteases in the thermolysin family. Proc. Natl. Acad. Sci. USA 107, 17569-
441 17574.
- 442 Giannini, G., Rappuoli, R., Ratti, G., 1984. The amino-acid sequence of two non-toxic
443 mutants of diphtheria toxin: CRM45 and CRM197. Nucleic Acids Res. 12, 4063-
444 4069.
- 445 Gudmundsdóttir, B.K., 1996. Comparison of extracellular proteases produced by *Aeromonas*
446 *salmonicida* strains, isolated from various fish species. J. Appl. Microbiol. 80, 105-
447 113.
- 448 Gudmundsdottir, B.K., Bjornsdottir, B., 2007. Vaccination against atypical furunculosis and
449 winter ulcer disease of fish. Vaccine. 25, 5512-5523.
- 450 Gudmundsdottir, B.K., Hastings, T.S., Ellis, A.E., 1990. Isolation of a new toxic protease
451 from a strain of *Aeromonas salmonicida* subspecies *achromogenes*. Dis. Aquat. Org.
452 9, 199-208.
- 453 Gudmundsdottir, B.K., Hvanndal, I., Bjornsdottir, B., Wagner, U., 2003. Analysis of
454 exotoxins produced by atypical isolates of *Aeromonas salmonicida*, by enzymatic and
455 serological methods. J. Fish. Dis. 26, 15-29.
- 456 Gudmundsdottir, B.K., Magnadottir, B., 1997. Protection of Atlantic salmon (*Salmo salar* L.)
457 against an experimental infection of *Aeromonas salmonicida* ssp. *achromogenes*. Fish
458 Shellfish Immunol. 7, 55-69.
- 459 Guevara, T., Yiallouros, I., Kappelhoff, R., Bissdorf, S., Stocker, W., Gomis-Ruth, F.X.,
460 2010. Proenzyme structure and activation of astacin metallopeptidase. J. Biol. Chem.
461 285, 13958-13965.
- 462 Häse, C.C., Finkelstein, R.A., 1993. Bacterial extracellular zinc-containing metalloproteases.
463 Microbiol. Rev. 57, 823-837.
- 464 Hooper, N.M., 1994. Families of zinc metalloproteases. FEBS Lett. 354, 1-6.

- 465 Hori, T., Kumasaka, T., Yamamoto, M., Nonaka, N., Tanaka, N., Hashimoto, Y., Ueki, U.,
466 Takio, K., 2001. Structure of a new 'aspzincin' metalloendopeptidase from *Grifola*
467 *frondosa*: implications for the catalytic mechanism and substrate specificity based on
468 several different crystal forms. *Acta Crystallogr.* 57, 361-368.
- 469 Hvannadal, I., 2003. A study of the gene enconding the bacterial protein toxin AsaP1 of
470 *Aeromonas salmonicida*. MSc Thesis. University of Iceland, Reykjavík.
- 471 Kraut, J., 1977. Serine proteases: structure and mechanism of catalysis. *Annu. Rev. Biochem.*
472 46, 331-358.
- 473 Laemmli, U., 1970. Cleavage of structural proteins during the assembly of the head of
474 bacteriophage T4. *Nature* 227, 680-685.
- 475 Magariños, B., Romalde, J.L., Santos, Y., Casal, J.F., Barja, J.L., Toranzo, A.E., 1994.
476 Vaccination trials on gilthead seabream (*Sparus aurata*) against *Pasteurella piscicida*.
477 *Aquaculture* 120, 201-208.
- 478 Magnadottir, B., Gudmundsdottir, B.K., 1992. A comparison of total and specific
479 immunoglobulin levels in healthy Atlantic salmon (*Salmo salar* L.) and in salmon
480 naturally infected with *Aeromonas salmonicida* subsp. *achromogenes*. *Vet. Immunol.*
481 *Immunopathol.* 32, 179-189.
- 482 Robbins, J.B., Schneerson, R., Trollfors, B., Sato, H., Sato, Y., Rappuoli, R., Keith, J.M.,
483 2005. The diphtheria and pertussis components of diphtheria-tetanus toxoids-pertussis
484 vaccine should be genetically inactivated mutant toxins. *J. Infect. Dis.* 191, 81-88.
- 485 Santos, Y., Bandin, I., Nunez, S., Gravningen, K., Toranzo, A.E., 1991. Protection of turbot,
486 *Scophthalmus maximus* (L.), and rainbow trout, *Oncorhynchus mykiss* (Richardson),
487 against vibriosis using two different vaccines. *J. Fish Dis.* 14, 407-411.
- 488 Schwenteit, J., Gram, L., Nielsen, K.F., Fridjonsson, O.H., Bornscheuer, U.T., Givskov, M.,
489 Gudmundsdottir, B.K., 2011. Quorum sensing in *Aeromonas salmonicida* subsp.

490 *achromogenes* and the effect of the autoinducer synthase AsaI on bacterial virulence.
491 Vet. Microbiol. 147, 389-397.
492 Seshadri, R., Joseph, S.W., Chopra, A.K., Sha, J., Shaw, J., Graf, J., Haft, D., Wu, M., Ren,
493 Q., Rosovitz, M.J., Madupu, R., Tallon, L., Kim, M., Jin, S., Vuong, H., Stine, O.C.,
494 Ali, A., Horneman, A.J., Heidelberg, J.F., 2006. Genome sequence of *Aeromonas*
495 *hydrophila* ATCC 7966T: jack of all trades. J. Bacteriol. 188, 8272-8282.
496 Wegerer, A., Sun, T., Altenbuchner, J., 2008. Optimization of an *E. coli* L-rhamnose-
497 inducible expression vector: test of various genetic module combinations. BMC
498 Biotechnol. 8, 2.
499 Zheng, L., Baumann, U., Reymond, J.L., 2004. An efficient one-step site-directed and site-
500 saturation mutagenesis protocol. Nucleic Acids Res. 32, e115.

501

502

503

Table 1: Primer used in the present study and their application

Primer	Sequence	Application
<i>asaP1</i> -nde-f	5'-CGA ATT CCA TAT GAT GAA AGT GAC TCC AAT AG-3'	
<i>asaP1</i> -bgl-h-r	5'-CGG AGA TCT GTT TTC GCT CGG GGT ATT C-3'	Cloning of <i>asaP1</i> in pJOE3075 (Wegerer et al., 2008)
<i>asaP1</i> -gln-f _{Glu294}	5'-CCG TGC CCG TAC CAT AGT CCA TCA GCT GAG TCA CTT CAA CG-3'	
<i>asaP1</i> -gln-r _{Glu294}	5'-GCT GAT GGA CTA TGG TAC CGG CAC GGG AAT CGC TCC-3'	
<i>asaP1</i> -ala1-f _{Glu294}	5'-CCG TGC CGG TAC CAT AGT CCA TGC GCT GAG TCA CTT CAA CG-3'	
<i>asaP1</i> -ala1-r _{Glu294}	5'-GCG CAT GGA CTA TGG TAC CGG CAC GGG AAT CGC TCC-3'	
<i>asaP1</i> -phe-f _{Tyr309}	5'-GCA GGT ACC GAC GAT CTG GGT TTC GGT CAG GCC AAT GCC CGC-3'	Construction of AsaP1 mutants by site directed mutagenesis
<i>asaP1</i> -phe-r _{Tyr309}	5'-CCG AAA CCC AGA TCG TCG GTA CCT GCC ACC ACG TTG AAG TG-3'	
<i>asaP1</i> -ala2-f _{Tyr309}	5'-GTG GCA GGT ACC GAC GAT CTG GGT CAG GCC AAT G-3'	
<i>asaP1</i> -ala2-r _{Tyr309}	5'-CCG GCA CC AGA TCG TCG GTA CCT GCC ACC ACG TTG AAG-3'	

504

505

506 **Table 2:** Microscopic changes detected in Atlantic salmon (mean weight, 30 g) 48 h post
 507 i.p. injection. N = 2.

Sample	Histopathological changes			
	Kidney	Heart	Spleen	Liver
AsaP1 _{wt} * [5 ng/ g fish]	b	c	a, b	a, b, d
AsaP1 _{wt} * [1 ng/ g fish]	b	-	a, b	b
AsaP1 _{rec} ** [5 ng/ g fish]	b	c	a	a, b, d
AsaP1 _{rec} ** [1 ng/ g fish]	b	-	-	b,d
PBS	-	-	-	-

* AsaP1_{wt}, native AsaP1 purified from ECP of *A. salmonicida* subsp. *achromogenes*, strain Keldur265-87

**AsaP1_{rec}, recombinant AsaP1 purified from a lysate of *E. coli* expressing the *asaP1* gene
 - = no pathological changes; a = hyperaemia; b = haemorrhage; c = vacuolar degeneration;
 d = liquefactive necrosa

508
 509
 510
 511
 512
 513

514

515 **Figure 1:** Growth of *E. coli* Pri3715 (a BL21 derivative) expressing AsaP1_{rec} and its four
516 mutants: AsaP1_{E294A}, AsaP1_{E294Q}, AsaP1_{Y309A} and AsaP1_{Y309F}, monitored by OD_{600 nm}
517 measurement at different times over a period of 30 h. An empty BL21 strain served as control.

518

519 **Figure 2:** Detection of AsaP1 and AsaP1 mutants by polyclonal murine α -AsaP1 antibody on
520 Western blot. Extracellular products (ECP) of *A. salmonicida* subsp. *achromogenes*
521 (Keldur265-87) served as a positive control. Lanes: (1) AsaP1_{E294A}, (2) AsaP1_{E294Q}, (3)
522 AsaP1_{Y309A}, (4) AsaP1_{Y309F}, (5) ECP.

523

524 **Figure 3:** Analysis of recombinant AsaP1_{rec} expression and secretion in *E. coli* by Coomassie
525 blue stained SDS-PAGE. Shown is the representative expression of the mutant AsaP1_{E294A}.
526 Other mutants as well as the recombinant AsaP1_{wt} show similar results. Lanes: (1)
527 extracellular proteins, (2) Periplasmic proteins, (3) Soluble cytosolic proteins, (4) insoluble
528 cytosolic proteins. Arrow indicates the size of unprocessed AsaP1_{E294A} (37kDa). Proteins can
529 be detected in all three fractions within the *E. coli* cell but not in the extracellular milieu.

530

531 **Figure 4:** Time course of stability and maturation for recombinant AsaP1_{rec} and AsaP1_{E294A} at
532 4 °C. Purified protein analysed after 1, 10 and 18 days by Coomassie blue stained SDS-
533 PAGE. Protein at 37 kDa shows the unprocessed precursor, whereas the protein bands at the
534 size of recombinant AsaP1_{rec} (22 kDa) show the matured protease domain.

535

536 **Figure 5: (A)** Antibody activity and **(B)** antibody endpoint titre against extracellular product
537 (ECP) of *Aeromonas salmonicida* subsp. *achromogenes* (Keldur265-87) detected in Arctic
538 charr serum 12 weeks post immunization with AsaP1mutants, AsaP1_{E294A}, AsaP1_{E294Q},
539 AsaP1_{Y309A} and AsaP1_{Y309F}. Data are expressed in a box blot, with the line representing the
540 median. Boxes indicate 25-75% percentiles and whiskers 0-100%. Significances were

Crystallization and preliminary X-ray diffraction studies of AsaP1_E294A and AsaP1_E294Q, two inactive mutants of the toxic zinc metallopeptidase AsaP1 from *Aeromonas salmonicida* subsp. *achromogenes*

Xenia Bogdanović,^a
 Rajesh Kumar Singh,^a‡ Johanna Hentschke,^b Bjarnheidur K. Gudmundsdóttir^b and Winfried Hinrichs^{a*}

^aInstitut für Biochemie, Universität Greifswald, Felix-Hausdorff-Strasse 4, D-17489 Greifswald, Germany, and ^bInstitute for Experimental Pathology, University of Iceland, Keldur, 112 Reykjavík, Iceland

‡ Current address: Chemical Engineering Division, National Chemical Laboratory, Dr Homi Bhabha Road, Pune 411008, India.

Correspondence e-mail:
 winfried.hinrichs@uni-greifswald.de

Received 29 April 2009
 Accepted 26 May 2009

Two mutants of the toxic extracellular zinc endopeptidase AsaP1 (AsaP1_E294Q and AsaP1_E294A) of *Aeromonas salmonicida* subsp. *achromogenes* were expressed in *Escherichia coli* and crystallized by the vapour-diffusion method. Crystals were obtained using several precipitants and different protein concentrations. Protein crystals were found in a monoclinic (*C*2) as well as an orthorhombic (*P*2₁2₁2₁) space group. The crystals belonging to the monoclinic space group *C*2 had unit-cell parameters $a = 103.4$, $b = 70.9$, $c = 54.9$ Å, $\beta = 109.3^\circ$ for AsaP1_E294A, and $a = 98.5$, $b = 74.5$, $c = 54.7$ Å, $\beta = 112.4^\circ$ for AsaP1_E294Q. The unit-cell parameters of the orthorhombic crystal obtained for AsaP1_E294A were $a = 57.9$, $b = 60.2$, $c = 183.6$ Å. The crystals of the two different mutants diffracted X-rays beyond 2.0 Å resolution.

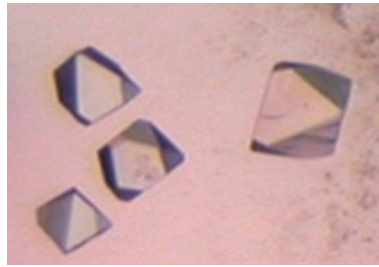
1. Introduction

Aeromonas salmonicida is a Gram-negative bacterium which has been known as a fish pathogen for over 90 years, but the mechanisms of its virulence are only partly understood. Both farmed and wild fish are affected in marine as well as freshwater environments. *A. salmonicida* has so far been divided into five subspecies (Pavan *et al.*, 2000; Holt *et al.*, 1994). *A. salmonicida* subsp. *salmonicida* is often referred to as the typical strain, whereas the others, based on the heterogeneity in this group, have been referred to as atypical strains (Wiklund *et al.*, 1994). One group of atypical *A. salmonicida*, *i.e.* subsp. *achromogenes*, has recently been found to form a homogeneous group of strains that cause atypical furunculosis, a systemic disease, in many species of fish (Austin *et al.*, 1998; Bjornsdóttir *et al.*, 2004; Gudmundsdóttir, Lange *et al.*, 2003; Gudmundsdóttir, Hvannadal *et al.*, 2003; Lund & Mikkelsen, 2004).

A. salmonicida subsp. *achromogenes* produces a toxic peptidase, AsaP1, which is a major virulence factor (Gudmundsdóttir *et al.*, 1990; Arnadóttir *et al.*, 2008). AsaP1 has not been detected in secretions from typical *A. salmonicida* (Gudmundsdóttir, Hvannadal *et al.*, 2003).

AsaP1 is a caseinolytic zinc metallopeptidase that is lethally toxic to both fish and mice (Gudmundsdóttir *et al.*, 1990; Gudmundsdóttir & Gudmundsdóttir, 2001). Sublethal doses of AsaP1 injected intramuscularly induce pathological changes in Atlantic salmon (*Salmo salar* L.) that are comparable to those seen in fish with atypical furunculosis (Gudmundsdóttir *et al.*, 1990).

Mature AsaP1 is composed of 172 amino acids and has a calculated molecular mass of 19 kDa. It is autocatalytically released from a 343-amino-acid proenzyme with a calculated molecular mass of 37 kDa (Arnadóttir *et al.*, 2008). AsaP1 contains the typical zinc-binding motif HExxH, where *x* is any amino-acid residue and the two histidines coordinate the zinc ion. The glutamate is most probably involved in catalysis. Three families, aspzincins, metzincins and gluzincins, can be distinguished among these zinc peptidases, in which the third zinc ligand is aspartate, histidine or glutamate, respectively (Hooper, 1994). AsaP1 belongs to the family of aspzincins, in which a



© 2009 International Union of Crystallography
 All rights reserved

GTxDxxYG loop is conserved and the aspartate within this sequence has been shown to act as a zinc ligand (Hori *et al.*, 2001; McAuley *et al.*, 2001).

For biochemical and structural characterization of AsaP1, an *Escherichia coli* expression system was established for two inactive mutants of AsaP1 created by site-directed mutagenesis (Hentschke, 2008). In this way, the glutamic acid at position 294 which is involved in the catalysis was replaced by an alanine (AsaP1_E294A) or by a glutamine (AsaP1_E294Q). Both mutants are inactive. Because of

the inactivity of the mutants, the propeptide still remains as part of the protein but its function (whether it plays a role in protease folding and acts as an intramolecular chaperone or whether it inhibits proteinase activity in the intracellular space) still remains unclear.

2. Protein expression and purification

Starting from a glycerol stock frozen at 193 K of *E. coli* BL21 containing the expression vector pJOE E3075 (Stumpf *et al.*, 2000; Hentschke, 2008) encoding the His-tagged sequence for AsaP1_E294Q and AsaP1_E294A, a pre-culture was prepared with 5 ml Luria/Miller medium containing 0.1 mg ml⁻¹ ampicillin. Cultures were incubated overnight at 310 K with 220 rev min⁻¹ shaking.

1 l Luria/Miller medium containing 0.1 mg ml⁻¹ ampicillin was freshly inoculated with the overnight preculture at 310 K and 220 rev min⁻¹ shaking. Protein expression was induced at an OD_{600 nm} between 0.5 and 1.0 absorption units by adding L-rhamnose to a final concentration of 1 mg ml⁻¹ and cultures were incubated at 295 K and 220 rev min⁻¹ for 16 h.

Cells were harvested by centrifugation at 5000 g and resuspended in 20 mM Tris-HCl pH 7.6 containing 300 mM NaCl. The cells were lysed by sonication and the homogenate was centrifuged for 1 h at 48 000 g and 277 K. The supernatant was filtered through a 0.2 µm syringe filter and loaded onto an Ni²⁺-charged immobilized metal-affinity (PorosMC) chromatography column with buffer A (20 mM Tris-HCl pH 7.6, 300 mM NaCl, 50 mM imidazole). The protein was eluted with buffer B (20 mM Tris-HCl pH 7.6, 300 mM NaCl, 200 mM imidazole) using a linear gradient from 0% to 100%. Fractions containing AsaP1 mutants were pooled and concentrated by ultrafiltration before loading onto a gel-filtration column (Superdex200). The buffer for gel filtration was composed of 20 mM Tris-HCl pH 7.6 and 300 mM NaCl. The protein concentration was determined by UV absorption ($\varepsilon_{280\text{ nm}} = 31\,400\text{ M}^{-1}\text{ cm}^{-1}$).

3. Crystallization

Initial screening for crystallization conditions was performed using a CyBio crystallization robot with the sitting-drop vapour-diffusion method in 96-well plates (CrystalQuick Lp). For crystallization, 0.3 µl protein solution (concentrated to 5–25 mg ml⁻¹) and 0.3 µl reservoir solution were mixed in each drop and equilibrated against 40 µl reservoir solution. From these initial screens (JBScreen Classic 1–10, Jena Bioscience) the first hits were found (1.8 M ammonium sulfate, 0.1 M MES-NaOH pH 6.5 for the monoclinic crystals of AsaP1_E294Q, 2.0 M ammonium sulfate, 0.1 M Tris-HCl pH 8.5 for the monoclinic crystals of AsaP1_E294A and 16% PEG 4000, 10% 2-propanol, 0.1 M HEPES pH 7.5, 0.2 M ammonium sulfate for the orthorhombic crystals of AsaP1_E294A). These crystallization conditions were further optimized using 24-well crystallization plates (Greiner Bio-One). Optimization of crystallization conditions was carried out using the hanging-drop vapour-diffusion method. Each well contained 500 µl reservoir solution and the drop was a mixture of 1 µl protein solution and 1 µl reservoir solution. Crystallization of both inactive mutants AsaP1_E294A and AsaP1_E294Q occurred under several conditions and at different protein concentrations. Usually, colourless crystals appeared within 4 d.

Crystals of AsaP1_E294Q suitable for data collection were obtained from a protein solution at 7–10 mg ml⁻¹. Drops comprised of 2 µl protein solution and 2 µl reservoir solution (0.2 M MES-NaOH pH 7.5 and 1.6 M ammonium sulfate) were equilibrated against 500 µl reservoir solution (Fig. 1a).

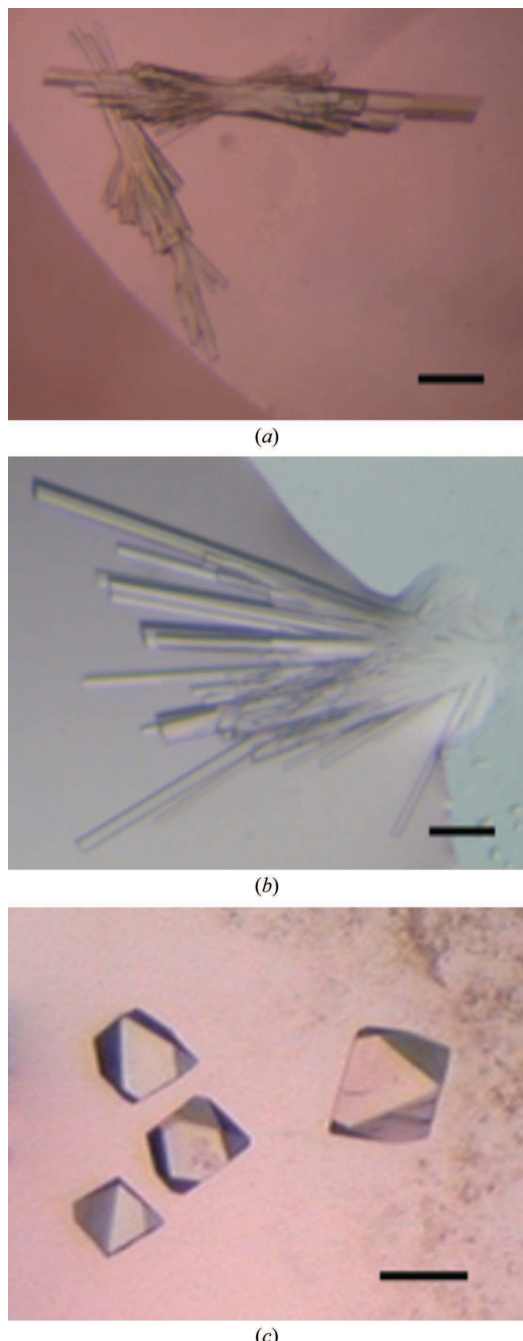


Figure 1

Crystals from the two different AsaP1 mutants E294Q and E294A grown by the hanging-drop vapour-diffusion method. (a) Monoclinic crystals of AsaP1_E294Q and (b) monoclinic crystals of AsaP1_E294A. (c) Orthorhombic crystals of AsaP1_E294A. The solid bar represents 200 µm.

Table 1

X-ray data-collection statistics of AsaP1_E294A and AsaP1_E294Q.

Values in parentheses are for the outer resolution shell.

Crystal	AsaP1_E294Q	AsaP1_E294A	AsaP1_E294A
X-ray source	EMBL X12 c/o DESY	Rigaku MicroMax007	EMBL X12 c/o DESY
Detector	MAR CCD 225	Rigaku CCD Saturn92	MARCCD 225
Wavelength (Å)	0.95369	1.5418	0.97784
Resolution range (Å)	99.0–2.0 (2.05–2.00)	35.2–2.1 (2.26–2.18)	90.0–2.2 (2.25–2.20)
Space group	C2	C2	P2 ₁ 2 ₁ 2 ₁
Unit-cell parameters			
<i>a</i> (Å)	98.5	103.4	57.8
<i>b</i> (Å)	74.5	70.9	60.2
<i>c</i> (Å)	54.7	54.8	183.6
α (°)	90.0	90.0	90.0
β (°)	112.4	109.3	90.0
γ (°)	90.0	90.0	90.0
Total reflections	92926	133664	204992
Unique reflections	24682 (1451)	21701 (2103)	33551 (7629)
Completeness (%)	98.9 (86.3)	98.9 (96.2)	99.4 (93.1)
R_{merge} (%)	10.1 (39.3)	9.7 (59.2)	13.3 (60.2)
$R_{\text{r.i.m.}}$ (%)	10.7 (53.3)	11.2 (83.1)	15.9 (50.7)
$R_{\text{p.i.m.}}$ (%)	5.5 (27.8)	4.4 (37.7)	6.0 (18.5)
Average $I/\sigma(I)$	18.7 (3.3)	8.8 (1.6)	19.3 (2.69)
<i>d</i> -spacing (Å)	2.05–2.00	2.26–2.18	2.25–2.20
Mosaicity (°)	1.5	0.7	0.9
Redundancy	3.8 (3.4)	6.2 (4.5)	6.1 (3.7)
Wilson <i>B</i> factor (Å ²)	23.7	44.5	41.7
No. of images	360	740	360

The crystallization condition for AsaP1_E294A (7–10 mg ml^{−1}) was found to be 0.1 M Tris–HCl pH 8.5 and 2.2 M ammonium sulfate (Fig. 1b). Bipyramidal shaped crystals appeared (Fig. 1c) using a crystallization condition composed of 15% PEG 4000, 0.1 M HEPES pH 7.5, 0.2 M ammonium sulfate and 10% 2-propanol.

4. Data collection and X-ray crystallographic analysis

Before mounting, crystals were transferred into and soaked with a suitable cryoprotectant for 30 s. For cryoprotection, the reservoir solution was mixed with glycerol to a final concentration of 20% (v/v) for the crystals of AsaP1_E294Q and AsaP1_E294A grown in 0.2 M MES–NaOH pH 7.5, 1.6 M ammonium sulfate and in 0.1 M Tris–HCl pH 8.5, 2.2 M ammonium sulfate, respectively. Crystals of AsaP1_E294A grown in 15% PEG 4000, 0.1 M HEPES pH 7.5, 0.2 M ammonium sulfate and 10% 2-propanol were transferred to a cryo-solution containing the reservoir solution and 20% PEG 400. Crystals were then flash-cooled to 110 K (Oxford Cryosystems).

Diffraction data were collected on the home source, a Rigaku rotating-anode X-ray generator (MicroMax007) with Osmic multiple layer optics (beam size 0.3 × 0.3 mm), with a CCD detector (Saturn92) and also on the EMBL beamline X12 at DESY, Hamburg with a MAR CCD 225 (MAR Research, Germany).

The crystals of AsaP1_E294A (0.2 M MES–NaOH pH 7.5, 1.6 M ammonium sulfate) and AsaP1_E294Q (0.1 M Tris–HCl pH 8.5, 2.2 M ammonium sulfate) belonged to the monoclinic space group C2 and showed the same packing in general, with unit-cell parameters $a = 103.4$, $b = 70.9$, $c = 54.9$ Å, $\beta = 109.3^\circ$ for AsaP1_E294A and $a = 98.5$, $b = 74.5$, $c = 54.7$ Å, $\beta = 112.4^\circ$ for AsaP1_E294Q. The crystals of AsaP1_E294A grown in 15% PEG 4000, 0.1 M HEPES pH 7.5, 0.2 M ammonium sulfate and 10% 2-propanol belonged to the orthorhombic space group P2₁2₁2₁, with unit-cell parameters $a = 57.9$, $b = 60.2$, $c = 183.6$ Å. The diffraction data from the crystals measured in-house were processed using the software *CrystalClear*1.3.6 (Pflugrath, 1999); the data from the crystal measured on EMBL beamline X12 were processed using *DENZO* and *SCALEPACK* from the *HKL* package (Otwinowski & Minor, 1997). To obtain values of $R_{\text{p.i.m.}}$ and $R_{\text{r.i.m.}}$, the data were processed with *MOSFLM* and *SCALA* from the *CCP4* suite (Collaborative Computational Project, Number 4, 1994).

For data collection of AsaP1_E294Q one needle was broken off the crystal cluster shown in Fig. 1(a). This mechanical stress probably led to the high mosaicity of 1.5°. The needle-shaped crystals of AsaP1_E294A (Fig. 1b) were easier to handle.

Assuming the presence of one molecule in the asymmetric unit for the crystals belonging to the monoclinic space group, the Matthews coefficients V_M for AsaP1_E294A and AsaP1_E294Q were calculated to be 2.58 and 2.53 Å³ Da^{−1}, respectively. The Matthews coefficient V_M for the crystal of AsaP1_E294A belonging to the orthorhombic space group was calculated to be 2.16 Å³ Da^{−1}, assuming the presence of two molecules in the asymmetric unit.

Molecular replacement using the program *Phaser* (McCoy, 2007) was successful using the peptidyl-Lys metalloendopeptidase from *Grifola frondosa* (PDB entry 1g12) as a search model. The polypeptide of the search model consisted of only the C-terminal protease domain (amino acids 182–348), which shares a sequence identity of 43% with residues 171–343 of the AsaP1 protease domain. Initial phasing also revealed interpretable electron density for the pro-peptide domain of both inactive AsaP1 mutants. Currently, model building and refinement of all data sets is in progress.

References

- Arnadóttir, H., Hvannadal, I., Andresdóttir, V., Burr, S. E., Frey, J. & Gudmundsdóttir, B. K. (2008). *J. Bacteriol.* **191**, 403–410.
- Austin, B., Austin, D. A., Dalsgaard, I., Gudmundsdóttir, B. K., Hoie, S., Thornton, J. M., Larsen, J. L., O'Hici, B. & Powell, R. (1998). *Syst. Appl. Microbiol.* **21**, 50–64.
- Bjornsdóttir, B., Gudmundsdóttir, S., Bambir, S. H., Magnadóttir, B. & Gudmundsdóttir, B. K. (2004). *J. Fish Dis.* **27**, 645–655.
- Collaborative Computational Project, Number 4 (1994). *Acta Cryst. D50*, 760–763.
- Gudmundsdóttir, B. K., Hastings, T. S. & Ellis, A. E. (1990). *Dis. Aquat. Organ.* **9**, 199–208.
- Gudmundsdóttir, B. K., Hvannadal, I., Bjornsdóttir, B. & Wagner, U. (2003). *J. Fish Dis.* **26**, 15–29.
- Gudmundsdóttir, S. & Gudmundsdóttir, B. K. (2001). *Vet. Immunol. Immunopathol.* **81**, 71–83.
- Gudmundsdóttir, S., Lange, S., Magnadóttir, B. & Gudmundsdóttir, B. K. (2003). *J. Fish Dis.* **26**, 331–338.
- Hentschke, J. (2008). Diploma thesis. Ernst-Moritz-Arndt University, Greifswald, Germany.
- Holt, J. G., Krieg, N. R., Sneath, P. H. A., Staley, J. T. & Williams, S. T. (1994). *Bergey's Manual of Determinative Bacteriology*, 9th ed. Baltimore: Williams & Wilkins.
- Hooper, N. M. (1994). *FEBS Lett.* **354**, 1–6.
- Hori, T., Kumakura, T., Yamamoto, M., Nonaka, T., Tanaka, N., Hashimoto, Y., Ueki, T. & Takio, K. (2001). *Acta Cryst. D57*, 361–368.
- Lund, V. & Mikkelsen, H. (2004). *Dis. Aquat. Organ.* **61**, 257–262.
- McAuley, K. E., Jia-Xing, Y., Dodson, E. J., Lehmbeck, J., Østergaard, P. & Wilson, K. S. (2001). *Acta Cryst. D57*, 1571–1578.
- McCoy, A. J. (2007). *Acta Cryst. D63*, 32–41.
- Otwinowski, Z. & Minor, W. (1997). *Methods Enzymol.* **276**, 307–326.
- Pavan, M. E., Abbott, S. L., Zorzosopoulos, J. & Janda, J. M. (2000). *Int. J. Syst. Evol. Microbiol.* **50**, 1119–1124.
- Pflugrath, J. W. (1999). *Acta Cryst. D55*, 1718–1725.
- Stumpf, T., Wilms, B. & Altenbuchner, J. (2000). *BIOspektrum*, **6**, 33–36.
- Wiklund, T., Dalsgaard, I., Eerola, E. & Olivier, G. (1994). *J. Appl. Bacteriol.* **76**, 511–520.

Xenia Bogdanović and Winfried Hinrichs*

Department of Molecular Structural Biology,
 Institute for Biochemistry, Ernst-Moritz-Arndt
 University, Greifswald, Germany

Correspondence e-mail:
 winfried.hinrichs@uni-greifswald.de

Received 22 October 2010
 Accepted 12 January 2011

Influence of temperature during crystallization setup on precipitate formation and crystal shape of a metalloendopeptidase

It is well known that protein crystallization is affected by several different parameters such as the composition of the reservoir solution, the protein concentration, the pH and the temperature. An effect of different temperatures during setup of crystallization experiments was observed for a metalloendopeptidase (AsaP1_{E294A}). Spontaneous protein precipitation was reduced and the crystal shape could be improved by decreasing the temperature during crystallization setup.

1. Introduction

X-ray crystallography enables us to visualize protein structures at an atomic level and to better understand the function of a protein. The first requirement for structure determination by X-ray crystallography is a well ordered single protein crystal. The nucleation and growth of protein crystals is dependent on several different factors such as the composition of the reservoir solution, the protein purity and concentration, the pH and the temperature. The parameters of successful crystallization trials are not predictable and it is only partly understood which effect is a consequence of a certain factor. The relevance of each parameter may differ considerably in importance for different proteins. For example, the crystallization of α -amylase and catalase is sensitive to temperature, while this is not the case for ovalbumin and ferritin (McPherson, 1990).

To investigate the influence of temperature, crystallization plates with identical crystallization conditions are often stored at different temperatures. Here, we report the effect of temperature during crystallization setup while mixing protein solution with reservoir solution. We observed that placing the crystallization plate on ice, cooling the reservoir solution (to about 277 K) and using pre-chilled pipette tips had a positive effect on the crystal shape and decreased precipitate formation. There was also a slight increase in diffraction quality.

The protein for which this effect was observed is an inactive mutant of the metalloendopeptidase AsaP1 (AsaP1_{E294A}), a major virulence factor of the fish-pathogenic bacterium *Aeromonas salmonicida* subsp. *achromogenes* (Gudmundsdóttir *et al.*, 1990; Arnadóttir *et al.*, 2008).

2. Materials and methods

Protein expression, purification and crystallization of AsaP1_{E294A} have recently been described (Bogdanović *et al.*, 2009). For the crystallization experiments reported in this manuscript, a protein solution with a concentration of 16–25 mg ml^{−1} in 20 mM Tris–HCl buffer pH 7.6 and 200 mM NaCl was used. The protein solution was placed on ice or stored in a refrigerator (~277 K) at all times. Crystallization was carried out manually using hanging-drop vapour diffusion in 24-well crystallization plates (Greiner Bio-One, Item No. 662102). Each well contained 500 µl reservoir solution and the drop consisted of a mixture of 2 µl protein sample and 2 µl reservoir solution. Preparation of each plate took about 20 min.

The crystallization condition for AsaP1_{E294A} (16–25 mg ml^{−1}) comprises 14% (w/v) PEG 4000, 0.1 M HEPES pH 7.5, 0.2 M



© 2011 International Union of Crystallography
 All rights reserved

ammonium sulfate and 10%(*v/v*) 2-propanol. This condition was repeated 24 times per plate for three crystallization plates in each of the four different crystallization experiments as explained below.

The first crystallization experiment was set up with the crystallization plate on the bench at 294–296 K and with reservoir solutions at about 294–296 K. The crystallization plate was subsequently stored in a temperature-controlled room at 293 K. The second experiment was performed with the crystallization plate on the bench at 294–296 K and reservoir solutions that had been pre-chilled overnight in a refrigerator (~ 277 K) and were kept on ice during the crystallization setup. The crystallization plates were stored at 293 K. In the third experiment the crystallization plate was placed on ice as were the pre-chilled (~ 277 K) reservoir solutions. Additionally, pipette tips were cooled to 253 K overnight in a freezer and were placed on ice during crystallization setup. The crystallization plates were stored at 293 K.

In a fourth experiment, crystallization plates were placed on ice as well as the reservoir solutions, which were additionally pre-chilled to 277 K overnight in a refrigerator. These crystallization plates were stored in a temperature-controlled room at 277 K.

The X-ray diffraction resolution of the crystals was tested using a rotating-anode X-ray generator (MicroMax-007, Rigaku) with Osmic multiple layer optics (beam size 0.3×0.3 mm) and a CCD detector (SATURN92, Rigaku).

Several crystals obtained in the first three crystallization experiments described above were tested using a cryoprotectant that consisted of the reservoir solution with 14%(*v/v*) PEG 400. Crystals were flash-cooled to 110 K in a stream of nitrogen (Oxford Cryosystems) and the diffraction images were analyzed using *CrystalClear* v1.3.6 (Pflugrath, 1999). Reflections from the test images were determined using the *difind* option of the software with default settings of $I/\sigma = 3.0$ and a minimum pixel value of 20. These reflections were sorted by their resolution. On the best image recorded for each experiment, the 95th percentile of all reflections was considered as the resolution. Complete data sets were not collected.

3. Results

Recently, the crystallization of AsaP1_{E294A} at a concentration of 7–10 mg ml⁻¹ has been reported using crystallization conditions comprising 2.0 M ammonium sulfate and 0.1 M Tris-HCl pH 8.5,

resulting in monoclinic crystals (space group *C2*), and 14%(*w/v*) PEG 4000, 0.1 M HEPES pH 7.5, 0.2 M ammonium sulfate and 10%(*v/v*) 2-propanol, resulting in orthorhombic crystals (*P2₁2₁2₁*) (Bogdanović *et al.*, 2009). In the crystallization experiments described here, we further characterized monoclinic crystals (*C2*) that were obtained using the same condition as used for the orthorhombic crystals but with a higher protein concentration (16–25 mg ml⁻¹; Fig. 1*a*). These crystals showed unit-cell parameters of $a = 149.55$, $b = 48.23$, $c = 55.35$ Å, $\beta = 110.65^\circ$, which differed from the previously published monoclinic cell (Bogdanović *et al.*, 2009).

At a protein concentration in the range 16–25 mg ml⁻¹, the first setup of crystallization trials with the crystallization plate on the bench and with reservoir solutions that were not chilled (about 294–296 K) produced crystals within 2 d with rough edges and flaws and considerable amounts of precipitate within the drop (Fig. 1*a*). Protein aggregation and precipitate formation could be detected as a light turbidity immediately upon mixing the protein solution with the reservoir solution. After 2 d the growth of crystals as well as the observed Ostwald ripening (Fig. 1*a*) stopped and the amount of precipitate persisted. Crystals were stable for several weeks up to months and no further changes were detected within the drops.

Precipitate formation and the growth defects of the crystals could be reduced (Fig. 1*b*) by cooling the reservoir solutions to approximately 277 K before mixing them with the protein solution. By placing the crystallization plate on ice during crystallization setup and by additional cooling of the pipette tips (~ 253 K) precipitate formation could be decreased even more and the shape of the crystals was also improved (Fig. 1*c*). In these experiments crystal growth again stopped after 2 d and crystals were stable for several weeks up to months.

The results were reproducible for different drops of the same crystallization experiment. All plates for these three experiments were stored at 293 K.

Crystallization conditions with a lower protein concentration (down to 14 mg ml⁻¹) or a reduced precipitant concentration [down to 10%(*w/v*) PEG 4000] showed the same effect of protein precipitation and similarly shaped but fewer crystals.

Only phase separation and no crystals could be detected for the fourth crystallization experiment, in which the crystallization plate was placed on ice and chilled reservoir solutions were used. These crystallization plates were stored at 277 K for several months.

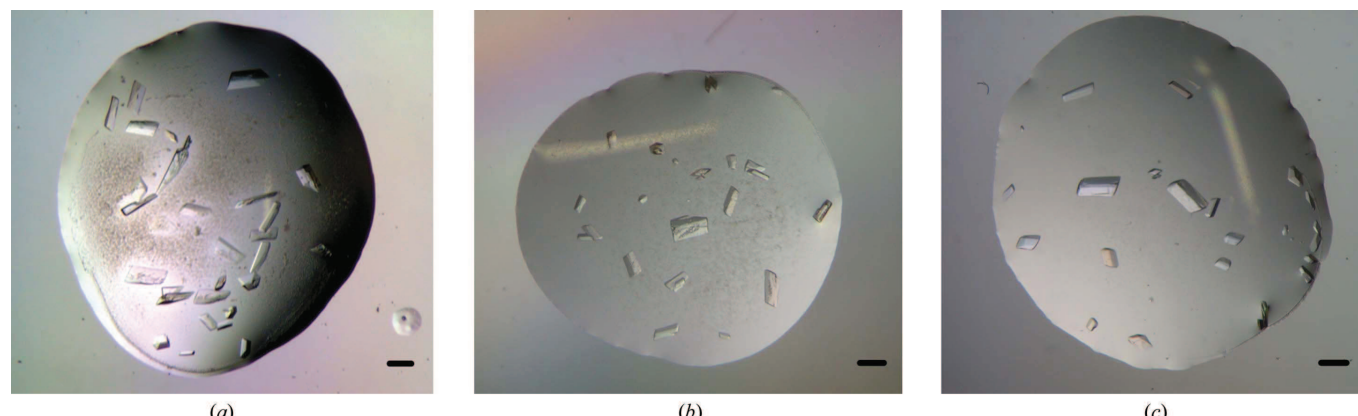


Figure 1

Influence of the temperature during crystallization setup on precipitate formation and crystal shape. Monoclinic crystals of AsaP1_{E294A} from three different crystallization setups are shown. Typical examples of 72 trials after 2–4 d when crystal growth has already stopped are presented. All plates were stored at 293 K for several weeks, but the crystals and precipitate remained unchanged. (a) Crystallization at about 294–296 K, (b) crystallization at about 294–296 K with pre-chilled reservoir solutions (~ 277 K) and (c) crystallization plate placed on ice during crystallization setup with pre-chilled reservoir solutions (~ 277 K) and pre-chilled pipette tips (253 K). The drop volume is 4 µl and the solid bar at the bottom right represents 200 µm.

For several typical crystals from each crystallization experiment diffraction images were recorded to test the resolution. For crystals obtained in the first, second and third crystallization experiments the resolution of the 95th percentile of all reflections from the best image was 3.83, 3.64 and 3.27 Å, respectively.

4. Discussion

The probability of crystal nucleation and crystal growth is higher the farther the system is pushed into the supersaturation region. On the other hand, the probability of excess nucleation and protein aggregation also increases (McPherson, 1990). Additionally, the crystal-growth velocity is high, which leads to growth defects and flaws in the crystals. Temperature can be one parameter that pushes the system into the supersaturation region. Fig. 1(a) shows a condition with protein aggregation and numerous crystals with growth defects and flaws as an example of a system that has been pushed far into the supersaturation region owing to a high protein concentration and probably owing to an elevated temperature. By decreasing the temperature while mixing the protein solution with the reservoir solution (Figs. 1b and 1c), disordered aggregation of the protein molecules (precipitate) can be reduced and the protein molecules tend to arrange in better ordered single crystals. This is reflected in the slightly better resolution of the corresponding crystals.

In the case of AsaP1_{E294A} the protein could not be concentrated to more than 25 mg ml⁻¹ without precipitating; thus, the solubility limit of the protein solution was reached. The solubility as a function of temperature was not investigated. The effect of temperature on protein solubility varies for different proteins as well as for diversified precipitant conditions and should be determined for the particular protein. Proteins in salt solutions seem to be more soluble at lower temperatures, whereas proteins in solutions of polyethylene glycol, methylpentanediol or other organic solvents are less soluble in the cold (McPherson, 1990). The crystallization condition for AsaP1_{E294A} contained polyethylene glycol as a precipitant, but protein precipitation was reduced in the cold. Taking into account the fact that the AsaP1_{E294A} protein is already at the solubility limit owing to the high protein concentration, the observed effect of temperature on protein precipitation could suggest retrograde solubility. Thus, the improvement in crystal quality that was noted could have been because pre-chilling the various components (tips, solutions and trays) of the crystallization setup led to a lower level of supersaturation in the drops.

Blow *et al.* (1994) showed that a separation of nucleation and crystal growth can be achieved by a temperature shift from 283 to 291 K for lysozyme. They also showed that the higher the lysozyme concentration and the longer the incubation time at 283 K the more stable the nuclei that were observed. In our experiments, the number of crystals is the same but their quality has improved. This would suggest that the experiment still reaches the same level of supersaturation. However, seeding experiments (Bergfors, 2003) have shown that crystal quality can be dependent on the quality of the seeds that serve as nuclei. It may be that this is what explains the improvement that we noticed here when we pre-chilled the crystallization setup. The initial nuclei were more ordered owing to the slight and brief decrease in temperature.

However, the temperature response of the protein seems to be complicated because there was no crystallization or protein precipitation in experiment 4. It is not clear if nucleation occurs under these conditions and only crystal growth is not supported at 277 K. The energy barrier for the formation of stable nuclei might be overcome by random fluctuations (Blow *et al.*, 1994) that will increase with temperature.

It may be that nucleation in the different experiments occurs while the crystallization plates that are set up in the cold are stored at 293 K and the temperature slowly increases. At lower temperature the protein solution will pass through the nucleation region and the metastable phase more slowly because of retarded diffusion. This could result in crystallization nuclei with better quality and, owing to a decreased growth velocity, to fewer imperfections within the crystals.

This approach might be useful for proteins that precipitate immediately when added to the precipitant in the drops.

References

- Arnadóttir, H., Hvannadal, I., Andresdóttir, V., Burr, S. E., Frey, J. & Gudmundsdóttir, B. K. (2008). *J. Bacteriol.* **191**, 403–410.
- Bergfors, T. (2003). *J. Struct. Biol.* **142**, 66–76.
- Blow, D. M., Chayen, N. E., Lloyd, L. F. & Saridakis, E. (1994). *Protein Sci.* **3**, 1638–1643.
- Bogdanović, X., Singh, R. K., Hentschke, J., Gudmundsdóttir, B. K. & Hinrichs, W. (2009). *Acta Cryst. F* **65**, 695–697.
- Gudmundsdóttir, B. K., Hastings, T. S. & Ellis, E. A. (1990). *Dis. Aquat. Organ.* **9**, 199–208.
- McPherson, A. (1990). *Eur. J. Biochem.* **189**, 1–23.
- Pflugrath, J. W. (1999). *Acta Cryst. D* **55**, 1718–1725.

Structure of inactive mutants of the aspzincin metalloendopeptidase AsaP1 in complex with its propeptide

Xenia Bogdanović¹, Johanna Schwenteit¹, Rajesh Kumar Singh^{1*}, Bjarnheidur K. Gudmundsdóttir² and Winfried Hinrichs¹

¹ Institut für Biochemie, Universität Greifswald, Felix-Hausdorff-Str. 4, D-17489 Greifswald, Germany.

² Institute for Experimental Pathology, University of Iceland, Keldur, 112-Reykjavík, Iceland

*Current address: Chemical Engg. Division, National Chemical Laboratory, Dr. Homi Bhabha Road, Pune, 411008. India.

Correspondence e-mail: winfried.hinrichs@uni-greifswald.de

Keywords

AsaP1, *Aeromonas salmonicida achromogenes*, zinc metalloendopeptidase, aspzincins, M35, propeptide

Abstract

The protease AsaP1 is an extracellular, toxic zincendopeptidase that is produced by the Gram-negative bacterium *Aeromonas salmonicida* subsp. *achromogenes*. *Aeromonas salmonicida* is a well-known fish pathogen for various fish species worldwide with negative economic impacts on aquaculture. AsaP1 belongs to the family of deuterolysin-like aspzincin metalloendopeptidases. Here we report the crystal structure analysis of two

different inactive mutants of AsaP1 that were solved in two different space groups at 2.0 Å resolution. Owing to proteolytic inactivity of the mutants the crystallized polypeptide comprises the propeptide domain and the globular protease with 172 and amino acid residues. The binding mode of the propeptide to the protease reveals insights in propeptide function, substrate binding and protease specificity. A lysine side chain of the propeptide is bound in the hydrophobic S1' pocket interacting in a specific manner with three carboxylate side chains. The active site is composed of two helices connected by a loop region comprising the conserved HExxH and GTxDxxYG motifs of aspzincins including the zinc coordinating amino acids His293, His297 and Asp306. These are the first crystal structure analyses of a precursor of deuterolysin-like aspzincin proteases so far.

Introduction

The Gram-negative bacterium *Aeromonas salmonicida* is a well-known fish pathogen with a world-wide distribution, infecting salmonids and numerous other fish species. Both cultivated and wild fish, in marine as well as in freshwater environments, are affected but the mechanisms of virulence are only partly understood. *A. salmonicida* is today classified in five subspecies: subsp. *salmonicida*, subsp. *achromogenes*, subsp. *masoucida*, ssp. *smithia*, subsp. *pectinolytica* [1] and it is the causative agent of typical or atypical furunculosis [2, 3] depending on whether the disease is caused by typical (*A. salmonicida* subsp. *salmonicida*) or atypical *A. salmonicida* strains.

The zincendopeptidase AsaP1 has been isolated from extracellular products (ECP) of several atypical strains and has been identified as a major exotoxin of a homologous group of strains of *A. salmonicida* subsp. *achromogenes* [4, 5]. In infections with *A. salmonicida* subsp. *achromogenes* several symptoms can be assigned to the expression of

AsaP1 like skin ulcers and lesions, degenerative changes in underlying muscles accompanied of liquefactive necrosis, pallor gills, and general anemia in various organs [6].

AsaP1 is a caseinolytic zinc metalloendopeptidase that is lethally toxic to both fish and mice [4, 7]. Sublethal doses of AsaP1 injected intramuscularly induce pathological changes in Atlantic salmon (*Salmon salar*, L.) that are comparable to those seen in fish with atypical furunculosis [4]. The expression of the protease is quorum-sensing regulated [8]. Mature AsaP1 is composed of 172 amino acid residues and has a calculated molecular mass of 19 kDa. The protease is released from a 343-amino-acid pre-pro-enzyme with a calculated molecular mass of 37 kDa [6].

AsaP1 is a member of the MEROPS protease clan MA and belongs to the deuterolysin metalloproteases (family M35) (<http://www.merops.org>). It is the first bacterial virulence factor within this group. Families in clan MA show a conserved HExxH motif in which the two histidine residues act as zinc ligands and the glutamic acid is involved in catalysis. Based on the structural topology of the active site and the third zinc ligand, this protease group is further divided into gluzincins, metzincins [9] and aspzincins [10] with an aspartate, glutamate or histidine as third zinc ligand, respectively. Besides the active-site helix the architecture of the active site differs significantly between aspzincins, gluzincins and metzincins. AsaP1 belongs to the family of aspzincins and thus the aspartate within the conserved GTxDxxYG motif acts as third zinc ligand. This motif is part of the loop at the active site of aspzincins. Peptidases in which the third zinc ligand is Asp also occur in families M6, M7 and M64. In gluzincins the glutamate within the conserved NExxSD acts as third zinc ligand, whereas the third zinc ligand of metzincins is a histidine of the loop region adjacent to the active-site helix within the conserved sequence HExxHxxGxxH. Methzincins are named after the methionine of a conserved β -

turn, the Met-turn, which is located near the catalytic zinc ion opposite to the catalytic water.

For structural characterization AsaP1 mutants were created by site-directed mutagenesis [11]. In this way, the glutamic acid in position 294 within the HExxH motif, which is crucial for catalysis, was replaced by an alanine or by a glutamine resulting in two inactive mutants AsaP1_{E294A} and AsaP1_{E294Q}, respectively. Recently, we reported crystallization conditions leading to single crystals of AsaP1_{E294A} and AsaP1_{E294Q} suitable for structural analysis by X-ray diffraction [12]. Here we describe the three dimensional structures of AsaP1_{E294A} and AsaP1_{E294Q} with its propeptide in two different space groups at a resolution of 2.0 Å.

Material and Methods

Protein expression, purification and crystallization

The expression, purification and crystallization of AsaP1_{E294A} and AsaP1_{E294Q} have been reported, recently [12]. In brief, AsaP1 was cloned, expressed heterologously in *E. coli* Pri3715 (a BL21 derivate), and purified to homogeneity by metal-affinity and size exclusion chromatography. The protein was crystallized by the hanging-drop vapor-diffusion method at 293 K out of a buffer containing 200 mM Tris-HCl pH 7.6 and 200 mM NaCl. In case of AsaP1_{E294Q} with a protein concentration at 7 – 10 mg ml⁻¹ the precipitant comprised 0.2 M MES pH 7.5 and 1.6 M ammonium sulfate leading to monoclinic crystals. The precipitant for monoclinic crystals of AsaP1_{E294A} (7–10 mg ml⁻¹) comprised 0.1 M Tris pH 8.5 and 2.2 M ammonium sulfate. Orthorhombic crystals of AsaP1_{E294A} were obtained with a protein concentration of 16 – 25 mg ml⁻¹ using a crystallization condition composed of 15% PEG 4000, 0.1 M HEPES pH 7.5, 0.2 M ammonium sulfate and 10% 2-propanol.

Data collection, structure determination and refinement

Diffraction data of crystals of AsaP1_{E294Q} and AsaP1_{E294A} were collected at the EMBL beamline X12 at DESY, Hamburg, using a MAR CCD 225 (MAR research, Germany). The monoclinic crystals of AsaP1_{E294Q} and AsaP1_{E294A} were soaked for 5 seconds in the corresponding reservoir solution containing 20%(v/v) glycerol for cryoprotection and were then flash frozen to 100 K. The orthorhombic crystal of AsaP1_{E294A} was soaked in the reservoir solution with 20%(v/v) PEG400 as cryoprotectant.

The data were processed using *DENZO* and *SCALEPACK* of the *HKL* package [13]. The structure of AsaP1_{E294A} in the monoclinic crystal form could be solved by molecular replacement using *PHASER* [14] with the peptidyl-Lys metalloendopeptidase (MEP) from *Grifola frondosa* (PDB entry 1g12) as a search model [15]. Tracing of the propeptide was possible using the program *ARP/wARP* [16]. The structure model was refined with *REFMAC5* [17] from the *CCP4* suite [18] using restrained and TLS refinement. The model was manually complemented using *COOT* [19]. The two other structures were solved by molecular replacement using *PHASER* [14] with the search model of AsaP1_{E294A}. The orthorhombic crystal of AsaP1_{E294A} contains two molecules in the asymmetric unit, which was verified by *SFCHECK* [18]. Stereochemistry was verified using *MOLPROBITY* [20] and *PROCHECK* [18]. Details of data collection and refinement are summarized in Table 1.

Results

Structure determination and refinement

The X-ray crystal structure of AsaP1_{E294A} of the monoclinic crystal was solved by molecular replacement at 2.0 Å resolution. The search model was the peptidyl-Lys

metalloendopeptidase (*Gf*MEP) from *Grifola frondosa* (PDB 1g12) with a sequence identity of 43% for the protease (162 residues). Phasing was successful although the propeptide domain with 171 amino acid residues was not present in the search model (Table 1). There is one molecule in the asymmetric unit of AsaP1_{E294A} that comprises residues Gly23 - Gln126, Glu143 - Asn155, Ala172 - Asp210, Gly214 - Ser341, one zinc ion at the active site, 200 water molecules, three sulfate ions, one chloride ion and one glycerol molecule. Missing amino acids could not be identified because of poor electron density. Owing to the gap between residues 155 - 172 the connection between the protease and the propeptide domain cannot be traced.

The structure of AsaP1_{E294Q} was solved by molecular replacement using AsaP1_{E294A} as search model (Table 1). The model comprises residues Gly23 – Arg130, Ser142 – Gln160, Ala172 – Asp210, Gly214 – Pro340, one zinc ion in the active site, 198 water molecules, three sulfate ions, two glycerol molecules and one 2-(N-morpholino)ethanesulfonic acid (MES) molecule. Again, the connection of the protease domain to the propeptide domain is not visible.

Orthorhombic crystals of AsaP1_{E294A} contain two molecules in the asymmetric unit (Table 1). The model for monomer A comprises residues Gly23 - Arg131, Ser142 - Val159, Gly173 - Pro340, one zinc ion in the active site and 138 water molecules. Monomer B comprises residues Gly23 - Gln126, Ser142 - Val159, Gly173 - Pro340, one zinc ion in the active site and 115 water molecules. Also in this crystal setting, the connection of the protease domain to the propeptide domain could not be traced.

In all structures the main chain torsion angles of amino acid residues are in the allowed regions without outliers of the Ramachandran plot and with more than 90% in the most favorable regions (for details see Table 1).

Overall structure

The monoclinic as well as the orthorhombic AsaP1 variants show an overall r.m.s. deviation for Ca-atoms of 0.4 Å for the protease and of 0.9 Å for the propeptide domain.

The propeptide domain consists of 171 amino acid residues and forms a separate domain.

The N-terminal domain of monoclinic AsaP1_{E294A}, respectively, comprises amino acids Gly23 - Asn155 which form the propeptide that is composed of one two-stranded β-sheet, two three-stranded β-sheets and several loop regions. The first β-sheet comprises β-strand 1, 2 and 7 (corresponding to residues 24 - 30, 39 - 46 and 102 - 108, respectively), the second comprises β-strand 3 and 6 (residues 52 - 55 and 94 - 97) and the third comprises β-strand 4, 8, and 9 (residues 68 - 72, 119 - 125 and 147 - 151). The β-strand 5 (82 - 84) is located as a separate strand apart from the propeptide domain binding to the active site of the protease.

The protease shows the typical fold of the M35 proteases family or aspzincins (Figure 1). One domain consists of one β-sheet and two α-helices. The β-sheet includes β-strand 10, 11 and 13 (residues 174 - 178, 247 - 251 and 269 - 272, respectively) interacting in a parallel manner and β-strand 12 (residues 260 - 262) antiparallel to β-strand 13. The β-strand 6 of the propeptide interacts antiparallel with β-strand 13, expanding the β-sheet of the protease. The β-sheet is stabilized by two disulfide bridges within its loop regions made of Cys181-Cys252 and Cys254-Cys273. The two α-helices within the N-terminal protease domain are helix 6 and helix 7 (residues 273 - 279 and 286 - 299, respectively). The C-terminal domain is composed of five α-helices (residues 214 - 222, 225 - 246, 310 - 326 and 328 - 338, respectively). The long α-helix 5 (residues 182 – 209) connects the N-terminal and the C-terminal domain of the protease.

Coordination sphere of the catalytic Zn²⁺ ion

In all three structures the active-site Zn²⁺ ion is coordinated to imidazole side chains of His293 and His297 of the HExxH motif within the active-site helix $\alpha 7$ and the carboxylate of Asp306 of the conserved GTxDxxYG motif. A monodentate binding mode of the carboxylate of Asp306 is supposed according to distance criteria [21]. Bond lengths for Zn²⁺ coordination are summarized in Table 2. In the monoclinic form of AsaP1_{E294A} tetrahedral coordination of the Zn²⁺ ion is achieved by a chloro ligand. The chloride coordinates instead of the catalytic water molecule typically found in other zinc metalloendopeptidases attacking the carbonyl C-atom of the substrate (Figure 2a and 3). In the asymmetric unit of the orthorhombic form of AsaP1_{E294A} both molecules show a water molecule coordinating the Zn²⁺ ions at distances of 2.39 Å and 2.40 Å, respectively (Figure 2b).

In AsaP1_{E294Q} the Zn²⁺ position was refined to occupancy of 40%. This is in agreement with two modeled alternative conformations of the Asp306 side-chain, which are twisted by about 30°. The first conformation with an occupancy of 40% points towards the Zn²⁺ ion. The alternative conformation with 60% occupancy points in the opposite direction of the Zn²⁺ ion and is stabilized by a hydrogen bond to the phenolic hydroxyl group of Tyr309 with a length of 2.54 Å (Figure 2c). Electron density for a 4th ligand is not observed.

The active site and substrate recognition

The active site is located in a crevice formed of the N-terminal and the C-terminal protease domains and is built of a helix-loop-helix motif. This motif starts with the active-site helix $\alpha 7$ containing the conserved H²⁹³ExxH motif. The following loop region contains the conserved motif G³⁰³TxDxxYG and the delimitation to the C-terminal

domain is built of helix α 8. In direction to the N-terminal protease domain β -strand 13 is located, which interacts in an antiparallel manner with β -strand 6 of the propeptide domain (Figure 1). The active site is thus blocked by the propeptide (Figure 4).

The interaction of the propeptide with the protease allows insights into substrate binding and protease specificity. The propeptide is located at the active site with Lys85 in P1' position and Leu83 in P2 position, both amino acids are within β -strand 6 (Figure 5a) that interacts with β -strand 13 of the protease in an antiparallel orientation. Specific interactions of AsaP1 protease to Lys85 can be assigned to the following amino acid residues: Phe259, Asp285, Asp330, Glu333 (Figure 5b). Whereas Asp330 is conserved among all aspzincins, Asp285 and Glu333 are only conserved among Lys-specific aspzincins (Figure 6). These negatively charged amino acid side chains are located at the bottom of the S1' binding pocket interacting with the positively charged amino group of the lysine side chain (Figure 5d). Asp285 and Glu333 are replaced by glutamine and alanine, respectively, in non-Lys-specific aspzincins. The methylene chain of the lysine residue interacts with Phe259 of the N-terminal protease domain, which is not strictly conserved but also found to be Tyr in Lys-specific aspzincins. In other aspzincins, hydrophobic amino acids like leucine or proline are common at this position. Thus a hydrophobic environment is established in the substrate binding site. Thr290 and Tyr334 are also part of the S1' binding pocket though their distance to the positively charged amino group of the lysine is $> 6 \text{ \AA}$. Thr290 is conserved among all aspzincins, whereas Tyr334 is only conserved among Lys-specific aspzincins and is often replaced with leucine in other aspzincins.

The P1 amino acid side chain (Ile84) is pointing into the opposite direction of the active site, because of the β -strand conformation. Leu83 binds to the S2 binding pocket. Within a radius of 4 \AA His297, Pro264, Pro66, Val262 interact with Leu83 in a hydrophobic

environment and the polypeptide backbone of Asp305 and Asp306 of the GTxD³⁰⁶xxYG loop (Figure 5e). The S2 binding pocket of the protease is rather unspecific in contrast to S1' (Figure 5c). Both amino acid residues, which bind to the active site, are not strictly conserved among aspzincins.

Crystal packing

In the crystal packing the quaternary structure is a homodimer for both AsaP1 mutants. In the orthorhombic packing the asymmetric unit consists of the homodimer, whereas in the monoclinic crystals the local twofold axis coincides with a crystallographic dyad (Figure 7a). Both inactive mutants AsaP1_{E294A/Q} are monomeric in solution as observed from gel-filtration chromatography (Supplementary Material, S1).

The connection of protease and propeptide could not be traced in any of the three structures and distance criteria are neither sufficient for finding the most probable connection. Possible interactions are that the propeptide binds intramolecular to the active site of the protease (1) or that it binds intermolecular to the other protease of the homodimer (2). Thus, for the homodimer that is detected in both crystal forms there are two possible dimer interfaces, depending on the connection of the propeptide domain to the protease (Figure 7b).

A PISA (PISA [22]) analysis revealed that both arrangements are predicted as stable in solution (Table 3). The arrangement with the propeptide in the active site of the protease of the other polypeptide shows that this interface is not significant for complexation and may be solely a result of crystal packing. For the interface with the intramolecular bound propeptide to the active site of the same polypeptide chain the data imply that this interface plays an auxiliary role in complexation.

Homologous structures of AsaP1

A DALI search [23] for the protease domain revealed two homologues proteases showing the aspzincin fold. The protein with the highest Z-score (28.10) is the Peptidyl-Lys metalloendopeptidase (*GfMEP*) from *Grifola frondosa* (pdb 1g12) [15] and the second is deuterolysin from *Aspergillus oryzae* (pdb 1eb6) [10] with a Z-score of 21.0. Both enzymes are structurally closely related to AsaP1 with a r.m.s. deviation for Ca-atoms of 2.0 Å for monoclinic AsaP1_{E294A} to deuterolysin and 1.0 Å to *GfMEP*, respectively. There are several other proteins containing a domain with a similar fold with a Z-score of 6.1 or less (Table 4).

The propeptide domain consists of a core region with 7 antiparallel β-strands arranged as a β-sandwich of a three stranded and a four stranded β-sheet (Figure 8). The homology search using DALI revealed seven proteins with a related fold (Table 4). Several proteins only consist of the target domain. The highest structural homology to the AsaP1 propeptide with a Z-score of 9.3 has an intracellular protease inhibitor from *Bacillus subtilis* (pdb 3isy). A Z-score of less than 7 was found for the FIXG-Related Protein from *Vibrio parahaemolyticus* rimd 221063 (pdb 2r39), the putative ApaA protein from *Bordetella Pertussis* (pdb 1xq4), the ApaG protein from *Xanthomonas axonopodis* pv. *citri* (pdb 2f1e) [24], the ApaG Protein from *Vibrio cholerae* (pdb 1xvs), and the ApaG Protein from *Shewanella oneidensis* mr-1 (pdb 1tza). The DALI search revealed also proteins with a higher molecular weight containing a sub-domain with the propeptide fold (Z-score 7.3 and less).

Discussion

Overall structure

Both inactive mutants AsaP1_{E294A} and AsaP1_{E294Q} crystallized in different space groups as homodimers with identical fold. The AsaP1 protease is coincident with the so far solved structures of M35 or aspzincin metalloendopeptidases [15, 25]. Due to inactivity of AsaP1_{E294A} and AsaP1_{E294Q} the structure of the propeptide is visible as a distinct domain. This is the first time that a propeptide structure is observed for the class of aspzincin metalloendopeptidases.

A sequence alignment of M35 proteases is shown in **Figure 9**. Apart from peptidyl-Lys metalloendopeptidase from *Pleurotus ostreatus* (*PoMEP*) all sequences show a signal sequence and a propeptide domain of comparable length and are autocatalytically processed to the mature enzyme. Although AsaP1 and *GfMEP*, respectively, share 43% amino acid sequence identity within their mature proteases there is no significant homology in their propeptide sequences.

The first 22 amino acid residues are a predicted signal sequence (SignalP 3.0 [26]), which is most likely cleaved off by transporting the protein via the cytosolic membrane into the periplasmic space by a sec-dependent, general secretory pathway [27].

Gaps in the structure, due to poor electron density, are most probably highly flexible regions. For example, the loop region Asp210 - Gly214, which is only visible in orthorhombic AsaP1_{E294A}, deuterolysin and *GfMEP*, indeed shows the highest r.m.s.d. within these three structures.

Due to the lack of electron density the connection of propeptide domain to the protease cannot be traced (residues 155– 171). Therefore it is not possible to specify unambiguously the biological unit (Figure 2). We suggest that the propeptide domain is bound to the active site of the protease of the same polypeptide and that the other

interface with weaker interaction is suitable to form the homodimer within the crystal lattices. This is in agreement with the observed monomeric fraction in gel-filtration experiments and the PISA analysis.

The domain interaction of protease and propeptide is most probably an intermediate in the autocatalytic maturation process of the protease, which could be trapped because of inactivity of the protease mutants.

Catalytic Zn²⁺ environment

The active site Zn²⁺ ion is coordinated by His293, His297 of the HExxH motif and Asp306 located in the GTxDxxYG motif downstream to the active-site helix, typical for M35 or aspzincin proteases [15, 25]. All binding distances of these conserved aspzincin motifs are in the expected range (Table 2)[21].

The aspartate in the AsaP1 mutants is found to bind in a monodentate manner, in contrast to the bifurcated interaction with the Zn²⁺ ion of aspzincins described by Hori *et al.* [15]. Generally, the fourth Zn²⁺ ligand is a water molecule that attacks as key nucleophile the carbonyl C atom of the peptide substrate. Both AsaP1 mutants are inactive because E294 is replaced by A or Q. In the wildtype enzyme this catalytic water ligand is activated by Zn²⁺ coordination and hydrogen bonding to glutamate of the HExxH motif. In AsaP1_{E294A} (monoclinic form) a chloro ligand is found in the position of the catalytic water molecule, as was observed elsewhere[28]. Polarization of the water by the carboxylate E294 is not possible and substitution by the negatively charged chloro ligand is a suitable alternative. In the orthorhombic form for both Zn²⁺ ions of the homodimer a weakly bound aqua ligand at 2.39Å and 2.40Å, respectively, is observed. In comparison to other Zn²⁺ metallopeptidases these distances seem to be rather long, but there are metallopeptidases without a watermolecule reported [29].

Tyr309 within the conserved GTxDxxYG motif was suggested to provide a hydrophobic environment to accommodate the hydrophobic lysine side chain of a substrate and to act as a hydrogen bond proton donor during catalysis to lower the energy of the oxyanion of the tetrahedral transition state [15]. The distance of the hydroxyl OH of Tyr309 to the carbonyl oxygen of the target peptide bond (Ile84O) is 2.80 Å and 2.61 for AsaP1_{E294A} in the orthorhombic and monoclinic crystals, respectively, but 5.31 Å in AsaP1_{E294Q}. Thus in both AsaP1_{E294A} structures Tyr309 occupies the proper position to reduce the transition-state energy. Equivalent proton donor residues are typical for proteases [30-33].

Substrate specificity

By mutation of catalytically important amino acids to an isosteric residue it is possible to crystallize a protease-substrate complex with intact substrate trapped at the active site [34-38]. On the basis of subsets of superimpositions of >1500 protease-ligand crystal structures for aspartic, serine, cysteine and metalloproteases [39] an extended β-strand conformation of the substrate was found to interact commonly with the active site of the protease. This interaction is also observed between the propeptide and the protease for the two inactive mutants of AsaP1 suggesting that the observed complex is analogous to an enzyme substrate complex, allowing insights of substrate binding and protease specificity. The substrate specificity of AsaP1 was not examined so far, but the highly specific interaction of the lysine residue with residues of the S1' pocket suggests at least a preference for lysine. Several amino acids that specifically interact with the Lys85 are found to be conserved in Lys-specific aspzincins [40, 41] but so far there were only two amino acids assigned for a determinant of a lysine-specificity. In AsaP1 there are three negatively charged amino-acids at the bottom of the S1'-pocket that could serve as

determinants for lysine-specific aspzincin proteases (Figure 6). The lysine specificity is so far only present in mushroom enzymes and therefore AsaP1 is obviously the first bacterial M35-protease with this specificity.

The conserved Tyr309 within the GTxDxxYG motif is supposed to interact with the hydrophobic methylen chain of lysine, contributing to the lysine specificity in GfMEP together with the aromatic ring of Phe259 [15]. In AsaP1 Tyr309 is part of the S1' binding pocket but the interactions to the lysine could not be considered specific, because of distances between both side chains of 5.2 Å and more (Figure 5). A mutation of Tyr309 to Phe in AsaP1 however shows a decreased activity [11].

With exception of PoMEP, all aspzincins identified so far are processed as a pre-pro-enzyme and contain a signal-sequence and a rather long propeptide region. It was shown that the maturation of AsaP1 is correlated to the caseinolytic activity and that recombinant AsaP1 is able to process inactive mutants (AsaP1_{E294A} and AsaP1_{E294Q}) to the size of the mature recombinant protease [11]. Based on a structural analysis of the complex formed by the inactive mutants with the propeptide, the polypeptide would be cleaved most likely at Ile84-Lys85, if the protease was active. The N-term of active AsaP1 starts at position 171 but there is no lysine in the direct environment, but it could be shown that AsaP1 is processed autocatalytically [11]. In other lysine-specific aspzincins the lysine at the N-term is also missing. Therefore a protease is suggested to activate the precursor [40].

By means of site-directed mutagenesis Lys85 was replaced by an alanine in inactive AsaP1_{E294Q} and AsaP1_{E294A} as well as for the recombinant expressed mature enzyme AsaP1_{rec}. AsaP1_{E294Q/K85A}, AsaP1_{E294A/K85A} and AsaP1_{rec/K85A} were expressed in *E. coli* yielding inclusion bodies indicating that Lys85 might be implemented in the folding mechanism of AsaP1, before it is autoproteolytically processed to the mature enzyme.

The propeptides of extracellular proteases often act as an intramolecular chaperone and inhibitor [42-55].

The activation mechanism of aspzincin proteases is not known so far. We suggest that the complex of mature AsaP1 with its propeptide is one intermediate within the processing of the protease, that could be trapped because of the inactivity of the mutants.

Homologous structures of AsaP1

AsaP1 belongs to the family of M35 or Deuterolysin like proteases and is structurally identical with other aspzincin proteases. Besides AsaP1, there are five proteases within the group of aspzinkin or M35 proteases. Penicillolysin from *Penicillium citrinumaus* (M35.001), Deuterolysin from *Aspergillus oryzae* (M35.002) and GfMEP (M35.004) are already reviewed [56-58]. The fifth protease is AVR-Pita peptidase from *Magnaporthe sp.* (M35.005) [59]. Even though these proteases are spread within plenty different organisms it was suggested that they have evolved from a common ancestor [40].

It is the first time that the propeptide structure could be shown for this class of proteases. For the propeptide domain structurally related proteins were found by DALI (Figure 8). The structure of ApaG and ApaA proteins show an Fn3 fold, but there is no sequence identity to other Fn3-fold proteins. The function of ApaG proteins is still unknown, but they might play a role in mediating protein-protein interactions [24]. In the Fix-G-related protein from *Vibrio parahaemolyticus* (pdb 2r39) one β -strand from the β -sandwich is interrupted by a loop insertion and thus the two β -sheets have one additional β -strand, which is only half as long as other β -strands of the sheet. The two β -sheets in the AsaP1 mutants do not form a real sandwich structure but are shifted against each other and therefore the amino-acid side chains of the two β -sheets could interact only marginally with each other (Figure 8a). Furthermore the fourth β -strand within the second β -sheet is

only composed of two amino acid residues, with the second being a proline. This β -strand is also shortened in the structure of the protease inhibitor from *Bacillus subtilis* (pdb 3isy) containing four amino acids (Figure 8b).

The single loop containing β -strand 6 is allocated apart from the core sandwich structure and interacts with the active site of AsaP1. It is only present in the protease-Inhibitor, but without strand conformation. Probably the β -strand conformation of the propeptide of AsaP1 is formed because of the interaction with the active site of the protease.

The protease inhibitor is referred to as an intracellular protein expressed from *B. subtilis* - a Gram-positive bacterium (pdb 3isy). Asap1 from *A. salmonicida* subsp. *Achromogenes* (Gram-negative) is a toxic extracellular protease.

The genomes von *B. subtilis*, *V. parahaemolyticus*, *B. pertussis*, *V. cholerae* and *S. oneidensis* are already sequenced but there is no homologue protease to AsaP1. Solely in *X. axonopodis* there is a homologue M35 Protease.

It is not clear whether the structural similarities of the proteins imply a comparable function. Based on the crystal structure, it is not possible to assign the function of the propeptide in case of AsaP1. We are in the process of purifying the AsaP1 propeptide to further study its function.

References:

1. Holt JG, Krieg NR, Sneath PHA, Staley JT, Williams ST: **Bergey's Manual of Determinative Bacteriology**, 9 edn. Baltimore: Williams and Wilkins; 1994.
2. Austin B, Austin DA, Dalsgaard I, Gudmundsdottir BK, Hoie S, Thornton JM, Larsen JL, O'Hici B, Powell R: **Characterization of atypical Aeromonas salmonicida by different methods**. *Syst Appl Microbiol* 1998, **21**(1):50-64.
3. Gudmundsdottir BK, Hvannadal I, Bjornsdottir B, Wagner U: **Analysis of exotoxins produced by atypical isolates of Aeromonas salmonicida, by enzymatic and serological methods**. *J Fish Dis* 2003, **26**(1):15-29.
4. Gudmundsdottir BK, Hastingst S, Ellis EA: **Isolation of a new toxic protease from a strain of Aeromonas salmonicida subspecies achromogenes**. *Diseases of Aquatic Organisms* 1990, **9**(3):199-208.
5. Gunnlaugsdottir B, Gudmundsdottir BK: **Pathogenicity of atypical Aeromonas salmonicida in Atlantic salmon compared with protease production**. *J Appl Microbiol* 1997, **83**(5):542-551.
6. Arnadottir H, Hvannadal I, Andressdottir V, Burr SE, Frey J, Gudmundsdottir BK: **The AsaP1 peptidase of Aeromonas salmonicida subsp. achromogenes is a highly conserved deuterolysin metalloprotease (family M35) and a major virulence factor**. *J Bacteriol* 2009, **191**(1):403-410.
7. Gudmundsdottir S, Gudmundsdottir B: **Induction of inflammatory cytokines by extracellular products and LPS of the fish pathogen Aeromonas salmonicida ssp. achromogenes in mice and mouse cell cultures**. *Vet Immunol Immunopathol* 2001, **81**(1-2):71-83.
8. Schwenteit J, Gram L, Nielsen KF, Fridjonsson OH, Bornscheuer UT, Givskov M, Gudmundsdottir BK: **Quorum sensing in Aeromonas salmonicida subsp. achromogenes and the effect of the autoinducer synthase AsaI on bacterial virulence**. *Vet Microbiol* 2011, **147**(3-4):389-397.
9. Hooper NM: **Families of zinc metalloproteases**. *FEBS Lett* 1994, **354**(1):1-6.
10. Fushimi N, Ee CE, Nakajima T, Ichishima E: **Aspzincin, a family of metalloendopeptidases with a new zinc-binding motif. Identification of new zinc-binding sites (His(128), His(132), and Asp(164)) and three catalytically crucial residues (Glu(129), Asp(143), and Tyr(106)) of deuterolysin from Aspergillus oryzae by site-directed mutagenesis**. *J Biol Chem* 1999, **274**(34):24195-24201.
11. Schwenteit J, Bogdanović X, Fridjonsson OH, Bornscheuer UT, Hinrichs W, Gudmundsdottir BK: **Construction of four toxoids of AsaP1, a lethal toxic aspzincin metalloendopeptidase of Aeromonas salmonicida subsp. achromogenes, and studies of its activity and processing**. submitted.
12. Bogdanovic X, Singh RK, Hentschke J, Gudmundsdottir BK, Hinrichs W: **Crystallization and preliminary X-ray diffraction studies of AsaP1_E294A and AsaP1_E294Q, two inactive mutants of the toxic zinc metallopeptidase AsaP1 from Aeromonas salmonicida subsp. achromogenes**. *Acta Crystallogr Sect F Struct Biol Cryst Commun* 2009, **65**(Pt 7):695-697.
13. Otwinowski Z, Minor W: **Processing of x-ray diffraction data collected in oscillation mode**. *Methods in Enzymology* 1997, **276**:307-326.
14. McCoy AJ, Grosse-Kunstleve RW, Adams PD, Winn MD, Storoni LC, Read RJ: **Phaser crystallographic software**. *J Appl Crystallogr* 2007, **40**(Pt 4):658-674.
15. Hori T, Kumazaka T, Yamamoto M, Nonaka N, Tanaka N, Hashimoto Y, Ueki U, Takio K: **Structure of a new 'aspzincin' metalloendopeptidase from Grifola**

- frondosa: implications for the catalytic mechanism and substrate specificity based on several different crystal forms.** *Acta Crystallogr D Biol Crystallogr* 2001, **57**(Pt 3):361-368.
16. Morris RJ, Perrakis A, Lamzin VS: **ARP/wARP and automatic interpretation of protein electron density maps.** *Methods Enzymol* 2003, **374**:229-244.
 17. Vagin AA, Steiner RA, Lebedev AA, Potterton L, McNicholas S, Long F, Murshudov GN: **REFMAC5 dictionary: organization of prior chemical knowledge and guidelines for its use.** *Acta Crystallogr D Biol Crystallogr* 2004, **60**(Pt 12 Pt 1):2184-2195.
 18. **The CCP4 suite: programs for protein crystallography.** *Acta Crystallogr D Biol Crystallogr* 1994, **50**(Pt 5):760-763.
 19. Emsley P, Cowtan K: **Coot: model-building tools for molecular graphics.** *Acta Crystallogr D Biol Crystallogr* 2004, **60**(Pt 12 Pt 1):2126-2132.
 20. Davis IW, Leaver-Fay A, Chen VB, Block JN, Kapral GJ, Wang X, Murray LW, Arendall WB, 3rd, Snoeyink J, Richardson JS *et al*: **MolProbity: all-atom contacts and structure validation for proteins and nucleic acids.** *Nucleic Acids Res* 2007, **35**(Web Server issue):W375-383.
 21. Harding MM: **Small revisions to predicted distances around metal sites in proteins.** *Acta Crystallogr D Biol Crystallogr* 2006, **62**(Pt 6):678-682.
 22. Krissinel E, Henrick K: **Inference of Macromolecular Assemblies from Crystalline State.** *Journal of molecular biology* 2007, **372**(3):774-797.
 23. Holm L, Rosenstrom P: **Dali server: conservation mapping in 3D.** *Nucleic Acids Res* 2010, **38 Suppl**:W545-549.
 24. Cicero DO, Contessa GM, Pertinhez TA, Gallo M, Katsuyama AM, Paci M, Farah CS, Spisni A: **Solution structure of ApaG from Xanthomonas axonopodis pv. citri reveals a fibronectin-3 fold.** *Proteins* 2007, **67**(2):490-500.
 25. McAuley KE, Jia-Xing Y, Dodson EJ, Lehmbeck J, Østergaard PR, Wilson KS: **A quick solution: ab initio structure determination of a 19 kDa metalloproteinase using ACORN.** *Acta Crystallogr D Biol Crystallogr* 2001, **57**(Pt 11):1571-1578.
 26. Bendtsen JD, Nielsen H, von Heijne G, Brunak S: **Improved prediction of signal peptides: SignalP 3.0.** *Journal of molecular biology* 2004, **340**(4):783-795.
 27. du Plessis DJF, Nouwen N, Driessens AJM: **The Sec translocase.** *Biochimica et Biophysica Acta (BBA) - Biomembranes* 2011, **1808**(3):851-865.
 28. Yen N, Bogdanović X, Palm G, Kühl O, Hinrichs W: **Structure of the Ni(II) complex of Escherichia coli peptide deformylase and suggestions on deformylase activities depending on different metal(II) centres.** *Journal of Biological Inorganic Chemistry* 2010, **15**(2):195-201.
 29. Lipscomb WN, Sträter N: **Recent Advances in Zinc Enzymology.** *Chemical Reviews* 1996, **96**(7):2375-2434.
 30. Holden HM, Tronrud DE, Monzingo AF, Weaver LH, Matthews BW: **Slow- and fast-binding inhibitors of thermolysin display different modes of binding: crystallographic analysis of extended phosphonamide transition-state analogues.** *Biochemistry* 1987, **26**(26):8542-8553.
 31. Grams F, Dive V, Yiotakis A, Yiallouros I, Vassiliou S, Zwilling R, Bode W, Stocker W: **Structure of astacin with a transition-state analogue inhibitor.** *Nat Struct Biol* 1996, **3**(8):671-675.
 32. Bode W, Walter J, Huber R, Wenzel HR, Tschesche H: **The refined 2.2-Å (0.22-nm) X-ray crystal structure of the ternary complex formed by bovine**

- trypsinogen, valine-valine and the Arg15 analogue of bovine pancreatic trypsin inhibitor.** *European Journal of Biochemistry* 1984, **144**(1):185-190.
33. Kim H, Lipscomb WN: **Comparison of the structures of three carboxypeptidase A-phosphonate complexes determined by x-ray crystallography.** *Biochemistry* 1991, **30**(33):8171-8180.
34. Prabu-Jeyabalan M, Nalivaika E, Schiffer CA: **Substrate Shape Determines Specificity of Recognition for HIV-1 Protease: Analysis of Crystal Structures of Six Substrate Complexes.** *Structure (London, England : 1993)* 2002, **10**(3):369-381.
35. Laco GS, Schalk-Hihi C, Lubkowski J, Morris G, Zdanov A, Olson A, Elder JH, Wlodawer A, Gustchina A: **Crystal Structures of the Inactive D30N Mutant of Feline Immunodeficiency Virus Protease Complexed with a Substrate and an Inhibitor†,‡.** *Biochemistry* 1997, **36**(35):10696-10708.
36. Phan J, Zdanov A, Evdokimov AG, Tropea JE, Peters HK, Kapust RB, Li M, Wlodawer A, Waugh DS: **Structural Basis for the Substrate Specificity of Tobacco Etch Virus Protease.** *Journal of Biological Chemistry* 2002, **277**(52):50564-50572.
37. Turk BE, Wong TY, Schwarzenbacher R, Jarrell ET, Leppla SH, Collier RJ, Liddington RC, Cantley LC: **The structural basis for substrate and inhibitor selectivity of the anthrax lethal factor.** *Nat Struct Mol Biol* 2004, **11**(1):60-66.
38. Fülöp V, Szeltner Z, Renner V, Polgár L: **Structures of Prolyl Oligopeptidase Substrate/Inhibitor Complexes.** *Journal of Biological Chemistry* 2001, **276**(2):1262-1266.
39. Madala PK, Tyndall JDA, Nall T, Fairlie DP: **Update 1 of: Proteases Universally Recognize Beta Strands In Their Active Sites.** *Chemical Reviews* 2010, **110**(6):PR1-PR31.
40. Nonaka T, Dohmae N, Hashimoto Y, Takio K: **Amino Acid Sequences of Metalloendopeptidases Specific for Acyl-Lysine Bonds from Grifola frondosa and Pleurotus ostreatus Fruiting Bodies.** *Journal of Biological Chemistry* 1997, **272**(48):30032-30039.
41. Nonaka T, Hashimoto Y, Takio K: **Kinetic Characterization of Lysine-Specific Metalloendopeptidases from Grifola frondosa and Pleurotus ostreatus Fruiting Bodies.** *Journal of Biochemistry* 1998, **124**(1):157-162.
42. Baker D, Sohl JL, Agard DA: **A protein-folding reaction under kinetic control.** *Nature* 1992, **356**(6366):263-265.
43. Braun P, Tommassen J: **Function of bacterial propeptides.** *Trends in Microbiology* 1998, **6**(1):6-8.
44. Carmona E, Dufour É, Plouffe C, Takebe S, Mason P, Mort JS, Ménard R: **Potency and Selectivity of the Cathepsin L Propeptide as an Inhibitor of Cysteine Proteases†.** *Biochemistry* 1996, **35**(25):8149-8157.
45. Demidyuk IV, Gromova TY, Polyakov KM, Melik-Adamyan WR, Kuranova IP, Kostrov SV: **Crystal Structure of the Protealysin Precursor.** *Journal of Biological Chemistry* 2010, **285**(3):2003-2013.
46. Eder J, Rheinnecker M, Fersht AR: **Folding of subtilisin BPN': characterization of a folding intermediate.** *Biochemistry* 1993, **32**(1):18-26.
47. Fu X, Inouye M, Shinde U: **Folding Pathway Mediated by an Intramolecular Chaperone.** *Journal of Biological Chemistry* 2000, **275**(22):16871-16878.
48. Gao X, Wang J, Yu D-Q, Bian F, Xie B-B, Chen X-L, Zhou B-C, Lai L-H, Wang Z-X, Wu J-W *et al*: **Structural basis for the autoprocessing of zinc**

- metalloproteases in the thermolysin family.** *Proceedings of the National Academy of Sciences* 2010, **107**(41):17569-17574.
49. Guevara T, Yiallouros I, Kappelhoff R, Bissdorf S, Stöcker W, Gomis-Rüth FX: **Proenzyme Structure and Activation of Astacin Metallopeptidase.** *Journal of Biological Chemistry* 2010, **285**(18):13958-13965.
50. Inouye M: **Intramolecular chaperone: the role of the pro-peptide in protein folding.** *Enzyme* 1991, **45**(5-6):314-321.
51. Khan AR, James MNG: **Molecular mechanisms for the conversion of zymogens to active proteolytic enzymes.** *Protein Science* 1998, **7**(4):815-836.
52. Li Y, Hu Z, Jordan F, Inouye M: **Functional Analysis of the Propeptide of Subtilisin E as an Intramolecular Chaperone for Protein Folding.** *Journal of Biological Chemistry* 1995, **270**(42):25127-25132.
53. Ramos C, Winther JR, Kielland-Brandt MC: **Requirement of the propeptide for in vivo formation of active yeast carboxypeptidase Y.** *Journal of Biological Chemistry* 1994, **269**(9):7006-7012.
54. Silen JL, Agard DA: **The [alpha]lytic protease pro-region does not require a physical linkage to activate the protease domain in vivo.** *Nature* 1989, **341**(6241):462-464.
55. van den Hazel HB, Kielland-Brandt MC, Winther JR: **The propeptide is required for in vivo formation of stable active yeast proteinase A and can function even when not covalently linked to the mature region.** *Journal of Biological Chemistry* 1993, **268**(24):18002-18007.
56. Ichishima E: **Penicillolysin.** In: *Handbook of Proteolytic Enzymes*. Edited by Barrett AJ, Rawlings,N.D. & Woessner,J.F., vol. 2 edn (eds). London Elsevier; 2004: 784-786.
57. Tatsumi H: **Deuterolysin.** In: *In Handbook of Proteolytic Enzymes*. Edited by Barrett AJ, Rawlings, N.D. & Woessner,J.F., vol. 2 end. London: Elsevier; 2004: 786-788.
58. Takio K: **Peptidyl-Lys metalloendopeptidase.** In: *In Handbook of Proteolytic Enzymes*. Edited by Barrett AJ, Rawlings,N.D. & Woessner,J.F. eds, vol. 2 edn. London: Elsevier; 2004: 788-792.
59. Zhou E, Jia Y, Singh P, Correll JC, Lee FN: **Instability of the Magnaporthe oryzae avirulence gene AVR-Pita alters virulence.** *Fungal genetics and biology : FG & B* 2007, **44**(10):1024-1034.
60. Corpet F: **Multiple sequence alignment with hierarchical clustering.** *Nucleic Acids Research* 1988, **16**(22):10881-10890.
61. Gouet P, Courcelle E, Stuart DI, M©toz F: **EScript: analysis of multiple sequence alignments in PostScript.** *Bioinformatics* 1999, **15**(4):305-308.

Table 1: X-Ray data-collection statistics of AsaP1_{E294A} and Asap1_{E294Q}.

	AsaP1 _{E294Q}	AsaP1 _{E294A}	AsaP1 _{E294A}
Pdb code	2x3a	2x3c	2x3b
A. Data collection			
Space group	C2	C2	P2 ₁ 2 ₁ 2 ₁
Unit-cell parameters			
<i>a</i> (Å)	98.5	102.0	57.9
<i>b</i> (Å)	74.5	72.0	60.2
<i>c</i> (Å)	54.7	55.0	183.6
α (°)	90.0	90.0	90.0
β (°)	112.4	109.8	90.0
γ (°)	90.0	90.0	90.0
Wavelength (Å)	0.9537	0.9778	0.9778
Resolution range (Å)	99.0 – 2.0 (2.05 - 2.00)	90.0 – 2.0 (2.05 – 2.0)	90.0 – 2.2 (2.25 - 2.20)
Completeness (%)	98.9 (86.3)	99.8 (100)	99.4 (93.1)
Multiplicity	3.8 (3.4)	5.7 (5.3)	6.1 (3.7)
Average $I / \sigma(I)$	18.7 (3.3)	23.6 (3.5)	19.3 (2.69)
R_{merge} (%)	10.1 (39.3)	8.8 (53.8)	13.3 (60.2)
$R_{\text{r.i.m.}}$ (%)	10.7 (53.3)	8.4 (42.7)	15.9 (50.7)
$R_{\text{p.i.m.}}$ (%)	5.5 (27.8)	3.4 (18.0)	6.0 (18.5)
Wilson B factor (Å ²)	25.8	29.4	41.7
B. Refinement			
No. of reflections	23411	37710	30802
R_{work} (%)	17.01	17.19	24.43
R_{free} (%)	20.46	21.43	29.33
F.O.M.	0.87	0.87	0.79
No. of atoms	2525	2451	4806
Average B-Factors (Å ²)			
Overall	22.1	26.4	27.8
Protein main chain	20.0	24.5	27.4
Protein side chains + water	23.9	28.0	28.2
R.m.s. deviations			
Bond lengths (Å)	0.023	0.022	0.017
Bond angles (°)	1.928	1.899	1.672
Ramachandran plot			
Most favored (%)	91.8	93.1	90.3
Additional allowed (%)	8.2	6.9	9.7

Values in parentheses correspond to values in the highest resolution shell

Table 2: selected binding distances of AsaP1_{E294A} and AsaP1_{E294Q} in [Å].

Crystal	AsaP1_E294Q	AsaP1_E294A	AsaP1_E294A
Space group	C2	C2	P2 ₁ 2 ₁ 2 ₁
Pdb entry	2x3a	2x3c	2x3b
Catalytic zinc-ion binding distance to			
Nε2 of His293	1.85	2.14	2.05
Nε2 of His297	2.35	1.97	1.95
Oδ1 of Asp306	2.84	1.85	2.81
Oδ2 of Asp306	2.01	2.72	1.91
Water molecule			
Chlorid ion		2.37	
Carbonyl-O of peptide bond Ile84-Leu85	2.98	3.75	3.72
Carbonyl-O of peptide bond Ile84-Leu85 to Tyr309 OH	5.31	2.61	2.80

Table 3: Details PISA analysis

	Interface 1	Interface 2
interface area Å ²	1728	1624
Δ ⁱ G kcal/mol	-12.9	1.0
P-value	0.246	0.765
CSS	0.148	0.091

CSS (complexation significance score) ranges from 0 to 1 as interface relevance to complexation increases.

Table 4: DALI search showing all proteins with a Z-score of 6 and higher for the protease part and the propeptide domain.

Pdb	Z-score	RMSD. (Å)	lali	nres	%id	Protein	source
Protease (amino acids 172-343)							
1g12	28.40	0.9	159	167	46	Peptidyl-Lys Metalloendopeptidase	<i>Grifola frondosa</i>
1eb6	21.1	1.9	157	177	24	Neutral protease II (Deuterolysin)	<i>Aspergillus oryzae</i>
2gtq	6.2	3.2	105	864	10	Aminopeptidase N	<i>Homo sapiens</i>
Propeptide (amino acids 1-172)							
3isy	9.3	2.7	102	117	12	Intracellular Proteinase Inhibitor	<i>Bacillus subtilis</i>
119m	7.3	3.4	92	681	9	Protein-Glutamine Glutamyltransferase E3	<i>Homo sapiens</i>
2r39	6.9	2.6	86	109	7	FIXG-Related Protein, chain A	<i>Vibrio parahaemolyticus</i> rimb 221063
1xq4	6.9	2.5	89	116	13	Protein ApaG	<i>Bordetella pertussis</i>
2f1e	6.7	2.4	89	116	13	Protein ApaG, chain A	<i>Xanthomonas axonopodis</i> pv. <i>citri</i>
2q3z	6.6	3.5	90	655	14	Transglutaminase 2, chain A	<i>Xanthomonas axonopodis</i> pv. <i>citri</i>
1xvs	6.6	2.6	89	124	13	Protein ApaG, chain B	<i>Vibrio cholerae</i>
1f13	6.5	3.0	90	721	6	Cellular Coagulation Factor XIII Zymogen	<i>Kluveromyces marxianus</i>
3abz	6.5	2.7	91	810	14	β -Glucosidase I, chain A	<i>Thermotoga neapolitana</i>
2x41	6.5	2.8	92	715	18	β -Glucosidase, chain A	<i>Pagrus major</i>
1g0d	6.5	3.5	90	666	11	Protein-Glutamine γ -Glutamyltransferase	<i>Shewanella oneidensis</i> mr-1
1tza	6.4	6.1	90	132	7	ApaG Protein	<i>Homo sapiens</i>
3ly6	6.4	6.1	90	683	14	Protein-Glutamine γ -Glutamyltransferase 2	<i>Bacteroides thetaiotaomicron</i>
2je8	6.1	2.7	85	841	11	β -Mannosidase, chain B	

Z score, the statistical significance of the similarity between AsaP1_{E294A} and neighbourhood protines; Root Mean Square Distance (RMSD), root-mean-square deviation of C-alpha atoms; lali, number of structurally equivalent residues; nres, total number of amino acids in the hit protein; %id, percentage of identical amino acids over structurally equivalent residues

Figure legends:

Figure 1: Structure of AsaP1_{E294A} the complex of AsaP1 protease with the propeptide domain. Zinc ion is displayed as magenta sphere; helices (α 1-8) of the protease are labeled in green, these from the propeptides (η 1-2) in pale green, sheets are marked in dark blue for the protease (β 10-14) and in light blue for the propeptide (β 1-9). Selected residues of AsaP1 are numbered to help orientate the reader. Zinc ligands are shown as sticks with typical color code for atoms.

Figure 2: Coordination of the active-site zinc-ion. The zinc ligands are represented as sticks with O atoms in red and N atoms in blue. The zinc ion is shown as magenta sphere **a)** Monoclinic AsaP1_{E294A} with chloride as green sphere. **b)** Orthorhombic AsaP1_{E294A} **c)** Monocline AsaP1_{E294Q}

Figure 3: Superposition of the active sites of all three mutants based on the active-site zinc ion. The orthorhombic AsaP1_{E294A} mutant is shown in light blue; the monoclinic AsaP1_{E294A} mutant is presented in dark blue. The monoclinic AsaP1_{E294Q} mutant is colored in green. The active-site zinc ion is shown as magenta sphere and the chloride ion found in the monoclinic AsaP1_{E294A} mutant is shown as green sphere. Amino acids at the active site are labeled and presented with the O atoms in red and the N atoms in blue.

Figure 4: The active site of the protease is blocked by the propeptide domain. **a)** Surface representation of the protease domain. **b)** The protease domain with a propeptide domain blocking the active site. Color coding: β -strands, blue; α -helices, green and loops grey. The zinc ion is magenta. In the propeptide β -strands, light blue; loops, grey.

Figure 5: Substrate specificity of AsaP1_{E294Q}. **a)** Interaction of β -strand 6 from the propeptide with the protease domain. **b)** Surface representation of the S1'- and the S2 binding pocket **c)**. Color scheme: Carbon atoms green; nitrogen atoms blue and oxygen atoms red. Amino acids Lys85 and Leu83 from the propeptide are represented as sticks and colored in cyan. **d)** Schematic drawing of the S1'- and S2 binding pocket **e)**. Shown are all amino acid residues in a radius of 6 Å. H-bonds are labeled in blue with the corresponding distances in Å. Hydrophobic interactions are marked in green, considering atoms with a distance up to 4 Å.

Figure 6: Multiple sequence alignment of AsaP1, with all M35 proteases with evidence at the protein level. AsaP1 AERSA (*A. salmonicida* subsp. *achromogenes*), EPRA1 AERHY (*Aeromonas hydrophila*), GfMEP GRIFR (*Grifola frondosa*), PLMP ARME (*Armillaria mellea*), PLMP PLEOS (*Pleurotus ostreatus*), Penicillolysin PENCI (*Penicillium citrinum*), Deuterolysin ASPOR (*Aspergillus oryzae*). Identical residues are presented in white on a red background, similar residues are indicated by red lettering on a white background. Secondary structure elements of AsaP1 are given above the sequence. The alignment was generated with MultAlin [60] and illustrated using ESPript 2.2 [61]. Highly conserved regions typical for aspzincin proteases are labeled in blue, possible determinants for lysine specificity are labeled in green.

Figure 7: Conserved dimeric arrangement observed in the two different crystal lattices of AsaP1_{E294A} and both possible interactions of propeptide and protease. **a)** Superposition of the C α -traces of the asymmetric unit of orthorhombic (blue) and monoclinic crystals (red) and the corresponding symmetry mate (orange). The local-twofold axis creating the dimer in the asymmetric unit of the orthorhombic crystal coincides with the crystallographic symmetry in the monoclinic crystal. **b)** The protease with two alternative positions of the propeptide domain. Zinc ion is displayed as magenta sphere; helices of the protease are labeled in green these from the propeptides in pale green, sheets are marked in dark blue for the protease and in light blue for the propeptides.

Figure 8: Structural comparision of **a)** AsaP1_{E294Q} propeptid **f)** protease inhibitor from *B. subtilis* (pdb 3isy), **g)** FixG-related protein from *V. parahaemolyticus* (pdb 2r39), **h)** different ApaG-proteins shown in different blues (putative ApaA protein from *Bordetella Pertussis* (pdb 1xq4), the ApaG protein from *Xanthomonas axonopodis* pv. *citri* (pdb 2f1e), the ApaG Protein from *Vibrio cholerae* (pdb 1xvs) [5]).

Figure 1:

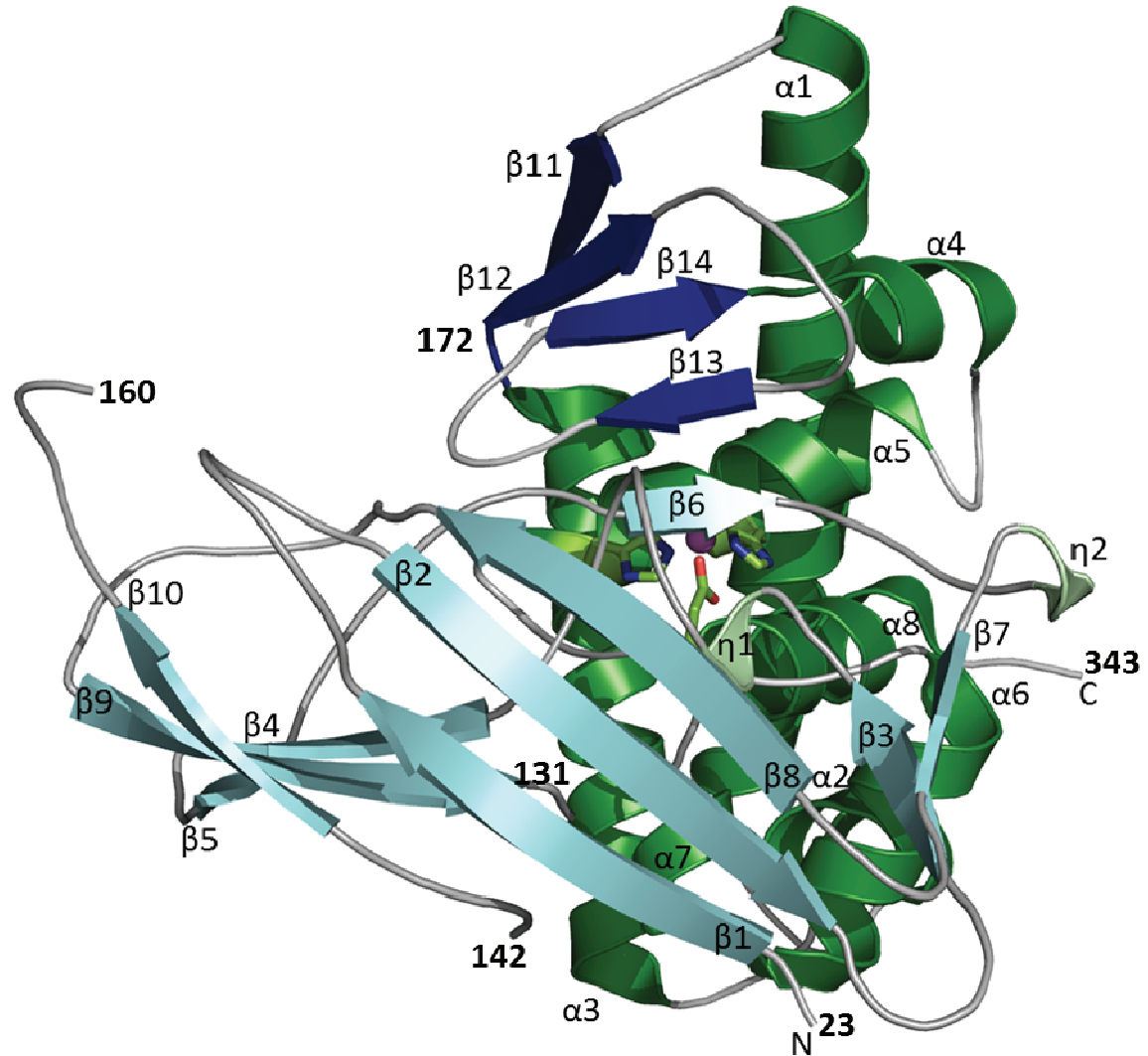


Figure 2:

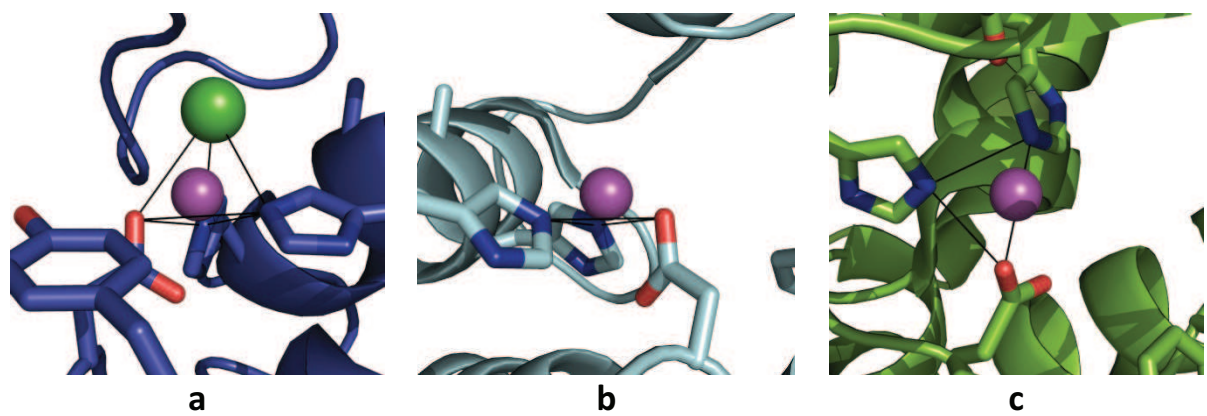


Figure 3:

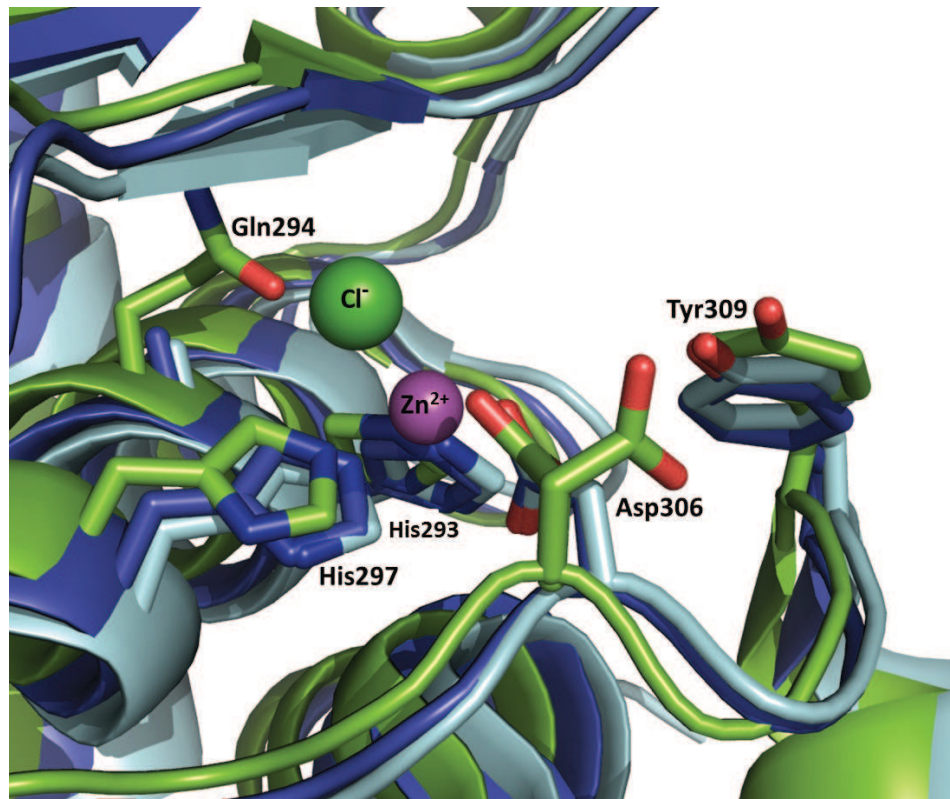


Figure 4

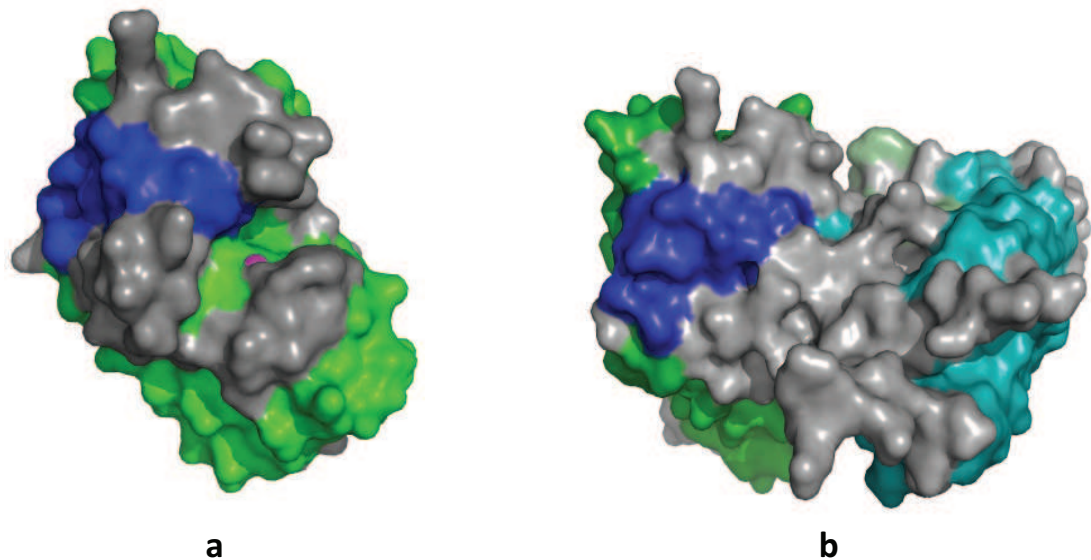


Figure 5:

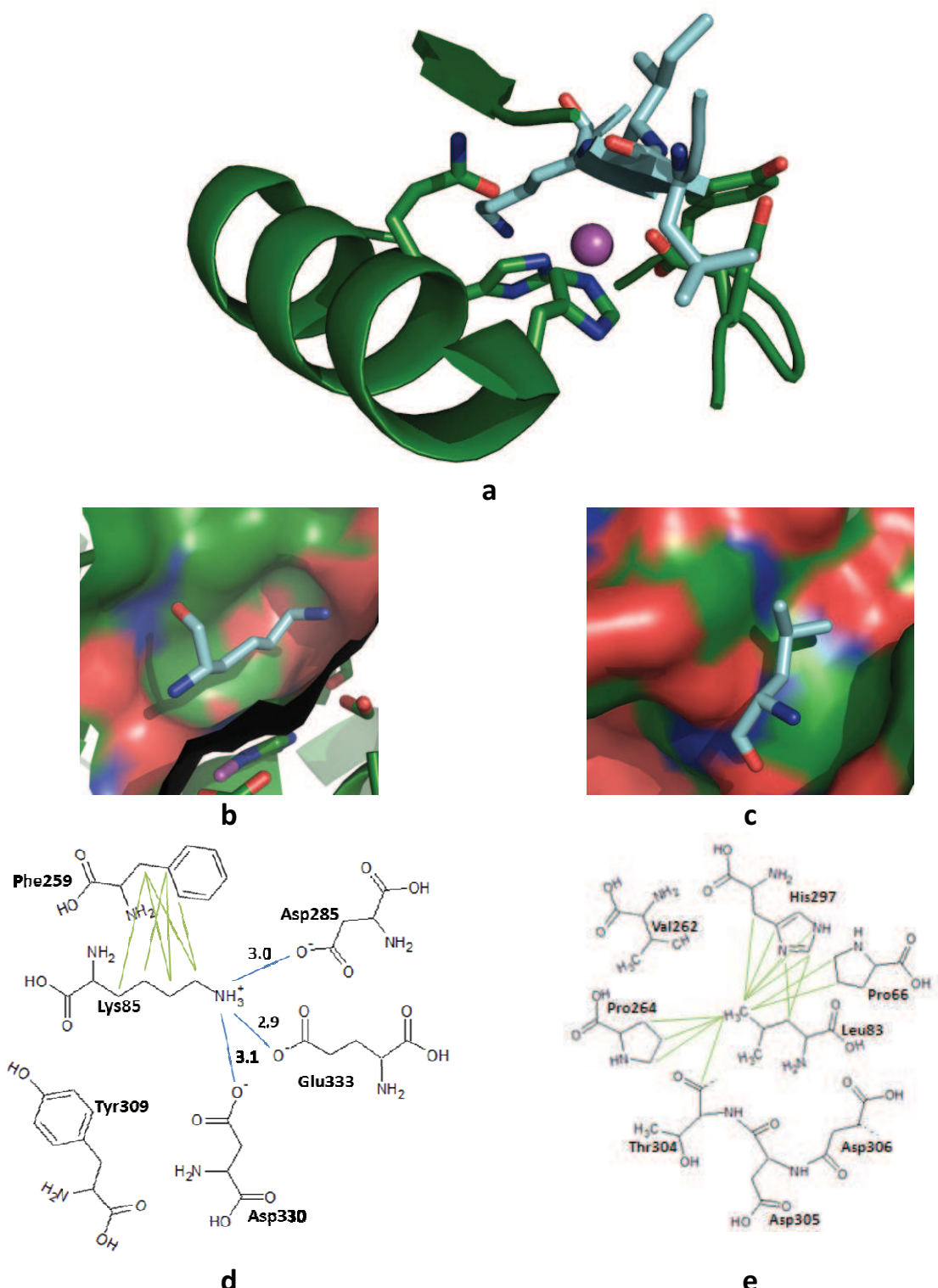


Figure 6:

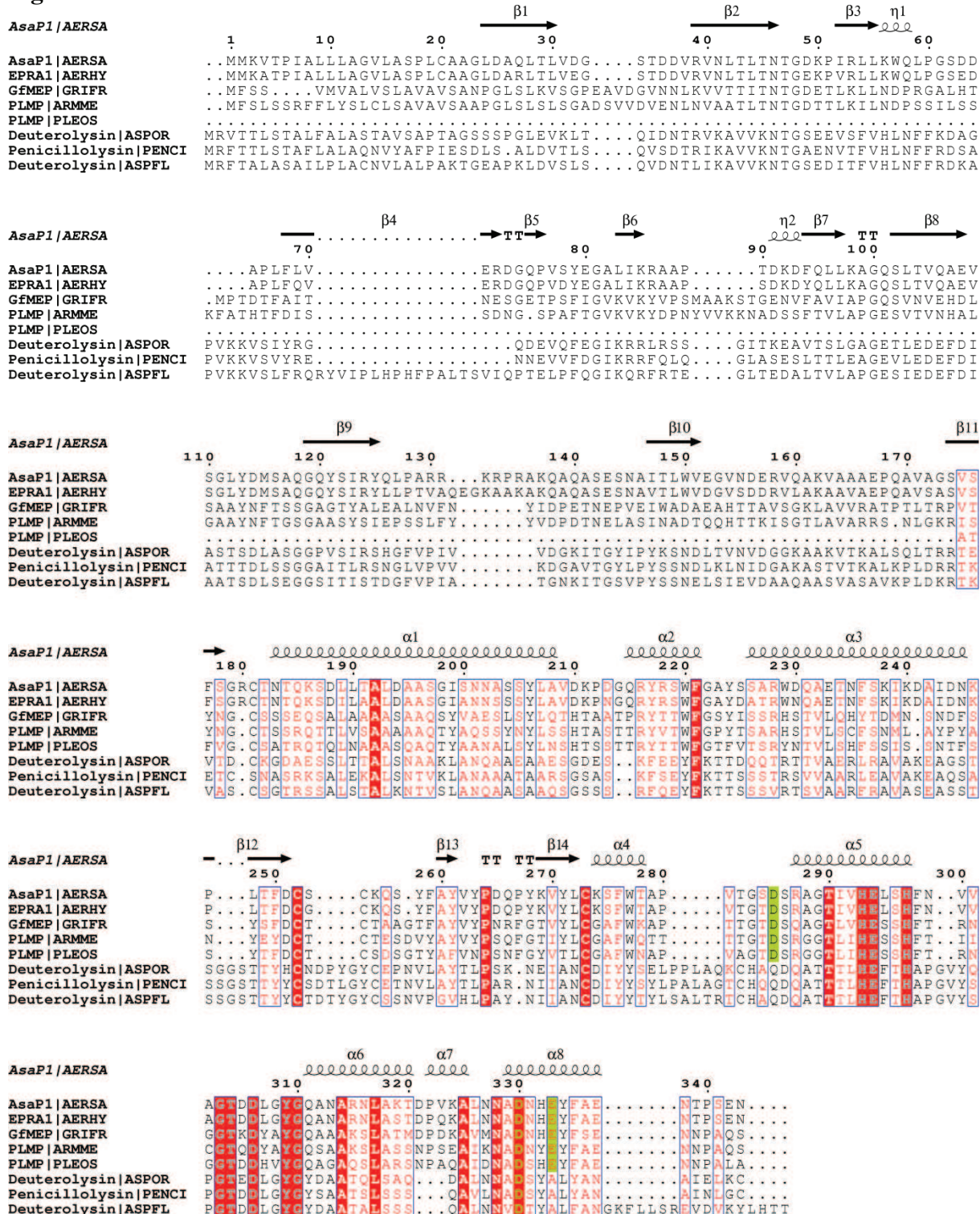


Figure 7:

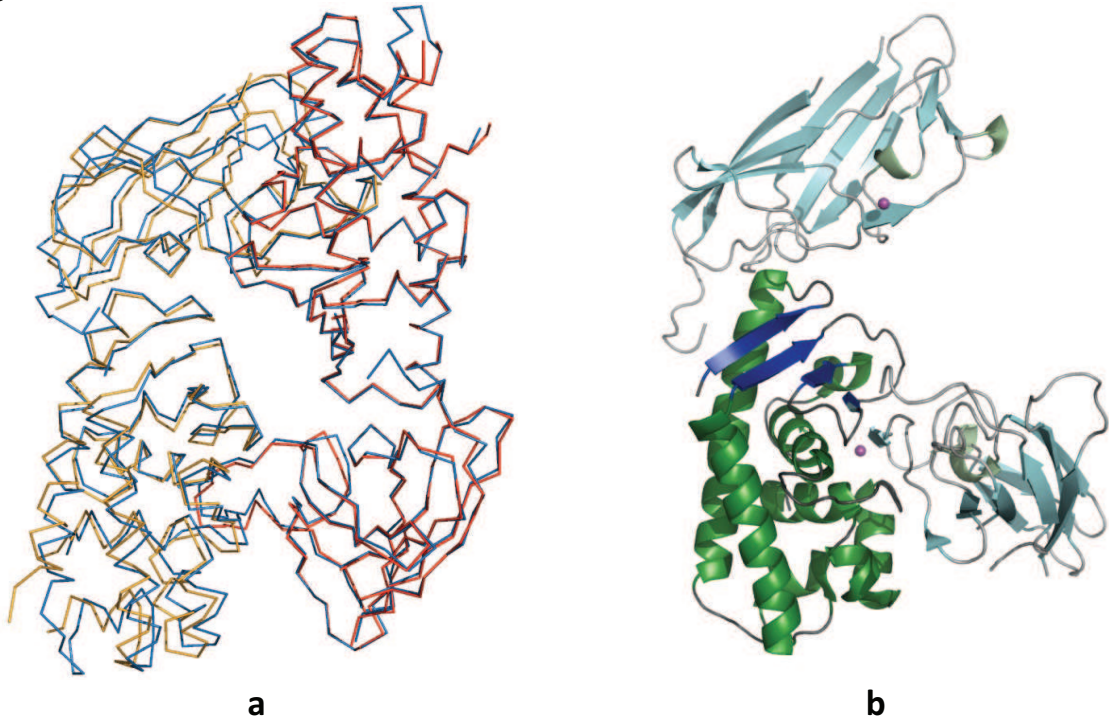
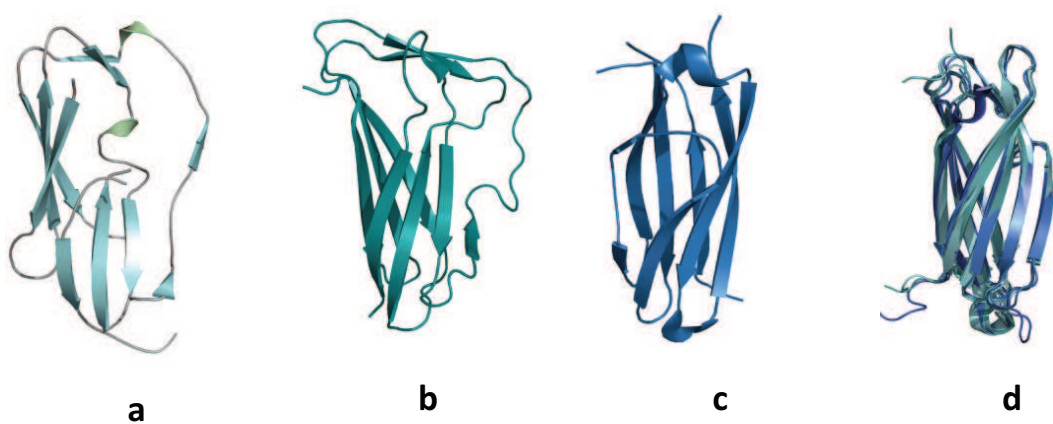


Figure 8:



Supporting Information

Structure of inactive mutants of the aspzincin metalloendopeptidase AsaP1 in complex with its propeptide

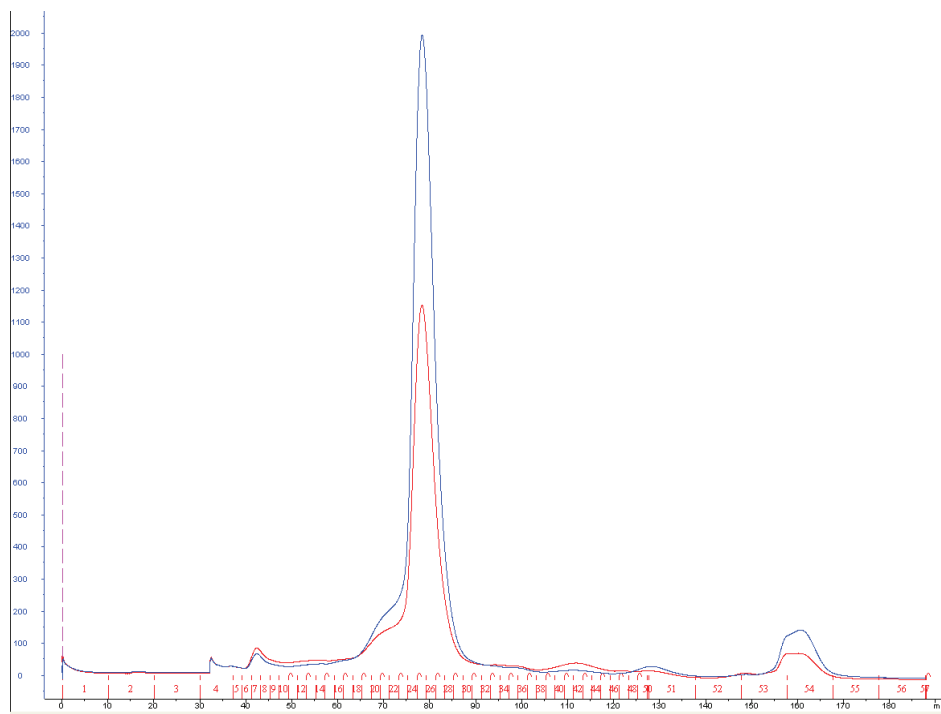
Xenia Bogdanović¹, Johanna Schwenteit¹, Rajesh Kumar Singh^{1*}, Bjarnheidur K. Gudmundsdóttir² and Winfried Hinrichs¹

¹ Institut für Biochemie, Universität Greifswald, Felix-Hausdorff-Str. 4, D-17489 Greifswald, Germany.

² Institute for Experimental Pathology, University of Iceland, Keldur, 112-Reykjavík, Iceland

*Current address: Chemical Engg. Division, National Chemical Laboratory, Dr. Homi Bhabha Road, Pune, 411008. India.

Correspondence e-mail: winfried.hinrichs@uni-greifswald.de



S1: Results fro gelfiltration chromatography of AsaP1_{E294Q}. Indicating a monomeric protein at a size corresponding to 37 kDa.

Xenia Bogdanović,^{a*} Martin Hessler,^b Gottfried J. Palm,^a Uwe T. Bornscheuer^b and Winfried Hinrichs^a

^aMolecular Structural Biology, Institute for Biochemistry, University of Greifswald, Felix-Hausdorff-Strasse 4, D-17489 Greifswald, Germany, and ^bBiotechnology and Enzyme Catalysis, Institute for Biochemistry, University of Greifswald, Felix-Hausdorff-Strasse 4, D-17489 Greifswald, Germany

Correspondence e-mail:
xenia.bogdanovic@uni-greifswald.de

Received 30 March 2010
Accepted 20 May 2010

Crystallization and preliminary X-ray diffraction studies of the putative haloalkane dehalogenase DppA from *Plesiocystis pacifica* SIR-I

DppA from *Plesiocystis pacifica* SIR-I is a putative haloalkane dehalogenase (EC 3.8.1.5) and probably catalyzes the conversion of halogenated alkanes to the corresponding alcohols. The enzyme was expressed in *Escherichia coli* BL21 and purified to homogeneity by ammonium sulfate precipitation and reversed-phase and ion-exchange chromatography. The DppA protein was crystallized by the vapour-diffusion method and protein crystals suitable for data collection were obtained in the orthorhombic space group $P2_12_12$. The DppA crystal diffracted X-rays to 1.9 Å resolution using an in-house X-ray generator.

1. Introduction

Haloalkane dehalogenases (EC 3.8.1.5) are α/β -hydrolase fold enzymes that catalyze the hydrolytic conversion of a broad spectrum of halogenated alkanes to the corresponding alcohols (Janssen, 2004). This reaction is of great environmental interest and haloalkane dehalogenases have therefore been extensively studied in recent years. Attempts have been made to enhance the speed of the catalytic reaction, to expand the substrate range and to increase the enantioselectivity (Bosma *et al.*, 2002; Schanstra *et al.*, 1996; Gray *et al.*, 2001; Chaloupkova *et al.*, 2003; Pries *et al.*, 1994; Holloway *et al.*, 1998). To date, only a handful of haloalkane dehalogenases have been crystallized (Franken *et al.*, 1991; Newman *et al.*, 1999; Marek *et al.*, 2000; Stsiapanava *et al.*, 2008; Mazumdar *et al.*, 2008), of which the enzymes from *Xanthobacter autotrophicus* GJ10, *Sphingomonas paucimobilis* UT26 and *Rhodococcus rhodochrous* NCIMB13064 have been extensively investigated in several further studies. They all share the α/β -hydrolase fold, which is a hallmark of this class of enzymes (Ollis *et al.*, 1992).

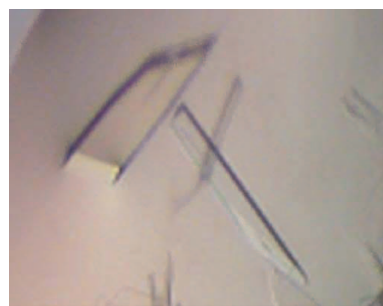
Plesiocystis pacifica SIR-1 is a myxobacterium which was isolated from the Japanese coast (Iizuka *et al.*, 2003). The strain is Gram-negative, chemoheterotrophic and strictly aerobic (Iizuka *et al.*, 2003). Its DNA sequence is available online at NCBI as a shotgun library (NCBI reference sequence NZ_ABCS00000000). The entry ZP_01908831.1 is tagged as a putative haloalkane dehalogenase with a calculated molecular weight of 32 kDa.

This haloalkane dehalogenase was chosen as it showed the highest sequence homology to another dehalogenase currently under study in an ongoing project and showed good alignment, with the residues of the catalytic triad (Asp-His-Asp) in reasonable positions.

2. Materials and methods

2.1. Protein expression and purification

The strain *P. pacifica* SIR-I was ordered from the German Collection of Microorganisms and Cell Cultures (DSMZ; DSM No. 14875) and was supplied as an actively growing culture on agar medium. Genomic DNA of *P. pacifica* SIR-I was amplified with the help of the GenomiPhi-Kit from GE Healthcare. The coding region of ZP_01908831.1 was cloned into a pET28a vector (without a His



© 2010 International Union of Crystallography
All rights reserved

tag) and expressed in *Escherichia coli* BL21 Gold. The cells were grown at 310 K to an OD₆₀₀ of 0.5, induced with IPTG (final concentration 0.1 mM) and incubated at 293 K overnight. Subsequently, the cells were harvested and resuspended in buffer A (10 mM Tris-HCl buffer pH 8). The cells were disrupted by adding lysozyme (incubation time of 1 h at 280 K on an orbital shaker) and further treatment with a French press (three rounds of disruption). The cell lysate was centrifuged at 8000g for 45 min to remove cellular debris.

Ammonium sulfate precipitation was carried out using 15% (w/v) ammonium sulfate in buffer A with an incubation time of 2 h at 280 K. Afterwards, the solution was centrifuged at 8000g for 30 min. The following purification steps were all performed using an ÄKTA Purifier (GE Healthcare). The cell lysate was applied onto a Butyl Sepharose column equilibrated with buffer A and eluted using a linear gradient from 15 to 0% ammonium sulfate. Fractions containing DppA were pooled and desalting by gel filtration (buffer A). Subsequently, the sample was applied onto a Q Sepharose ion-exchange column with buffer A, eluted using a linear gradient from 0 to 1 M NaCl and desalting by gel filtration (buffer A). The sample was then applied onto a high-resolution Resource Q ion-exchange column equilibrated with buffer A and eluted with a linear gradient from 0 to 1 M KCl. Finally, the protein solution was desalting (buffer A) and concentrated with Amicon Ultra spin columns (exclusion size 10 kDa) from Millipore.

2.2. Crystallization

Initial screening for crystallization conditions was performed by the sitting-drop vapour-diffusion method using a crystallization robot (HTPC, CyBio) and 96-well plates (CrystalQuick LP, Greiner Bio-One). The drops contained 0.3 µl protein solution (at 8 mg ml⁻¹ in buffer A) and 0.3 µl reservoir solution and were equilibrated against 40 µl reservoir solution. From these initial screens (JBScreen Classic 1–10, Jena Bioscience) several hits were observed. The crystallization conditions were further optimized using 24-well crystallization plates (Greiner Bio-One) with the hanging-drop vapour-diffusion method. Each well contained 500 µl reservoir solution and the drop volume was a mixture of 1 µl protein solution and 1 µl reservoir solution.

2.3. Data collection and X-ray crystallographic analysis

For cryoprotection, the reservoir solution was mixed with 50% (v/v) PEG 400 to give a final concentration of 5% (v/v) PEG 400. Before

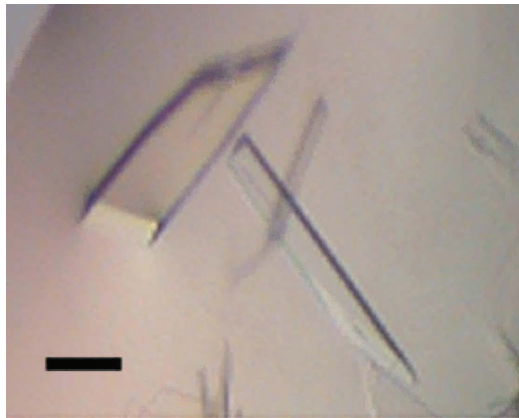


Figure 1

Crystals of the haloalkane dehalogenase DppA grown by the hanging-drop vapour-diffusion method. The crystal which was used for data collection (the leftmost crystal) has a thickness of approximately 40 µm. The solid bar represents 100 µm.

Table 1
X-ray data-collection statistics for DppA.

Values in parentheses are for the outer resolution shell.

X-ray source	Rigaku MicroMax-007
Detector	Saturn 92
Wavelength (Å)	1.5418
Resolution range (Å)	38.68–1.95 (2.02–1.95)
Space group	P2 ₁ 2 ₁ 2
Unit-cell parameters (Å)	<i>a</i> = 47.3, <i>b</i> = 108.5, <i>c</i> = 67.3
Total reflections	139903
Unique reflections	25613
Completeness (%)	98.5 (97.4)
<i>R</i> _{merge} (%)	12.0 (43.7)
<i>R</i> _{r.i.m.} (%)	13.7 (57.9)
<i>R</i> _{p.i.m.} (%)	6.4 (32.7)
Average <i>I</i> / <i>σ</i> (<i>I</i>)	7.0 (2.3)
<i>d</i> -spacing (Å)	2.02–1.95
Mosaicity (°)	1.00
Multiplicity	5.46 (4.13)
Wilson <i>B</i> factor (Å ²)	26.0
No. of images	258

the crystal was mounted, it was transferred into and soaked in this cryoprotectant for 30 s. The crystal was then flash-cooled to 110 K in a stream of nitrogen (Oxford Cryosystems).

Diffraction data were collected using a rotating-anode X-ray generator (MicroMax007, Rigaku) with Osmic multiple-layer optics (beam size 0.3 × 0.3 mm) and a CCD detector (Saturn 92, Rigaku).

The diffraction data were integrated and scaled using the software *CrystalClear* v.1.3.6 (Pflugrath, 1999). To obtain values of *R*_{p.i.m.} and *R*_{r.i.m.} the data were scaled with *SCALA* (Evans, 2006).

3. Results and discussion

The DppA protein was expressed in *E. coli* BL21 Gold and purified to homogeneity by ammonium sulfate precipitation and reversed-phase and ion-exchange chromatography. A final concentration of 8 mg ml⁻¹ was used for crystallization experiments.

Crystals of DppA protein could be obtained with several precipitants from the initial screen using the vapour-diffusion method. The crystallization conditions were further optimized and tiny needles that were too small for data collection appeared after several days in most cases (0.1 M sodium acetate pH 4.6, 28–31% PEG 400, 0.1 M MgCl₂; 0.1 M sodium phosphate–citrate pH 4.2, 0.2 M K₂HPO₄, 1.6 M NaH₂PO₄; 0.1 M Na HEPES pH 7.5, 1.8–2.2 M ammonium sulfate, 2% PEG 400; 0.1 M Na HEPES pH 7.5, 1.5–1.8 M ammonium sulfate, 0.2 M NaCl; 0.1 M Na MES pH 6.5, 1.8–2.0 M ammonium sulfate, 5% PEG 400; 0.1 M Na MES pH 6.5, 1.5–1.8 M ammonium sulfate). In one condition, comprised of 0.1 M Na MES pH 6.5, 1.8 M ammonium sulfate and 5% PEG 400, one crystal with an appropriate size for data collection (40 × 110 × 200 µm) was obtained after 4 d (Fig. 1).

This crystal of DppA diffracted X-rays to a resolution of 1.95 Å on a rotating-anode X-ray generator. The integration limit was set to an average *I*/*σ*(*I*) of 2. The data statistics are reported in Table 1.

The crystal of DppA belonged to the orthorhombic space group P2₁2₁2 (No. 18), with unit-cell parameters *a* = 47.3, *b* = 108.5, *c* = 67.3 Å.

Assuming the presence of one molecule in the asymmetric unit, the Matthews coefficient *V*_M was calculated to be 2.6 Å³ Da⁻¹.

The structure could be solved by molecular replacement using the program *Phaser* (McCoy *et al.*, 2007) with the haloalkane dehalogenase from *X. autotrophicus* GJ10 (PDB code 1edb; Verschueren *et al.*, 1993), which has a sequence identity of 50%, as a search model. A unique solution was obtained with a monomer in the asymmetric unit

with a likelihood score of 483.81 and a *Z* score of 21.51. Refinement is currently in progress.

References

- Bosma, T., Damborsky, J., Stucki, G. & Janssen, D. B. (2002). *Appl. Environ. Microbiol.* **68**, 3582–3587.
- Chaloupkova, R., Sykorova, J., Prokop, Z., Jesenska, A., Monincova, M., Pavlova, M., Tsuda, M., Nagata, Y. & Damborsky, J. (2003). *J. Biol. Chem.* **278**, 52622–52628.
- Evans, P. (2006). *Acta Cryst. D* **62**, 72–82.
- Franken, S. M., Rozeboom, H. J., Kalk, K. H. & Dijkstra, B. W. (1991). *EMBO J.* **10**, 1297–1302.
- Gray, K. A., Richardson, T. H., Kretz, K., Short, J. M., Bartnek, F., Knowles, R., Kan, L., Swanson, P. E. & Robertson, D. E. (2001). *Adv. Synth. Catal.* **343**, 607–617.
- Holloway, P., Knoke, K. L., Trevors, J. T. & Lee, H. (1998). *Biotechnol. Bioeng.* **59**, 520–523.
- Iizuka, T., Jojima, Y., Fudou, R., Hiraishi, A., Ahn, J.-W. & Yamanaka, S. (2003). *Int. J. Syst. Evol. Microbiol.* **53**, 189–195.
- Janssen, D. B. (2004). *Curr. Opin. Chem. Biol.* **8**, 150–159.
- Marek, J., Vevodova, J., Kuta Smatanova, I., Nagata, Y., Svensson, L. A., Newman, J., Takagi, M. & Damborsky, J. (2000). *Biochemistry*, **39**, 14082–14086.
- Mazumdar, P. A., Hulecki, J. C., Cherney, M. M., Garen, C. R. & James, M. N. G. (2008). *Biochim. Biophys. Acta*, **1784**, 351–362.
- McCoy, A. J., Grosse-Kunstleve, R. W., Adams, P. D., Winn, M. D., Storoni, L. C. & Read, R. J. (2007). *J. Appl. Cryst.* **40**, 658–674.
- Newman, J., Peat, T. S., Richard, R., Kan, L., Swanson, P. E., Affholter, J. A., Holmes, I. H., Schindler, J. F., Unkefer, C. J. & Terwilliger, T. C. (1999). *Biochemistry*, **38**, 16105–16114.
- Ollis, D. L., Cheah, E., Cygler, M., Dijkstra, B., Frolov, F., Franken, S. M., Harel, M., Remington, S. J., Silman, I., Schrag, J., Sussman, J. L., Verschueren, K. H. G. & Goldman, A. (1992). *Protein Eng.* **5**, 197–211.
- Pflugrath, J. W. (1999). *Acta Cryst. D* **55**, 1718–1725.
- Pries, F., van den Wijngaard, A. J., Bos, R., Pentenga, M. & Janssen, D. B. (1994). *J. Biol. Chem.* **269**, 17490–17494.
- Schanstra, J. P., Ridder, I. S., Heimeriks, G. J., Rink, R., Poelarends, G. J., Kalk, K. H., Dijkstra, B. W. & Janssen, D. B. (1996). *Biochemistry*, **35**, 13186–13195.
- Stsiapanava, A., Koudelakova, T., Lapkouski, M., Pavlova, M., Damborsky, J. & Kuta Smatanova, I. (2008). *Acta Cryst. F* **64**, 137–140.
- Verschueren, K. H. G., Kingma, J., Rozeboom, H. J., Kalk, K. H., Janssen, D. B. & Dijkstra, B. W. (1993). *Biochemistry*, **32**, 9031–9037.

Cloning, functional expression, biochemical characterization, and structural analysis of a haloalkane dehalogenase from *Plesiocystis pacifica* SIR-1

Martin Hessler · Xenia Bogdanović · Aurelio Hidalgo ·
Jose Berenguer · Gottfried J. Palm ·
Winfried Hinrichs · Uwe T. Bornscheuer

Received: 23 January 2011 / Revised: 30 March 2011 / Accepted: 9 April 2011
© Springer-Verlag 2011

Abstract A haloalkane dehalogenase (DppA) from *Plesiocystis pacifica* SIR-1 was identified by sequence comparison in the NCBI database, cloned, functionally expressed in *Escherichia coli*, purified, and biochemically characterized. The three-dimensional (3D) structure was determined by X-ray crystallography and has been refined at 1.95 Å resolution to an R-factor of 21.93%. The enzyme is composed of an α/β-hydrolase fold and a cap domain and the overall fold is similar to other known haloalkane dehalogenases. Active site residues were identified as Asp123, His278, and Asp249 and Trp124 and Trp163 as halide-stabilizing residues. DppA, like DhLA from *Xanthobacter autotrophicus* GJ10, is a member

of the haloalkane dehalogenase subfamily HLD-I. As a consequence, these enzymes have in common the relative position of their catalytic residues within the structure and also show some similarities in the substrate specificity. The enzyme shows high preference for 1-bromobutane and does not accept chlorinated alkanes, halo acids, or halo alcohols. It is a monomeric protein with a molecular mass of 32.6 kDa and exhibits maximum activity between 33 and 37°C with a pH optimum between pH 8 and 9. The K_m and k_{cat} values for 1-bromobutane were 24.0 mM and 8.08 s⁻¹. Furthermore, from the 3D-structure of DppA, it was found that the enzyme possesses a large and open active site pocket. Docking experiments were performed to explain the experimentally determined substrate preferences.

Martin Hessler and Xenia Bogdanović contributed equally to this work.

Electronic supplementary material The online version of this article (doi:10.1007/s00253-011-3328-x) contains supplementary material, which is available to authorized users.

M. Hessler · U. T. Bornscheuer (✉)
Department of Biotechnology and Enzyme Catalysis,
Institute of Biochemistry, Greifswald University,
Felix-Hausdorff-Str. 4,
17487 Greifswald, Germany
e-mail: uwe.bornscheuer@uni-greifswald.de

X. Bogdanović · G. J. Palm · W. Hinrichs
Department of Molecular Structural Biology,
Institute of Biochemistry, Greifswald University,
Felix-Hausdorff-Str. 4,
17487 Greifswald, Germany

M. Hessler · A. Hidalgo · J. Berenguer
Departamento de Biología Molecular, Centro de Biología
Molecular Severo Ochoa (UAM-CSIC),
Universidad Autónoma de Madrid,
C/Nicolás Cabrera, 1,
28049 Madrid, Spain

Keywords Haloalkane dehalogenase · *Plesiocystis pacifica* · Biochemical characterization · Structure

Introduction

Haloalkane dehalogenases (HLDs, E.C. 3.8.1.5) catalyze the hydrolytic dehalogenation of haloalkanes to the corresponding alcohols by cleavage of a carbon–halogen bond. The first HLD was isolated by Keuning et al. from *Xanthobacter autotrophicus* GJ10 (Keuning et al. 1985). This enzyme is also, by far, the best characterized HLD described in literature.

Structurally, HLDs belong to the α,β-hydrolase superfamily (Ollis et al. 1992; Holmquist 2000; Carr and Ollis 2009). The three-dimensional (3D) structure is composed of two domains: (1) the α,β-hydrolase main domain, strictly conserved in various members of the superfamily and (2) the helical cap domain, variable in terms of number and the arrangement of secondary structure elements. Currently,

five unique crystal structures of HLDs are available in the Protein Data Bank: DhLA from *X. autotrophicus* GJ10 (Franken et al. 1991), DhaA from *Rhodococcus* sp. TDTM0003 (Newman et al. 1999), LinB from *Sphingobium japonicum* (*Sphingomonas paucimobilis*) UT26 (Marek et al. 2000), DmbA from *Mycobacterium tuberculosis* H37Rv (Mazumdar et al. 2008), and DbjA from *Bradyrhizobium japonicum* USDA110 (Prokop et al. 2010). The HLD from *Plesiocystis pacifica* described here was identified with a BLAST search, where a consensus sequence of several known HLDs served as template.

HLDs were subdivided into three subfamilies HLD-I, HLD-II, and HLD-III (Chovancova et al. 2007) according to their substrate specificity on one hand, and the position of functionally important residues on the other hand: Asp–His–Asp (catalytic triad) and Trp–Trp (halide-stabilizing residues) in HLD-I, Asp–His–Glu and Asn–Trp in HLD-II, and Asp–His–Asp and Asn–Trp in HLD-III.

The catalytic triad consists of the key nucleophile (Asp), the general base (His), and a catalytic acid. The nucleophile and the base are highly conserved in all α/β -hydrolases, whereas the catalytic acid varies both in amino acid identity and position. The nucleophile is located on the nucleophile elbow, a sharp turn after β -strand 5, and the base is located after β -strand 8, whereas the catalytic acid, aspartic acid, or glutamic acid, is located after β -strand 7 or β -strand 6, respectively. Krooshof et al. (1997) shifted the catalytic acid Asp260 (after β 7) to position Asn148 (after β 6) by site-directed mutagenesis of Asp260 to Asn and Asn148 to Asp/Glu and demonstrated that the catalytic triad can be rearranged in DhLA haloalkane dehalogenase.

The dehalogenase reaction follows a two-step catalytic mechanism (Verschueren et al. 1993b). In the first step of the reaction, the nucleophile forms a covalently-bound ester intermediate with the substrate by releasing the halide ion. In the second step, a water molecule in form of a hydroxide ion, produced by the general base His, attacks the intermediate ester and the alcohol product is released. In the first reaction step, the transition state is stabilized by the side chains of the halide-stabilizing residues Trp/Trp or Asn/Trp, respectively. The first step is unique for dehalogenases, whereas the second reaction step is typical for α/β -hydrolases, and the characteristic feature to stabilize the transition state for the second reaction step is the oxyanion hole. This is typically composed of the amide nitrogen atoms from the Trp following the key nucleophile and a second backbone nitrogen of a residue located after β -strand 3.

Nowadays, various practical applications for HLDs are known, and its number increases with the growing knowledge of their properties and structure–function relationships: bioremediation of environmental pollutants (Stucki and Thüer 1995), in biosensors for toxic chemicals (Bidanova et al. 2010), industrial biocatalysis (Swanson

1999; Prokop et al. 2009; Janssen 2007), decontamination of warfare agents (Prokop et al. 2006a,b), as well as cell imaging and protein analysis (Los and Wood 2007). The identification of the biological role of HLDs is one of the great challenges in their research. The genes encoding for HLDs are widely distributed among various bacterial species, including the tissue-colonizing organisms, e.g., *Mycobacterium tuberculosis* or *Mycobacterium bovis*.

Plesiocystis pacifica SIR-1 was first described by Iizuka et al. (2003). The strain is a Gram-negative marine myxobacterium and was isolated from the Japanese coast located in the Pacific Subtropical Zone. The organism was sequenced, and the sequence was published online by Shimkets et al. (2007): DppA (accession no. ZP_01908831.1) has been annotated as “putative haloalkane dehalogenase”.

In this work, we describe the cloning, functional expression, and biochemical characterization of DppA and discuss its properties based on the crystal structure, for which we recently reported the purification and crystallization conditions leading to single crystals of DppA suitable for structural analysis by X-ray diffraction (Bogdanović et al. 2010).

Materials and methods

Chemicals

All chemical were purchased from Sigma-Aldrich (Weinheim, Germany). The following buffers were prepared for activity determination: acetate buffer 50 mM, pH 5.0 (acetate5.0); acetate buffer 50 mM, pH 5.7 (acetate5.7); sodium phosphate buffer 50 mM, pH 6.2 (NaPP6.2); sodium phosphate buffer 50 mM, pH 7.2 (NaPP7.2); sodium phosphate buffer 50 mM, pH 8.2 (NaPP8.2); TRIS buffer 50 mM, pH 8.2 (TRIS8.2); TRIS buffer 50 mM, pH 8.7 (TRIS8.7); TRIS buffer 50 mM, pH 9 (TRIS9.0); Borate buffer 50 mM, pH 8.2 (Borate8.2); Borate buffer 50 mM, pH 9.2 (Borate9.2); Borate buffer 50 mM, pH 10.2 (Borate10.2).

Identification of the putative protein sequence of HLD from *P. pacifica*

Protein sequences of 19 known HLDs were used to create a consensus sequence serving as template in a BLAST search to identify novel HLDs based on putative annotations. From the hits, all non-S1-organisms were excluded, and from the remaining handful, homology models were built with SwissModel and aligned with the known structure of the HLD DhLA from *X. autotrophicus* GJ10 (PDB-code: 2dhc) to verify that the required catalytic residues occurred in the active site and that they were also at the expected place. DppA was the only protein, which possessed the

typical catalytic triad Asp–His–Asp and gave good overlapping with the active site of DhlA and was therefore chosen for further investigation. For later expression in *E. coli*, the codon usage of *P. pacifica* was analyzed online at <http://gcua.schoedl.de>. The similarity was considered high enough (data not shown) for direct expression of the gene in *E. coli*.

Isolation of genomic DNA from *P. pacifica*

The strain *P. pacifica* DSM14875 was ordered from the German Collection of Microorganisms and Cell Cultures (DSMZ, Braunschweig, Germany). The genomic DNA was amplified using the GenomiPhi DNA Amplification Kit (GE Healthcare, Munich, Germany) according to the manual provided by the manufacturer. The amplification product was directly used for subsequent PCR.

Cloning of the *dppA* gene from *P. pacifica*

Primers for amplification of *dppA* were derived from the sequence deposited at NCBI by Shimkets et al. (2007). The forward and reverse primers had 5' extensions, which carried NdeI and BamHI restriction sites (forward primer: 5'-CATATGGAATTCTCGCCACCCCCGACGAC-3'; reverse primer: 5'-GGATCCTCACTGCCGAAGGCAGCGA-3'). After digestion, the gene was subcloned into the TOPO vector with the TOPO TA Cloning Kit (Invitrogen, Darmstadt, Germany) and putative positive clones were selected by blue/white screening. The correct sequence was confirmed by sequencing (GATC, Konstanz, Germany). For expression in *E. coli*, the gene was subcloned into a pET28a vector (Invitrogen, Carlsbad, CA, USA) with an N-terminal His-tag (pET28a-dppA-NHIS).

Expression and purification of the DppA HLD

E. coli BL21-Gold(DE3) cells carrying plasmid pET28a-dppA-NHIS were used for inoculation of a pre-culture, which was subsequently used for inoculation of the main culture. The pre-culture consisted of 10 ml lysogeny broth (LB) medium and 30 µg/ml kanamycin. After inoculation, it was incubated overnight in a 50-ml shake flask at 37°C and 200 rpm. The main culture was prepared in LB medium as well, and, after inoculation, incubated at 37°C at 200 rpm until the cultivation reached an OD₆₀₀ of ~0.5–1. After induction with IPTG (final concentration 0.5 mM) and further incubation at 20°C for 20 h, cells were harvested by three alternating centrifugation and washing steps (sodium phosphate buffer, 50 mM, pH 7.5, 4°C) followed by a final centrifugation step. Cell disruption and protein purification was carried out according to the BD TALON protocol (Clontech, Mountain View, CA, USA).

Purification was monitored by SDS-PAGE. Protein concentration was determined at room temperature by the Bradford method using bovine serum albumin (fraction IV) as standard. SDS polyacrylamide gel electrophoresis (SDS-PAGE) was performed with running gel (12% (w/v)) and stacking gel (4% (w/v)). Protein bands were stained with Coomassie Brilliant Blue G-250.

Determination of activity

Activity was determined as described elsewhere (Marvanova et al. 2001) with some modifications of the protocol: the reaction was routinely carried out with 1-bromobutane in HEPES buffer (50 mM, pH 8.2) at 35°C. An appropriate dilution of the enzyme was added together with the substrate to reach a final concentration of 50 mM. The reaction was performed in closed microreaction tubes to prevent evaporation of the substrates. The final reaction volume was 1 ml. The assay described by Iwasaki et al. (1952) was used for colorimetric determination of halide concentrations. Typical reaction time was 4 min. Samples of 100 µl were withdrawn and poured into the microtiter plate. The latter already contained one of the solutions for the Iwasaki assay, namely the one that contains nitric acid, to stop the reaction. The second Iwasaki solution was added to each well simultaneously, after the reaction had been finished. This was because the formation of the dye in the Iwasaki assay is a function of time. Reaction progress was monitored at 460 nm in 96-well microtiter plates with a BMG Labtech Fluostar Optima photometer (Offenburg, Germany). One unit (U) of activity corresponds to the release of 1 µmol halide released by the enzyme per minute.

Crystallization

Purification and crystallization of DppA have recently been reported (Bogdanović et al. 2010). In brief, DppA was cloned without His-Tag, expressed heterologously in *E. coli* BL21-Gold(DE3) and purified to homogeneity by hydrophobic interaction, size exclusion, and ion exchange chromatography. The protein was crystallized by the hanging-drop vapor-diffusion method at 20°C out of 10 mM Tris–HCl buffer pH 8 at a protein concentration of 8 mg ml⁻¹. The precipitant comprised 0.1 M NaMES (pH 6.5), 1.8 M (NH₄)₂SO₄, and 5% PEG 400.

Data collection and crystallographic computing

For cryoprotection, the reservoir solution was mixed with 50% (v/v) PEG 400 to a final concentration of 5% (v/v) PEG 400. The crystal was flash-cooled to -163.15°C (Oxford Cryosystems). Diffraction data were collected at a rotating-anode X-ray generator (MicroMax007, Rigaku)

with Osmic multiple layer optics (beam size 0.3×0.3 mm) and a CCD detector (SATURN92, Rigaku). Diffraction data were indexed, integrated, and scaled using the software CrystalClear 1.3.6 (Pflugrath 1999). For values of $R_{\text{p},\text{i.m}}$ and $R_{\text{r.i.m}}$, data were scaled with SCALA (Pries et al. 1994). The DppA structure was solved by molecular replacement using the program PHASER (McCoy et al. 2007) with a search model of DhlA from *X. autotrophicus* (PDB entry 1EDB, (Verschueren et al. 1993b)). Starting from the existing model and the amino acid sequence of DppA, several cycles of map improvement alternated with automated model building were performed using the program ARP/wARP (Morris et al. 2003). Afterwards the structure model was manually refined with REFMAC5 (Vagin et al. 2004) and COOT (Emsley and Cowtan 2004) from the CCP4 suit (Collaborative Computational Project 1994) using restrained and TLS refinement. The final model contains 2,311 non-hydrogen protein atoms, 260 water molecules, and 4 sulfate molecules. Stereochemistry was verified using MOLPROBITY (Davis et al. 2007) and PROCHECK (Collaborative Computational Project 1994).

Bioinformatics analysis and molecular modeling

The BLAST search (Altschul et al. 1990; 1997) was used to identify homologous sequences of DppA, which were then aligned by ClustalW (Thompson et al. 1994) and ESPript 2.2 (Gouet et al. 1999). Dockings were carried out with YASARA, which makes use of AutoDock. CAVER was used for the calculation of possible entrance tunnels (Petrek et al. 2006). Active site volumes were calculated with CASTp (Dundas et al. 2006). Visualization was performed with PyMOL.

Results

The *dppA* gene from *P. pacifica* was found by a BLAST search against the consensus sequence created with 19 known HLDs. The open reading frame consists of 894 nucleotides, which encodes for a protein of 297 amino acids (aa) in length.

A BLAST (Altschul et al. 1990, 1997) search with the DppA protein sequence was made to confirm the results of the first BLAST with the consensus sequence on one hand, and to find the most related HLDs on the other hand. Furthermore, conserved and therefore possibly important residues for catalytic activity were identified in a subsequent multi-sequence alignment. The BLAST search against the nr-database resulted in a number of hits, where the first 16 almost exclusively were HLDs or at least putative HLDs (Table S1, supporting information). The first hit with a sequence identity of 61% is the putative HLD from *Erythrobacter litoralis* HTCC2594. A BLAST against the

protein database showed that among the well-characterized HLDs, DppA shows by far the highest homology with DhlA from *X. autotrophicus* (50% sequence identity). The other four HLDs with known structure only have a sequence identity of around 30%. Figure 1 shows a multiple alignment of these HLDs, which is discussed below in detail.

Cloning, recombinant expression, and purification of DppA

After isolation of the genomic DNA from *P. pacifica*, PCR was used to specifically amplify the *dppA* gene. The resulting fragment was subcloned into a TOPO vector and subsequently cloned into the pET28a vector, which also carried an N-terminal His-tag.

Sequencing confirmed successful cloning of the desired gene, but also revealed some deviations between the cloned sequence and the information deposited in the NCBI database. Besides five silent mutations, two mutations (A247P and R265G) were identified at the protein level and were attributed to deviations between the strain used from DSMZ and the strain used for sequencing by Shimkets et al. (2007) (Figure S1, supporting information).

Next, the protein DppA was functionally expressed in *E. coli* BL21-Gold(DE3) as confirmed by initial qualitative tests for dehalogenase activity. After cell disruption, the vast majority of the protein was found in the soluble fraction and was subsequently purified by metal ion affinity chromatography using a Ni-NTA-Sepharose affinity column. As the protein in the crude cell extract was already quite pure (Fig. 2), specific activity only slightly increased from 1.80 to 2.44 U/mg in the conversion of 1-bromobutane. The theoretical size was calculated to be 32.6 kDa, whereas the actual size was estimated from the polyacrylamide gel to be about 35 kDa.

Effects of temperature and pH on enzyme activity

The influence of temperature on the enzyme activity was investigated in the range between 20°C and 45°C (data not shown). The enzyme shows a broad activity maximum with almost no deviation in activity between 30°C and 37°C. It retains 75% of its maximum activity between 25°C and 45°C, thus over a range of 20°C. The effect of pH on enzyme activity was investigated in the range between pH 5–10 (data not shown). DppA shows maximum activity between pH 8–9. The enzyme retains most of its activity between pH 7 and 9.5. Under very acidic and alkaline conditions, though, activity rapidly decreases.

Substrate range and determination of kinetic parameters

DppA was investigated for its activity towards a variety of substrates from different classes (Table 1). The enzyme accepts

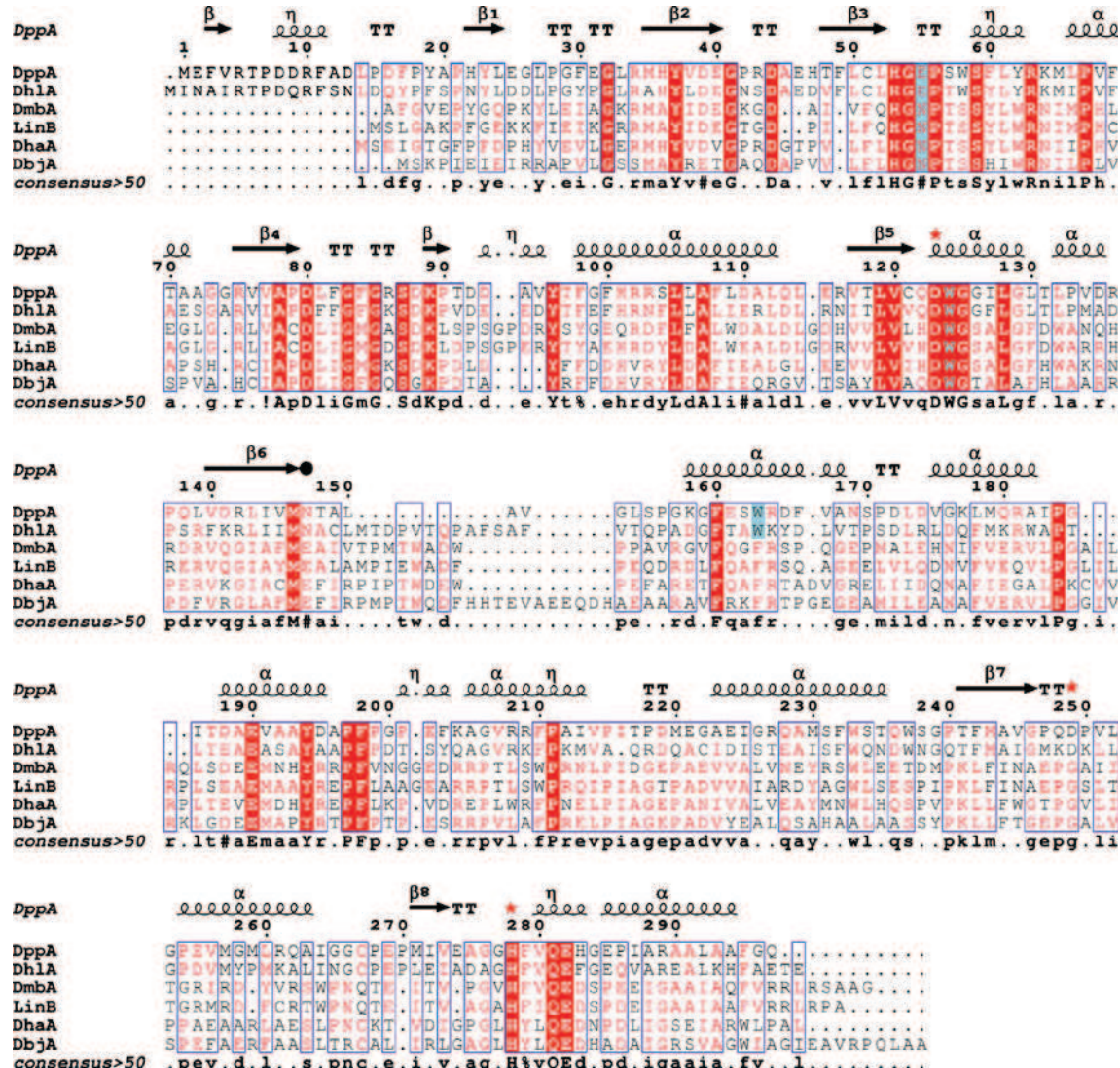


Fig. 1 Multiple sequence alignment of structurally described haloalkane dehalogenases. *DppA* *P. pacifica* dehalogenase, *DhlA* *X. autotrophicus* dehalogenase, *DmbA* *M. tuberculosis* dehalogenase, *LinB* *S. japonicum* dehalogenase, *DhaA* *Rhodococcus* sp. dehalogenase, *DbjA* *B. japonicum* dehalogenase. Identical residues are presented in white on a red background; similar residues are indicated by red lettering on a white background. Secondary structure elements of DppA are given above the

bromoalkanes of short and medium chain length. The highest activity was measured with 1-bromobutane. Activity increases with chain length from 1-bromopropane to 1-bromobutane and subsequently decreases from 1-bromobutane to 1-bromodecane with the exception of 1-bromoheptane, for which higher activity than towards 1-bromohexane was observed. In addition to 1-bromobutane also 2-bromobutane, as well as multiple substituted alkanes (1,2-dibromoethane, 1,2-dibromopropane), were converted. Chlorinated substrates, haloacids, haloalcohols, and the halogenated epoxide epibromohydrene were not converted at all.

The kinetic parameters K_m and k_{cat} of DppA were determined for a set of substrates (Table 2). 1-

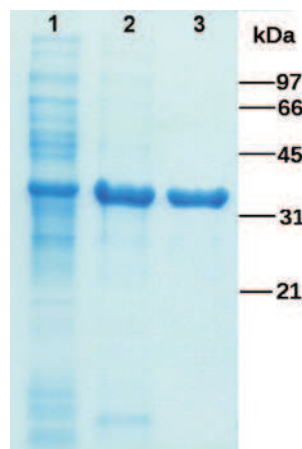
sequences. Residues of the catalytic triad of DppA are labeled with a red star, the glutamic acid of the catalytic triad found in DhaA, LinB, and DmbA is labeled with a black circle. Residues forming the anion hole or the chloride-binding site are marked in light blue. The alignment was generated with MultAlin (Corpet 1988) and printed using ESPript 2.2 (Gouet et al. 1999)

Bromopropane, 1-bromobutane, and 1-bromopentane showed the highest activities, but substantially differed in their K_m values, which were determined to 45.2, 24.0, and 2.51 mM, respectively. The K_m values further decreased with increasing chain length, which indicates higher affinity towards substrates with longer chains. Values for k_{cat} increased from 1-bromopropane to 1-bromopentane and subsequently decreased from 1-bromopentane to 1-bromoheptane.

Analysis of the crystal structure of DppA

DppA was crystallized in the orthorhombic space group $P2_12_12$ with one molecule in the asymmetric unit. The

Fig. 2 SDS-PAGE analysis of DppA. *Lane 1* before induction, *lane 2* crude cell extract, *lane 3* after His-tag purification



crystal structure was determined at 1.95 Å resolution to an R-factor of 21.93% and R_{free} of 24.80% and shows clear electron density from residues 1–297. Except for Asn147 and Pro56, the main-chain dihedral angles of all residues are in the allowed regions of the Ramachandran plot, with over 97.8% in the most favorable regions. Statistics of diffraction data and refinement are summarized in Table 3.

The DppA molecule has a globular shape and is composed of two domains. The core domain comprises residues 1–157 and 214–297 and shows the canonical α/β -hydrolase fold with a central, mixed β -sheet composed of eight β -strands, of which only one is antiparallel (β 2). The central β -sheet is flanked on both sides by α -helices; two are on one side (α I and α XI) and four are on the other side of the sheet (α 3, α 4, α 9, and α 10). The second domain, the cap structure (residues 158–213), is located at the C-terminal end of the β -sheet and is composed of α -helices α 5, α 6, α 7, and α 8, which are all connected by loops (Fig. 3).

The cap domain is inserted between β 6 and β 7 and covers the active site. The overall structure of DppA is very similar to those of other structurally known dehalogenases; the root mean square deviation (rmsd) (calculated with DALI (Holm and Rosenstrom 2010)) of 296 equivalent $C\alpha$ atoms of DppA and DhlA (Verschueren et al. 1993b) (pdb 1B6G) is 1.4 Å, the rmsd of 272 equivalent $C\alpha$ atoms of DppA and DhaA (Newman et al. 1999) (pdb 1BN7) is 2.3 Å, the rmsd of 270 equivalent $C\alpha$ atoms of DppA and LinB (Oakley et al. 2004) (pdb 1MJ5) is 2.2 Å, the rmsd of 265 equivalent $C\alpha$ atoms of DppA and DbjA (Prokop et al. 2010) (pdb 3A2N) is 2.2 Å, and the rmsd of 269 equivalent $C\alpha$ atoms of DppA and DmbA (Mazumdar et al. 2008) (pdb 2QVB) is 2.2 Å (Table S3, supporting information). The secondary structure elements of the core domain are well-conserved between dehalogenases, whereas the cap domains show greater differences.

Active site of DppA

The catalytic residues are proposed to be Asp123, His278, and Asp249. The key nucleophile (Asp123) is located between β 5

Table 1 Relative activity of HLD towards halogenated substrates as determined with purified enzymes from *P. pacifica* (DppA), *X. autotrophicus* (DhlA), and *S. japonicum* (LinB), and with crude extracts from *R. erythropolis* Y2 (DhaA)

Substrate	Activity [%]			
	DppA	DhlA	DhaA	LinB
α -Haloalkanes				
1-Chloropropane	0	165 ^a	4 ^b	135 ^c
1-Chlorobutane	0	100 ^{a,e}	100 ^{b,c}	100 ^{b,e}
1-Chloropentane	0	16 ^d	107 ^b	120 ^c
1-Bromopropane	85	94 ^a	197 ^b	+
1-Bromobutane	100 ^e	87 ^d	+	234 ^c
1-Bromopentane	77	103 ^d	+	+
1-Bromohexane	20			
1-Bromoheptane	33			
1-Bromooctane	13			
1-Bromononane	11			
1-Bromodecane	2			
α/β -Haloalkanes				
1,2-Dichloropropane	0	2 ^d	0 ^b	+
1,2-Dibromoethane	31	303 ^a	552 ^b	355 ^c
1,2-Dichloroethane	0	323 ^a	0 ^b	0 ^c
1,2-Dibromopropane	25			
Non- α -haloalkanes				
1,2,3-Trichloropropane	0			
2-Bromobutane	46			
Haloalcohols				
3-chloro-1,2-Propanediol	0			
2-Chloroethanol	0	0 ^a	–	131 ^b
Haloacids				
2-Chloropropionic acid	0	0 ^a	–	–
2-Bromobutyric acid	0			
2-Bromopropionic acid	0			
Bromoacetic acid	0			
Chloroacetic acid	0			
Sodium-fluoride acetate	0			
Haloepoxides				
Epibromohydrin	0	416 ^d	+	–

Activities of each enzyme are shown as relative values of the activity towards 1-bromobutane (DppA) and 1-chlorobutane (DhlA, DhaA, LinB). (+) and (–) indicate predictions of activity based on computer-automated structure evaluation published by Damborsky et al. (2001)

^a Keuning et al. (1985)

^b Damborsky et al. (2001)

^c Nagata et al. (1997)

^d Janssen et al. (1991)

^e Specific activities of enzymes in U/mg protein: 4.50 (DppA), 1.86 (DhlA), crude extracts (DhaA), 52.1 (LinB)

and α 3 (on the nucleophilic elbow). The base, His278, is located on the loop immediately after β 8. The distance of Oδ1

Table 2 Kinetic parameters of DppA for a set of substrates

	K_m [mM]	k_{cat} [sec $^{-1}$]	k_{cat}/K_m [mM $^{-1} \times$ sec $^{-1}$]
1,2-Dibromoethane	1.57	0.38	0.24
1,2-Dibromopropane	1.96	1.97	1.00
1-Bromopropane	45.2	5.85	0.13
1-Bromobutane	24.0	8.08	0.34
1-Bromopentane	2.51	9.94	3.96
1-Bromohexane	1.70	2.69	1.58
1-Bromoheptane	0.75	1.39	1.84

of Asp123 to Nε2 of His278 is 3.11 Å. The catalytic acid of DppA is Asp249 that is found in the loop after β7. This is the same topology of the triad that is found in most α/β-hydrolase

Table 3 Data collection and refinement statistics

	DppA (pdb 2×T0)
A. Data collection	
Space group	$P2_12_12$
Unit-cell parameters	
a (Å)	47.3
b (Å)	108.5
c (Å)	67.3
Wavelength (Å)	1.5418
Resolution range (Å)	38.68–1.95 (2.02–1.95)
Completeness (%)	98.5 (97.4)
Multiplicity	5.46 (4.13)
Average $I/\sigma(I)$	7.0 (2.3)
R_{merge} (%)	12.0 (43.7)
$R_{r.i.m.}$ (%)	13.7 (57.9)
$R_{p.i.m.}$ (%)	6.4 (32.7)
Wilson B factor (Å 2)	26.0
B. Refinement	
Resolution	67.31–1.95
No. of reflections	25,826
R_{work} (%)	21.93
R_{free} (%)	24.80
No. of atoms	2,596
Average B-Factors (Å 2)	
Overall	26.2
Protein main chain	24.3
Protein side chains+water	27.9
R.m.s. deviations	
Bond lengths (Å)	0.023
Bond angles (°)	1.854
Ramachandran plot	
Ramachandran favored (%)	97.8
Ramachandran allowed (%)	1.4

Values in parentheses correspond to values in the highest resolution shell

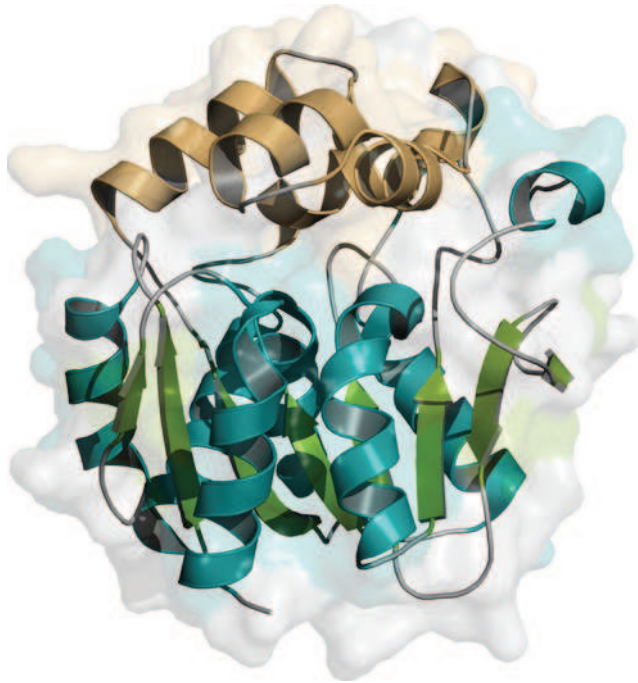


Fig. 3 Ribbon diagram showing the tertiary structure of DppA. Loops, β-strands, and α-helices of the main domain are marked in gray, green, and cyan, respectively. Helices of the cap domain are labeled in orange

fold enzymes (Ollis et al. 1992). The distance from Nε1 of His278 to Oδ1 of Asp249 is 3.75 Å and to Oδ2 2.88 Å showing the syn-conformation for the aspartate–histidine couple, where the aspartic acid makes a bifurcated hydrogen bond to the imidazole side chain of the histidine. This arrangement is very common for α/β-hydrolase fold enzymes as well as for serine proteases (Schrag et al. 1992) and is also found in DhlA. In contrast, the catalytic acid (glutamic acid) in DhaA, LinB, DbjA, and DmbA is located after β6. The glutamate–histidine couple makes one hydrogen bond, showing the anti-conformation (Fig. 4).

The halide-stabilizing residues in DppA are Trp124 and Trp163. These residues correspond in position and function to Trp125 and Trp175 in DhlA. The second halide-stabilizing residue varies in both amino acid identity and location among HLDs and is found to be an asparagine in LinB, DhaA, DmbA, and DbjA.

The oxyanion hole is composed of the amide NH Trp124 (Trp125 in DhlA, Trp109 in LinB, Trp118 in DhaA, Trp110 in DmbA, and Trp104 in DbjA) and the amide group Glu55 (Glu56 in DhlA, Asn38 in LinB, Asn52 in DhaA, Asn39 in DmbA, and Asn38 in DbjA). Both form a hydrogen bond to Oδ2 of the nucleophile increasing its nucleophilicity and thus stabilizing the negatively charged transition state that occurs during hydrolysis.

The active site region is predominantly formed by the hydrophobic residues Trp124, Ile127, Phe160, Trp163,

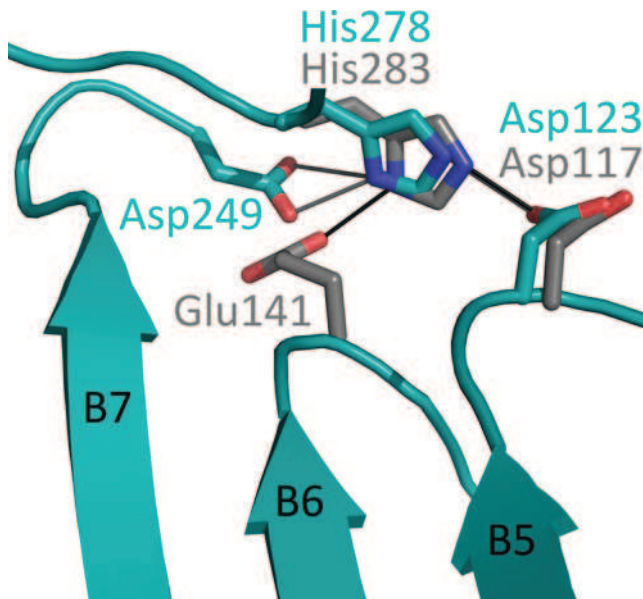


Fig. 4 Different arrangements of the catalytic triad shown by superposition of DppA and DhaA. Amino acids are labeled with color and numbering according to DppA (light blue) and DhaA (gray). Numbering of β -strands is based on the central β -sheet. The H-bond network of the DppA catalytic triad is labeled with gray lines (syn-conformation) that of DhaA with black lines (anti-conformation)

Pro211, Val214, Leu252, and Phe279. The proposed catalytic residues are the only hydrophilic residues within this pocket. We observed electron density in the active site cavity, which was interpreted as water.

Figure 5 shows important residues of the active site known from DhlA (Verschueren et al. 1993c) in a structure alignment with DppA. The catalytic triad of DppA shows good alignment with that from DhlA (Asp123, His278, His249, Asp249), as well as the halide-stabilizing tryptophan in the conserved part of the enzyme (Trp124 and Trp125 from DppA and DhlA, respectively). This does not hold for some

Fig. 5 Some important residues of the active sites in a structure alignment of DppA (green) and DhlA (blue) with its co-crystallized substrate 1,2-dibromoethane. The position of 1-chlorobutane results from docking experiments with DppA

residues shown in Fig. 5, which are part of the cap domain; e.g., Trp163 and Trp175 and Phe160, and Phe172 from DppA and DhlA, respectively. The corresponding residue of Phe128 in DppA is Ile127, which is a significantly smaller residue.

DppA was analyzed with CASTp and CAVER and compared to other HLDs. Its hydrophobic active site pocket is connected to the surrounding solvent via two tunnels, the main and the slot tunnel, which represent an important structural feature of HLDs (Marek et al. 2000). The entrance to the main tunnel is formed by residues Trp163, Leu178, Ala182, Gln248, Pro250, Val251, and Gly277. The entrance to the slot tunnel is surrounded by residues Val152, Leu154, Ser155, Pro156, Met230, Val256, Met259, and Ala263. Main tunnels of DhlA and DppA are located at approximately equivalent positions (entrances between α 4 and α 5), but significantly differ in volume and shape (Fig. 7). The slot tunnels of the two enzymes are located at different positions: in case of DhlA between α 4' and α 4, and in case of DppA near the end of the loop between β 6 and α 4. The entrance of the latter was found to be blocked in DhlA (Fig. 6). At this site, DppA shows a gap in the sequence alignment (Fig. 1). DppA has an active site that is relatively open to the surrounding solvent and possesses a large molecular surface. The active site cavity of DhlA in contrast is deeply buried in the protein and has very limited access to solvent molecules (Fig. 7) (Verschueren et al. 1993a). DhaA and LinB are more accessible (Petrek et al. 2006) and DmbA and DbjA show the highest accessibility of their active site pockets to the solvent (Damborsky et al. 2010).

Docking experiments

Dockings were made with 1,2-dibromoethane, 1-bromobutane, and 1-chlorobutane to find structural explanations for the

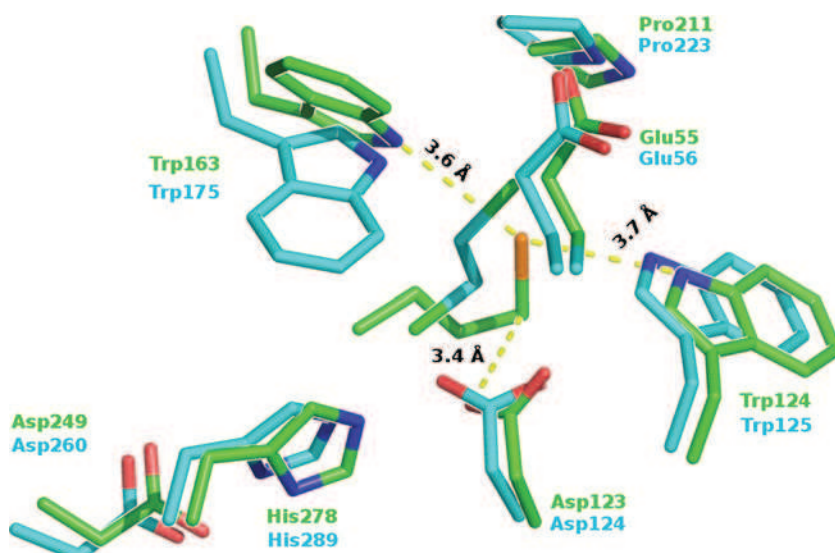
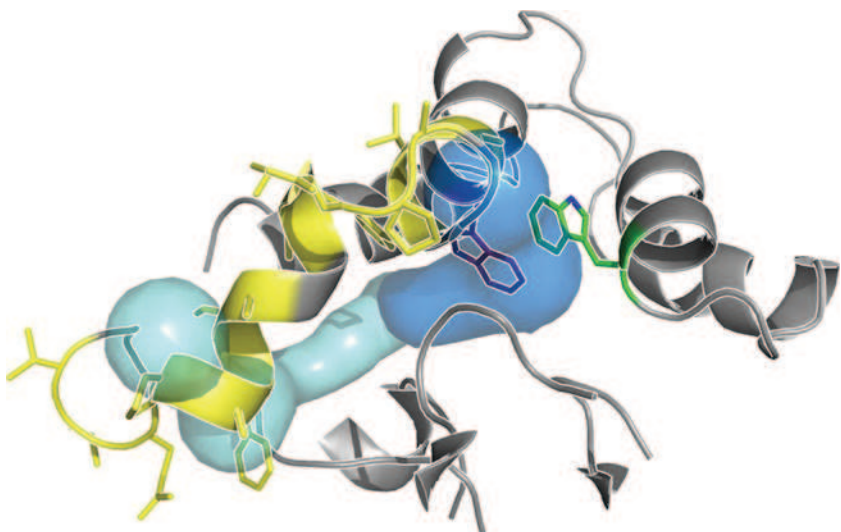


Fig. 6 Entrance tunnels of DppA calculated with CAVER superposed with the structure of DhLA (pdb 1BE0). Residues that form the direct repeats in DhLA are shown in yellow. Trp194 and Trp175 are shown in green and purple, respectively. Main tunnel of DppA is shown in blue, slot tunnel in cyan



substrate specificity. 1,2-Dibromoethane and 1-bromobutane were docked in reasonable positions and conformations for the hydrolytic reaction to take place (Fig. 5). The halogen of the substrate was oriented between the $N_{\varepsilon 1}$ from Trp163 and

Trp124 with a distance of 3.6 and 3.7 Å, respectively. The C_{α} of 1-bromobutane is located at 3.4 Å from the $O_{\delta 1}$ from Asp123, the nucleophile, and thus in a reasonable position for a nucleophilic attack.

Dockings with 1-bromobutane were superposed with DhLA (pdb 2DHC), which had been crystallized with 1,2-dichloroethane. Orientation within the active site and distances between the substrates' functional groups and the catalytic residues are similar. In case of DhLA, Trp125 $N_{\varepsilon 1}$ and Trp175 $N_{\varepsilon 1}$ are at 3.6 and 3.2 Å, respectively, from the chlorine to be cleaved off (Verschueren et al. 1993c).

1,2-Dibromoethane was docked in a similar orientation, which appeared reasonable for the hydrolytic reaction. 1-Chlorobutane was also docked in the active site pocket, but was not oriented in a way that would allow coordination of the halogen by Trp163 and Trp124.

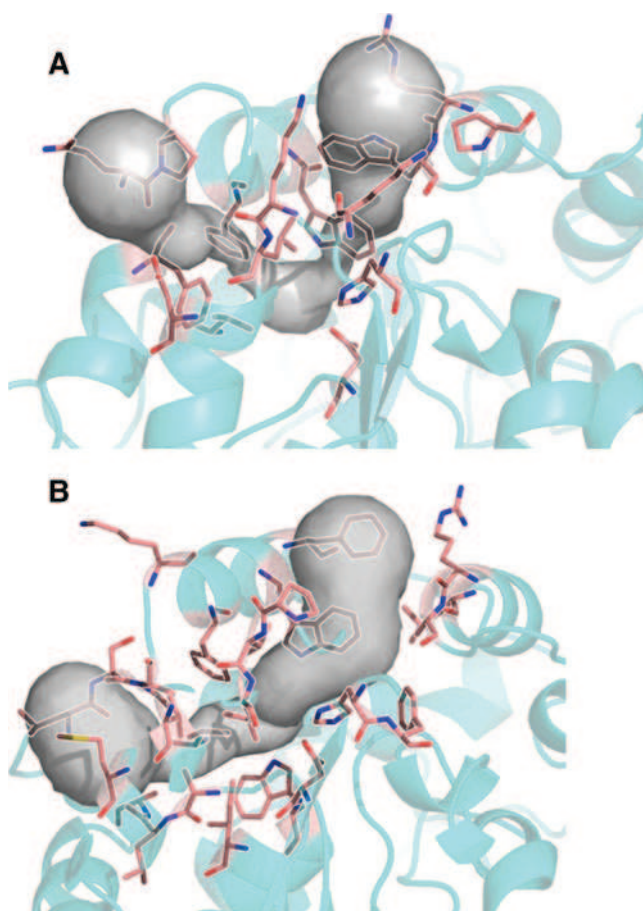


Fig. 7 Main tunnels and slot tunnels of DhLA (a) and DppA (b) calculated by CAVER (Petrek et al. 2006). Residues that form the tunnels are shown in red

Discussion

DppA exhibits in agreement with other characterized HLDs a wide substrate range. Similarly to other HLDs such as DhaA, LinB, DhLA, and DbjA, DppA shows activity towards short and medium chain α -haloalkanes as well as towards short α,ω -haloalkanes (Keuning et al. 1985; Janssen et al. 1991; Nagata et al. 1997; Damborsky et al. 2001; Sfetsas et al. 2009). However, unlike these HLDs, DppA does not show activity towards any of the tested chlorinated substrates. DppA therefore appears to form its own specificity class. Compared to other HLDs, it shows similarities with DhLA: with increasing chain length, activity towards α -haloalkanes drops drastically (Keuning et al. 1985; Janssen et al. 1991); this is also reflected by the drop of k_{cat} from 1-bromopentane to 1-bromohexane (Table 2). They both accept short α,β -haloalkanes but do not convert short haloalcohols like 2-chloroethanol (Keuning

et al. 1985), which is probably due to the hydroxyl group being too close to the halogen for the substrate to bind in the hydrophobic active site (Damborsky et al. 2001). The best substrate of DhlA, 1,2-dichloroethane, is not converted by DppA. In contrast, the activities of DhaA and LinB towards α -haloalkanes are not that restricted in terms of chain length and the enzymes also convert short-chain haloalcohols (Damborsky et al. 2001; Janssen et al. 1991; Nagata et al. 1997). All of the HLDs mentioned above prefer short (C_2 – C_4), terminally halogenated substrates over larger ones, although some of them also convert these with partially significant activities (Damborsky et al. 2001; Jesenska et al. 2005; Sfetsas et al. 2009).

Based on a BLAST search, we have identified DppA in the NCBI database as novel putative haloalkane dehalogenase. The highest sequence identity (61%) was found with the putative dehalogenase from *Erythrobacter litoralis* HTCC2594, whereas the enzyme from *X. autotrophicus* as an experimentally confirmed HLD had only 50% identity. Only 30% identity was found for other HLDs with known crystal structures (Tables S1 and S2, supporting information). This indicates a closer phylogenetic relation of DppA with DhlA than with DhaA, DbjA, DmbA, and LinB. An alignment with five structurally described HLDs (Fig. 1) maintains the closer phylogenetic relation of DppA and DhlA.

This multiple alignment contains members of subfamilies HLD-I (DhlA) and HLD-II (DhaA, LinB, DbjA, and DmbA) (Sfetsas et al. 2009; Chovancova et al. 2007). It does not contain members of the subfamily HLD-III, as this subfamily still remains less well characterized. However, recently, Jesenská et al. characterized two members of this family, DrbA from *Rhodopirellula baltica* SH1 and DmbC from *Mycobacterium bovis* 5033/66 (Jesenska et al. 2009). But to this day, there are no crystal structures available for this group. The information derived from Fig. 1 show that DppA most probably belongs to HLD-I, which is the same subfamily as found for the closest relative DhlA (Chovancova et al. 2007).

In many positions in the active site, DppA and DhlA show identical residues, which are also well-aligned (Fig. 5). The catalytic triad of DppA contains Asp123 (nucleophile), Asp249 (acid), and His278 (base) (Figs. 1 and 4). The nucleophile Asp123 and the general base His278 can be found at the conserved positions after β 5 and β 8, respectively. In DppA and DhlA, the catalytic acid is situated at the most common position after β 7 (Ollis et al. 1992). In DhaA, DbjA, DmbA and LinB, the catalytic acid is a glutamic acid and located after β 6. Trp124 is the first halide-stabilizing residue, which is conserved in all six enzymes. The second halide-stabilizing residue is most probably Trp163. It is located in the cap domain in the α 4 helix (like in DhlA) and not in the main domain after β 3

(like in DhaA, DbjA, DmbA, and LinB) (Janssen 2004). At the latter position DppA has a Glu, which would be expected to be an Asn (like in DhaA, DbjA, DmbA, and LinB) if it was supposed to act as a halide-stabilizing residue.

The alignment of DppA and DhlA shows a gap at the N-terminal beginning of the cap domain of DppA (after position 150, Fig. 1). At this site in DhlA, two short-sequence repeats (a 15-bp perfect repeat at positions 156–160 and 165–169, and a 9-bp imperfect repeat at positions 161–163 and 172–174) can be found (Fig. 6). These repeats were predicted to have evolved from an ancestor of today's dehalogenases during adaptation to the beginning release of industrially produced 1,2-dichloroethane in the last century (Pries et al. 1994). In a subsequent study, it was shown that these repeats have an effect on the ability of DhlA to convert 1,2-dichloroethane (Pikkemaat and Janssen 2002): after removal of one copy of the repeats, DhlA lost its activity towards 1,2-dichloroethane, while it was still able to convert 1,2-dibromoethane. Thus, the ancestral dehalogenase was predicted to have been active on brominated, but not on chlorinated substrates (Janssen et al. 2005). The fact, that DppA lacks these repeats is therefore in agreement with the observation, that DppA does not accept chlorinated substrates.

The slot tunnel of DhlA is formed by, among others, residues Phe164 and Pro168. In case of DppA, this tunnel does not exist according to CAVER. A possible reason is Val251, which probably makes this tunnel too narrow in DppA. However, during catalysis the cap domain undergoes movements that might open this tunnel (Otyepka and Damborsky 2002). The entrance of the slot tunnel of DppA is the site where in DhlA, the first copies of the direct repeats which are missing in DppA, are located. Consequently, the entrance of this tunnel is completely blocked, mainly by residues Pro159, Ala160, and Phe161 (Fig. 6). The slot tunnel of DppA is also significantly wider than that from DhlA and thus might not only be used by water molecules, but also by haloalkanes and its corresponding alcohols. The main tunnel was reported to have important influence on specificity of a HLD (Chaloupkova et al. 2003). The entrance of this tunnel in DppA is blocked in DhlA by Trp194, which causes the tunnel in DhlA to pass below this residue.

The second copies of the repeats are located at the end of α 4', at the beginning of α 4 and in the loop between them. They do not seem to have any direct influence on the shape of the entrance tunnels. The direct repeats were proposed to have an influence on substrate specificity by “pushing Trp175 downstream the sequence” (Pikkemaat and Janssen 2002). They therefore reposition it and take influence on the adaptation towards new substrates (Pikkemaat and Janssen 2002). Alignment of the structures of DppA and

DhlA shows that the two halide-stabilizing tryptophans differ significantly in position and orientation (Fig. 5). As a consequence, Trp175 forces (1) the tunnel in DhlA to be much narrower (2) and the halide to be cleaved off to be in different position from that in DppA. The structural differences observed agree with the differences in specificity. This holds especially for the inactivity of DppA towards 1,2-dichloroethane, as the direct repeats missing in DppA were proposed in DhlA to have evolved during adaption towards 1,2-dichloroethane. The two enzymes might originate from a common ancestor, where one of them has been exposed to 1,2-dichloroethane and the other not.

Docking experiments showed a good orientation for 1-bromobutane in the active site pocket. The halide is almost coplanar with the N_{ε1} from Trp163 and Trp124, where Asp123 is, in terms of distance, reasonably positioned for the nucleophilic attack (Fig. 5). Superposing of this result with the DhlA (pdb code: 2DHC) confirmed that the orientation found for 1-bromobutane is very likely to be productive (Fig. 5). The dockings with 1-chlorobutane on the other hand showed an orientation of the substrate with the halide pointing towards the outside (data not shown). The distances between the halide and the N_{ε1} from Trp163 and Trp124 were significantly higher (5.9 and 5.4 Å, respectively). This could be a reason why 1-chlorobutane is not converted and might be a hint that 1-chlorobutane acts as a competitive inhibitor. Similar results have been reported for LinB (Nagata et al. 1997).

Crystal structure

The structure of DppA has been deposited in the Protein Data Bank (PDB) under the entry 2XT0.

Acknowledgments We thank the German Research Foundation (DFG, Grant Bo1862/4-1) for their financial support.

References

- Altschul SF, Gish W, Miller W, Myers EW, Lipman DJ (1990) Basic local alignment search tool. *J Mol Biol* 215:403–410
- Altschul SF, Madden TL, Schäffer AA, Zhang J, Zhang Z, Miller W, Lipman DJ (1997) Gapped BLAST and PSI-BLAST: a new generation of protein database search programs. *Nucleic Acids Res* 25:3389–3402
- Bidmanova S, Chaloupkova R, Damborsky J, Prokop Z (2010) Development of an enzymatic fiber-optic biosensor for detection of halogenated hydrocarbons. *Anal Bioanal Chem* 398:1891–1898
- Bogdanović X, Hessler M, Palm GJ, Bornscheuer UT, Hinrichs W (2010) Crystallization and preliminary X-ray diffraction studies of the putative haloalkane dehalogenase DppA from *Plesiocystis pacifica* SIR-I. *Acta Crystallogr F Struct Biol Cryst Commun* 66:828–830
- Carr PD, Ollis DL (2009) Alpha/beta hydrolase fold: an update. *Protein Pept Lett* 16:1137–1148
- Chaloupkova R, Sykorova J, Prokop Z, Jesenska A, Monincova M, Pavlova M, Tsuda M, Nagata Y, Damborsky J (2003) Modification of activity and specificity of haloalkane dehalogenase from *Sphingomonas paucimobilis* UT26 by engineering of its entrance tunnel. *J Biol Chem* 278:52622–52628
- Chovancova E, Kosinski J, Bujnicki JM, Damborsky J (2007) Phylogenetic analysis of haloalkane dehalogenases. *Proteins* 67:305–316
- Collaborative Computational Project N (1994) The CCP4 suite: programs for protein crystallography. *Acta Crystallogr D Biol Crystallogr* 50:760–763
- Corpet F (1988) Multiple sequence alignment with hierarchical clustering. *Nucleic Acids Res* 16:10881–10890
- Damborsky J, Rorije E, Jesenska A, Nagata Y, Klopman G, Peijnenburg WJGM (2001) Structure-specificity relationships for haloalkane dehalogenases. *Environ Toxicol Chem* 20:2681–2689
- Damborsky J, Chaloupkova R, Pavlova M, Chovancova E, Brezovsky J (2010) Structure-function relationships and engineering of haloalkane dehalogenases. In: Timmis KN (ed) *Handbook of hydrocarbon and lipid microbiology*. Springer Berlin Heidelberg, pp 1081–1098
- Davis IW, Leaver-Fay A, Chen VB, Block JN, Kapral GJ, Wang X, Murray LW, Arendall WB 3rd, Snoeyink J, Richardson JS, Richardson DC (2007) MolProbity: all-atom contacts and structure validation for proteins and nucleic acids. *Nucleic Acids Res* 35(Web Server issue):W375–W383
- Dundas J, Ouyang Z, Tseng J, Binkowski A, Turpaz Y, Liang J (2006) CASTp: computed atlas of surface topography of proteins with structural and topographical mapping of functionally annotated residues. *Nucleic Acids Res* 34(Web Server issue):W116–W118
- Emsley P, Cowtan K (2004) Coot: model-building tools for molecular graphics. *Acta Crystallogr D Biol Crystallogr* 60(Pt 12 Pt 1):2126–2132
- Franken SM, Rozeboom HJ, Kalk KH, Dijkstra BW (1991) Crystal-structure of haloalkane dehalogenase—an enzyme to detoxify halogenated alkanes. *EMBO J* 10:1297–1302
- Gouet P, Courcelle E, Stuart DI, Metzger F (1999) ESPript: analysis of multiple sequence alignments in PostScript. *Bioinformatics* 15:305–308
- Holm L, Rosenstrom P (2010) Dali server: conservation mapping in 3D. *Nucleic Acids Res* 38(Web Server issue):W545–W549
- Holmquist M (2000) Alpha/beta-hydrolase fold enzymes: structures, functions and mechanisms. *Curr Protein Pept Sci* 1:209–235
- Iwasaki I, Utsumi S, Ozawa T (1952) New colorimetric determination of chloride using mercuric thiocyanate and ferric ion. *Bull Chem Soc Jpn* 25:226
- Janssen DB (2004) Evolving haloalkane dehalogenases. *Curr Opin Chem Biol* 8:150–159
- Janssen DB (2007) Biocatalysis by dehalogenating enzymes. *Adv Appl Microbiol* 61:233–252
- Janssen D, Wijngaard A, Waarde J, Oldenhuis R (1991) In: Hinchee RE, Olfenbuttel RF (eds) *On-site bioreclamation*, 1st edn. Butterworth-Heinemann, Boston, pp 539–547
- Janssen DB, Dinkla IJT, Poelarends GJ, Terpstra P (2005) Bacterial degradation of xenobiotic compounds: evolution and distribution of novel enzyme activities. *Environ Microbiol* 7:1868–1882
- Jesenska A, Pavlova M, Strouhal M, Chaloupkova R, Tseinska I, Monincova M, Prokop Z, Bartos M, Pavlik I, Rychlik I, Möbius P, Nagata Y, Damborsky J (2005) Cloning, biochemical properties, and distribution of mycobacterial haloalkane dehalogenases. *Appl Environ Microbiol* 71:6736–6745
- Jesenska A, Monincova M, Koudelakova T, Hasan K, Chaloupkova R, Prokop Z, Geerlof A, Damborsky J (2009) Biochemical characterization of haloalkane dehalogenases DrbA and DmbC:

- representatives of novel subfamily. *Appl Environ Microbiol* 75:5157–5160, AEM 00199-00209
- Keuning S, Janssen DB, Witholt B (1985) Purification and characterization of hydrolytic haloalkane dehalogenase from *Xanthobacter-autotrophicus* Gj10. *J Bacteriol* 163:635–639
- Krooshof GH, Kwant EM, Damborsky J, Koca J, Janssen DB (1997) Repositioning the catalytic triad aspartic acid of haloalkane dehalogenase: effects on stability, kinetics, and structure. *Biochemistry* 36:9571–9580
- Iizuka T, Jojima Y, Fudou R, Hiraishi A, Ahn J-W, Yamanaka S (2003) *Plesiocystis pacifica* gen. nov., sp. nov., a marine myxobacterium that contains dihydrogenated menaquinone, isolated from the Pacific coasts of Japan. *Int J Syst Evol Microbiol* 53(Pt 1):189–195
- Los GV, Wood K (2007) The HaloTag: a novel technology for cell imaging and protein analysis. *Meth Mol Biol* 356:195–208
- Marek J, Vevodova J, Smatanova IK, Nagata Y, Svensson LA, Newman J, Takagi M, Damborsky J (2000) Crystal structure of the haloalkane dehalogenase from *Sphingomonas paucimobilis* UT26. *Biochemistry* 39:14082–14086
- Marvanova S, Nagata Y, Wimmerova M, Sykorova J, Hynkova K, Damborsky J (2001) Biochemical characterization of broad-specificity enzymes using multivariate experimental design and a colorimetric microplate assay: characterization of the haloalkane dehalogenase mutants. *J Microbiol Meth* 44:149–157
- Mazumdar PA, Hulecki JC, Cherney MM, Garen CR, James MNG (2008) X-ray crystal structure of *Mycobacterium tuberculosis* haloalkane dehalogenase Rv2579. *Biochim Biophys Acta* 1784:351–362
- McCoy AJ, Grosse-Kunstleve RW, Adams PD, Winn MD, Storoni LC, Read RJ (2007) Phaser crystallographic software. *J Appl Crystallogr* 40(Pt 4):658–674
- Morris RJ, Perrakis A, Lamzin VS (2003) ARP/wARP and automatic interpretation of protein electron density maps. *Meth Enzymol* 374:229–244
- Nagata Y, Miyauchi K, Damborsky J, Manova K, Ansorgova A, Takagi M (1997) Purification and characterization of a haloalkane dehalogenase of a new substrate class from a gamma-hexachlorocyclohexane-degrading bacterium, *Sphingomonas paucimobilis* UT26. *Appl Environ Microbiol* 63:3707–3710
- Newman J, Peat TS, Richard R, Kan L, Swanson PE, Affholter JA, Holmes IH, Schindler JF, Unkefer CJ, Terwilliger TC (1999) Haloalkane dehalogenases: structure of a *Rhodococcus* enzyme. *Biochemistry* 38:16105–16114
- Oakley AJ, Klvana M, Otyepka M, Nagata Y, Wilce MC, Damborsky J (2004) Crystal structure of haloalkane dehalogenase LinB from *Sphingomonas paucimobilis* UT26 at 0.95 Å resolution: dynamics of catalytic residues. *Biochemistry* 43:870–878
- Ollis DL, Cheah E, Cygler M, Dijkstra B, Frolow F, Franken SM, Harel M, Remington SJ, Silman I, Schrag J, Sussman JL, Verschueren KHG, Goldman A (1992) The alpha/beta-hydrolase fold. *Protein Eng* 5:197–211
- Otyepka M, Damborsky J (2002) Functionally relevant motions of haloalkane dehalogenases occur in the specificity-modulating cap domains. *Protein Sci* 11:1206–1217
- Petrek M, Otyepka M, Banas P, Kosinova P, Koca J, Damborsky J (2006) CAVER: a new tool to explore routes from protein clefts, pockets and cavities. *BMC Bioinform* 7:316
- Pflugrath JW (1999) The finer things in X-ray diffraction data collection. *Acta Crystallogr D Biol Crystallogr* 55(Pt 10):1718–1725
- Pikkemaat MG, Janssen DB (2002) Generating segmental mutations in haloalkane dehalogenase: a novel part in the directed evolution toolbox. *Nucleic Acids Res* 30:E35
- Pries F, van den Wijngaard AJ, Bos R, Pentenga M, Janssen DB (1994) The role of spontaneous cap domain mutations in haloalkane dehalogenase specificity and evolution. *J Biol Chem* 269:17490–17494
- Prokop Z, Damborsky J, Oplustil F, Jesenska A, Nagata Y (2006a) Method of detoxification of yperite by using haloalkane dehalogenases. US Patent WO/2006/128390
- Prokop Z, Oplustil F, DeFrank J, Damborsky J (2006b) Enzymes fight chemical weapons. *Biotechnol J* 1:1370–1380
- Prokop Z, Damborsky J, Janssen DB, Nagata Y (2009) Method of production of optically active halohydrocarbons and alcohols using hydrolytic dehalogenation catalysed by haloalkane dehalogenases. US Patent WO/2006/079295
- Prokop Z, Sato Y, Brezovsky J, Mozga T, Chaloupkova R, Koudelakova T, Jerabek P, Stepankova V, Natsume R, van Leeuwen JG, Janssen DB, Florian J, Nagata Y, Senda T, Damborsky J (2010) Enantioselectivity of haloalkane dehalogenases and its modulation by surface loop engineering. *Angew Chem Int Ed* 49:6111–6115
- Schrag JD, Winkler FK, Cygler M (1992) Pancreatic lipases: evolutionary intermediates in a positional change of catalytic carboxylates? *J Biol Chem* 267:4300–4303
- Sfetsas CC, Milios L, Skopelitou K, Venieraki A, Todou R, Flemetakis E, Katnikas P, Labrou NE (2009) Characterization of 1,2-dibromoethane-degrading haloalkane dehalogenase from *Bradyrhizobium japonicum* USDA110. *Enzyme Microb Technol* 45:397–404
- Shimkets L, Ferriera S, Johnson J, Kravitz S, Beeson K, Sutton G, Rogers Y-H, Friedman R, Frazier M, Venter JC (2007) Direct Submission to NCBI database.
- Stucki G, Thüer M (1995) Experiences of a large-scale application of 1,2-dichloroethane degrading microorganisms for groundwater treatment. *Environ Sci Technol* 29:2339–2345
- Swanson PE (1999) Dehalogenases applied to industrial-scale biocatalysis. *Curr Opin Biotechnol* 10:365–369
- Thompson JD, Higgins DG, Gibson TJ (1994) CLUSTAL W: improving the sensitivity of progressive multiple sequence alignment through sequence weighting, position-specific gap penalties and weight matrix choice. *Nucleic Acids Res* 22:4673–4680
- Vagin AA, Steiner RA, Lebedev AA, Potterton L, McNicholas S, Long F, Murshudov GN (2004) REFMAC5 dictionary: organization of prior chemical knowledge and guidelines for its use. *Acta Crystallogr D Biol Crystallogr* 60(Pt 12 Pt 1):2184–2195
- Verschueren KHG, Franken SM, Rozeboom HJ, Kalk KH, Dijkstra BW (1993a) Refined X-ray structures of haloalkane dehalogenase at pH 6.2 and pH 8.2 and implications for the reaction-mechanism. *J Mol Biol* 232:856–872
- Verschueren KHG, Kingma J, Rozeboom HJ, Kalk KH, Janssen DB, Dijkstra BW (1993b) Crystallographic and fluorescence studies of the interaction of haloalkane dehalogenase with halide-ions—studies with halide compounds reveal a halide binding-site in the active-site. *Biochemistry* 32:9031–9037
- Verschueren KHG, Seljee F, Rozeboom HJ, Kalk KH, Dijkstra BW (1993c) Crystallographic analysis of the catalytic mechanism of haloalkane dehalogenase. *Nature* 363:693–698